Modern Aspects of the Jahn−Teller Effect Theory and Applications To Molecular Problems

Isaac B. Bersuker*

Institute for Theoretical Chemistry, Department of Chemistry & Biochemistry, The University of Texas at Austin, Austin, Texas 78712

Received December 4, 2000

Contents

* To whom correspondence should be addressed. Phone: 512-471-4671. Fax: 512-471-8696. E-mail: bersuker@eeyore.cm.utexas.edu.

I. Introduction

A. The Role and Place of Jahn−Teller Vibronic Coupling Effects in Theoretical Chemistry

I begin this review with a statement that the so-called Jahn−Teller (JT) effect (hereafter JTE), pseudo-JTE (PJTE), and Renner−Teller effect (RTE), jointly JT vibronic coupling effects, are *not* limited to a restricted variety of molecular polyatomic systems in specific electronic states, as it is often presented in the literature. In fact, what follows from the many works on this topic, partly cited in this review, is that the JT vibronic coupling theory is *an approach* to (*a tool* for) solving molecular and crystal problems, which is in principle applicable to any system with more than two atoms. Practically, this approach is most efficient when there are two or more coinciding (degenerate) or relatively close in energy (pseudodegenerate) electronic states that become sufficiently strongly mixed when the nuclei displace from their initial reference configuration.

The term "*relatively* close in energy" should be understood literally, which means that the absolute value of the energy gap between vibronically coupled energy levels may be large, provided other constants have appropriate values (see section II.C.1). This statement essentially enlarges the range of systems that can be treated by the JT approach because degenerate and close in energy states, ground or excited, are present in almost all systems. In fact, there are no a priori exclusions from treatments by this approach, and only considerations of smallness of the vibronic coupling and/or other preferences

10.1021/cr0004411 CCC: $36.00
Published on Web 03/13/2001

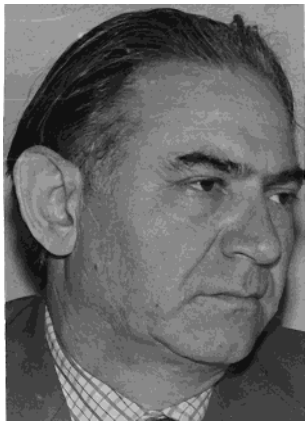

I. B. Bersuker obtained his scientific degrees of "Candidat of Sciences" (∼Ph. D.) and "Doctor of Sciences" in 1957 and 1964, respectively, from Leningrad University, in the group of Professor V. A. Fock, one of the authors of the Hartree–Fock method. From 1964 to 1993, I. B. Bersuker headed the Laboratory of Quantum Chemistry at the Institute of Chemistry of the Academy of Sciences of the USSR, Moldavian Branch (later, Academy of Sciences of Moldova), in Kishinev. He is a full Member of this Academy. In 1993, I. B. Bersuker became a Senior Research Scientist of the University of Texas at Austin. In his Ph.D. dissertation, I. B. Bersuker revealed the influence of core polarization on optical transition in atoms. His main interests afterward were in the Jahn–Teller (JT) and pseudo-JT (PJT) effect theory and applications. Among his main achievements, presented by 325 publications including 12 books and 25 major reviews, he predicted tunneling splitting in JT systems, proved that the PJT effect is the only source of instability of high-symmetry configurations of polyatomic systems, introduced orbital vibronic constants and vibronic molecular orbitals, revealed the coexistence of trigonal and tetragonal JT distortions, worked out the theory of vibronic chemical activation by coordination to transition metals, developed the general idea of vibronic stereochemistry and crystal chemistry, and created the vibronic theory of ferroelectricity and structural phase transitions. In more recent years he suggested and worked out a method of combined quantum/classical (QM/MM) modeling for large organometallic and metallobiochemical systems with charge transfer between the QM and MM fragments and a more "industrial oriented" electron-conformational method of pharmacophore identification and bioactivity prediction in drug design and toxicology. I. B. Bersuker supervised more than 50 Ph.D. theses, served in many Scientific Councils and Editorial Boards, received a variety of awards for scientific merit, and has the USSR registered Scientific Discovery N 202 (1979).

(other ways to treat the problem, if possible) may restrain one from its application. To a great extent, we can speak about systems that were already considered with regard to their vibronic coupling effects and systems that were not considered as yet.

With respect to the mainstream computational chemistry which overwhelmingly considers electronic structure calculations of polyatomic systems with fixed nuclei and nuclear dynamics along the adiabatic potential energy surface (APES), the JT vibronic effects are important extensions which take into account the coupling between the electronic and nuclear motions. The latter, in general, are not just small vibrations. Even if the nuclear motions can be presented by small vibration (which may take place in the absence of electronic degeneracy and/or strong pseudodegeneracy), APES that determines the vibrational frequency, especially the anharmonicity, is controlled by the vibronic coupling with other electronic states.

However, in the majority of molecular systems with more than two atoms, degenerate and pseudo-degenerate states are inevitable, ground or excited. Consider a simple triatomic ABC. If A = B = C, the molecule has a 3-fold axis of symmetry and hence doubly degenerate E terms in the configuration of a regular triangle. If the triangle is distorted, the E term splits, so the APES has the form of a conical intersection at the point of degeneracy (section II.B.1). If one of the atoms differs from the others or they are all different, there is no electronic degeneracy in the configuration of a regular triangle but there is still pseudo-degeneracy with a possible PJTE.

However, in principle there may be degeneracy in the configuration of a distorted triangle ABC if the distortion compensates the differences in the electronic structure of the atoms. Hence, even when the atoms are different, the ABC system has a conical intersection on its APES. Although this conical intersection may be displaced from the stable configuration of the minimum of the APES, it still may affect the observable properties (see, e.g., the Berry phase implications in section II.E). The nearer to the APES minimum, the more significant is this conical intersection.

In the presence of electronic degeneracy or pseudo-degeneracy, conventional electronic structure calculations with fixed nuclei, strictly speaking, do not predict observable properties. The calculated APES in these cases loses a significant part of its physical meaning as the potential energy of the nuclei because of the nonadiabacity,[1−3] and the spatial configuration of the system at the minimum of the APES may not coincide with observed geometry because of the JT dynamics. This is why the vibronic coupling theory is an unavoidable extension of the mainstream theoretical and computational chemistry. The number of works to develop this important trend in application to molecular problems is increasing rapidly (see refs 1−34), as it is reflected also in this review.

An important point is also the modeling (analytical) aspect of the JTE and PJTE theory. The JT vibronic coupling theory starts from a high-symmetry nuclear configuration of the polyatomic system (the reference configuration[1]) and includes the coupling to the nuclear displacements from this configuration (vibronic coupling) as a perturbation to the electronic states, the latter thus becoming dependent on nuclear coordinates. If the vibronic coupling terms (linear, quadratic, etc., in nuclear coordinates) mix two or more electronic states, the resulting APES is very peculiar with important consequences for the observable properties. The latter can be determined by solving the system of coupled equations for the nuclear motions (section II.A).

The first part of this problem, the calculation of the APES, can be solved numerically without involving the vibronic coupling theory. This can be done by electronic structure calculations with fixed nuclei. However, as it is widely recognized, the results of numerical computations have the value of a computer experiment and, as any other experimental data, may serve as a basis of the theory if properly accumulated and generalized. The latter means to put the data in correspondence with *analytical models* obtained by simplification and reasonable assumptions introduced in the general principles. The perturbational

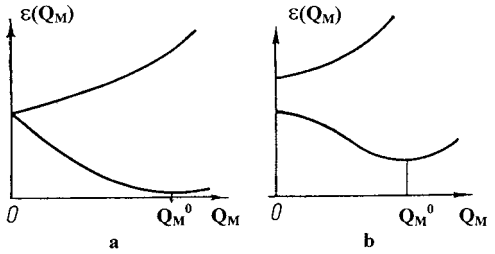

Figure 1. Adiabatic potential energy of interacting atoms or groups of atoms as a function of the inverse coordinate of their rapprochement Q_M ($Q_M = 0$ when the interatomic distance is infinite, Q_M^0 is the point of equilibrium): (a) the interacting atoms are identical, the system is degenerate at infinite—the bonding curve is similar to the JTE one; (b) the interacting atoms (groups) are different, the bonding curve is similar to the PJTE one.

approaches in the JT vibronic coupling theory serve as such analytical models that allow us *to rationalize the numerical data*.

The second part of the problem that considers observable properties by solving the system of equation of nuclear motions is *a novel extension of computational chemistry*.

The brief introduction to the role of the JT vibronic effects will be incomplete without mentioning the stimulating broader approach to the understanding and applications of the ideas that underlie these effects.

During the past decade, attempts have been made to generalize and extend the JTE ideas in order to explain phenomena which, at first sight, seem to be unrelated to JT subjects.[35−38] The most important and most relevant to the JTE is *the state of broken symmetry in the universe*, which can be regarded as resulting from a sequence of symmetry breaking (SB) that took place during the long period of cooling after the *big bang*. Any SB can be considered similar to a phase transition that takes place at a temperature $T = T_0$, at which the molar free energies of the high (1) and low (2) symmetry states coincide: $U_1 - T_0S_1 = U_2 - T_0S_2$. Since the entropy in the state of higher symmetry *ceteris paribus* is larger than in that of lower symmetry, $S_1 > S_2$, the SB takes place when there is *a triggering mechanism that lowers the potential energy with lowering the symmetry*, $U_1 > U_2$. With this inequality, the free energy is lower in the high-symmetry configuration at $T > T_0$ and in the low-symmetry one at $T < T_0$. The JT vibronic coupling effects are just such distortion mechanisms on the polyatomic level that includes molecular systems and crystals.[1−3,5,11,33,35−38]

The SB induced by JT vibronic effects requires degeneracy or pseudo-degeneracy. The linkage of SB to degeneracy seems to be of general validity. It was recognized also in the field of elementary particle interactions. As stated in ref 39 (cited also in ref 38), "*broken symmetry is always associated with a degeneracy*". With inclusion of PJT instability, the spectrum of phenomena resulting in broken symmetry enlarges essentially. In particular, interatomic and intermolecular interactions produce bonded states of lower symmetry which can be regarded as triggered by a JT or PJT-type instability.[37] Figure 1 illustrates this statement. It is seen that the energies of the two interacting systems, which are degenerate or pseudo-degenerate at large distances R between them (the coordinate Q_M is inversely proportional to R), undergo further splitting at smaller R (larger Q_M) resulting in bonding. The energy behavior as a function of Q_M in Figure 1a and 1b is quite similar to the one in the JTE and PJTE, respectively. In this respect, molecular and intermolecular bonding may be regarded as a SB. Together with the transitions gas−liquid[37] and liquid−crystal,[35] the whole picture of SB in matter, beginning with atoms, can be arranged as a sequence of SB which take place consequently by cooling the system[37] (Figure 2): atoms → molecules → liquids → crystal (I) → crystal (II) → and so on, all of them being triggered by the same mechanism of the JTE and PJTE in their extended formulation as a source of instability due to degeneracy or pseudo-degeneracy.

Note that, as mentioned above, the sequence of SB in the elementary particle systems by cooling, beginning with the big bang, are also related to degeneracies.[39] With them included, *the global picture of formation of matter from the big bang by cooling is controlled by a sequence of SB triggered by the JT-type coupling of degenerate (pseudo-degenerate) states to particle motions (transformations) that lower the symmetry*.

Among other extensions (analogues) of the JTE ideas, see meson−nucleon interaction in quantum field theory,[40] α-cluster description of light nuclei,[41] heavy nuclei giant resonances,[42] interaction of light with matter,[43] Yang−Mills gauge forces,[38] entanglement in quantum measurements,[38] etc.

B. What Is and Is Not Considered in This Review

This review on JT effect *theory* and limited applications is addressed to a wide range of readers, chemists and physicists, not just experts in this field.

As follows from section I.A, the JT vibronic coupling (JTE, PJTE, and RTE) theory is an approach to the investigation of polyatomic (molecular and crystal) systems which affects practically all their observable properties based on atomic and electronic structure. Vibronic coupling effects are important in molecular and crystal stereochemistry, all-range spectroscopy (from microwave and EPR, to infrared, visible, UV, photoelectron, X-ray, and γ-ray spectroscopy), reactivity and chemical activation, reaction mechanisms, electron transfer, redox properties, structural phase transition, ferroelectricity, colossal magneto-resistance, high-temperature superconductivity, etc. It is obvious that any review of reasonable size cannot consider all these fields; limitations are absolutely necessary.

The limitations of this review are related to objects, methods, and the time scale of publications. First, we refer the reader to a series of books and reviews that fully consider the general theory and earlier works in this field.[1−34] In general, we try not to repeat material from these publications, although earlier results are mentioned again if it is necessary in the context of new achievements and for the integrity of the presentation. This also pertains to the basic

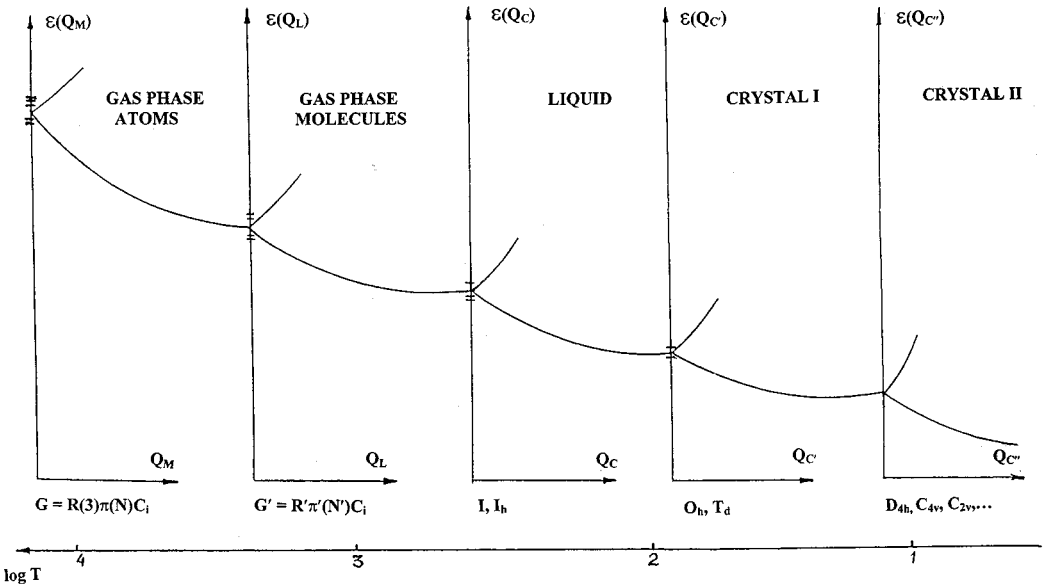

Figure 2. Conventional scheme of consequent temperature-dependent symmetry breaking triggered by JTE and/or PJTE. $G = R(3)\pi(N)C_i$ is the symmetry of an atomic gas, where $R(3)$ is the group of rotations of the free atom, $\pi(N)$ is the group of permutation and C_i is inversion; the primed values have the same meaning for the gas of molecules. Crystal I and crystal II denote two crystal phases with decreasing symmetry, respectively. Q_M, Q_L, Q_C, $Q_{C'}$, and $Q_{C''}$ are the coordinates of symmetry breaking.

equations of the JTE and PJTE theory that are given briefly in section II.A to outline the terminology and denotations used and to facilitate a better understanding of the reviewed material. In general (but not exclusively), this review is concerned with works published in approximately the last 10−15 years.

Second, only essential JT, PJT, and RT works are considered, i.e., publications in which these vibronic effects play a central role. The many interesting papers in which the vibronic effects are just mentioned or referred to for interpretation of the results, especially experimental results, without significant analysis are not reviewed here. The number of such papers (e.g., on X-ray analysis, electron diffraction, ESR, NMR, electron and vibrational spectroscopy) in which observed configuration distortions are attributed to JT vibronic effects is in the thousands, and there is no sense in including them in this review, although a separate bibliographic collection could be useful (such a bibliographic review of all JT papers published through 1979 is given in ref 11).

Third, we restrain this review from considering crystal problems and cooperative effects, although the latter are mentioned occasionally. The vibronic coupling effects in crystals are presently used to explain a variety of the most interesting properties including such important topics as crystal lattice formation, structural phase transitions, ferroelectricity, high-temperature superconductivity, and colossal magnetoresistance. These works form a whole trend, which is now in fast development and requires separate consideration. Some of these topics were reviewed earlier.[1−3,5,7,11,13,15,16,19,24,25,28,29,31,33] Some important topics related to the JT vibronic coupling theory in section III.F are just mentioned, not reviewed in detail.

With these limitations, we divide the publications to be reviewed here in two parts: advances in general theory and molecular geometry and spectra. The separation between these sections is conventional; many theoretical achievements, mostly those published together with specific applications, are presented in the second part of this review.

II. Advances in General Theory

A. Basic Formulations

This section introduces the reader to the main formulations of the JTE, PJTE, and RTE. The deduction of the formulas is in most cases omitted; they can be easily found in the corresponding references.[1−4] The notions introduced in this section serve as a basis for all subsequent discussions.

A rough formulation of the JTE comes from the authors of the first publication:[44] *the nuclear configuration of any nonlinear polyatomic system in a degenerate electronic state is unstable with respect to nuclear displacements that lower the symmetry and remove the degeneracy*. This formulation is not sufficiently rigorous and may lead to confusion. Indeed, at first sight, it follows from this formulation that the JTE implies that if the electronic term is degenerate, the system distorts itself spontaneously and *a distorted nuclear configuration should be observed*. Strictly speaking, this statement is not true. In fact, for free molecular systems, in general, distorted nuclear configuration may not be observable (because of the JT dynamics) and the degeneracy of the system as a whole is not always removed either. On the other hand, the limitation by linear molecules in this formulation does not hold either (section II.C.2). The main effect of electronic degeneracy is in producing a *special coupling between the electronic and nuclear motion* that results in a series of observable effects, which are jointly called the JT vibronic coupling

effects. They include also distorted nuclear configurations that can be observed under certain restraining conditions.

In a more rigorous presentation it is worthwhile to separate the JT effect from the JT theorem. The JT theorem refers to the APES of the system which, although not observable directly, may serve as an indirect qualitative measure of many observable effects. Its formulation is as follows:[1] *If the APES of a polyatomic system has two or more branches that intersect in one point (degeneracy point Q_0), then at least one of them has no extremum at this point. Two kinds of cases are exceptions: (1) linear molecules (linear configurations at the point Q_0) and (2) 2-fold spin (Kramers) electronic degeneracy.*

The proof of this theorem is straightforward. Divide the Hamiltonian of the system into three parts

$$H = H_r + H_Q + V(r,Q) \tag{1}$$

where H_r contains the pure electronic part, H_Q is the nuclear kinetic energy, and $V(r,Q)$ includes electron−nuclear and nuclear−nuclear interactions; r and Q stand for the sets of electronic and symmetrized nuclear coordinates, respectively. Expand the function $V(r, Q)$ with respect to small nuclear displacement from the initial[1] configuration $Q_\alpha = 0$, $\alpha = 1,2,...,N$

$$V(r, Q) = V(r, 0) + \sum_\alpha (\partial V/\partial Q_\alpha)Q_\alpha + {}^1/_2 \sum_{\alpha,\beta} (\partial^2 V/\partial Q_\alpha \partial Q_\beta)_0 Q_\alpha Q_\beta + ... \tag{2}$$

The terms

$$W(r, Q) = V(r, Q) - V(r, 0) = \sum_\alpha (\partial V/\partial Q_\alpha)Q_\alpha + {}^1/_2 \sum_{\alpha,\beta} (\partial^2 V/\partial Q_\alpha \partial Q_\beta)_0 Q_\alpha Q_\beta + ... \tag{3}$$

are called *vibronic coupling terms*. For small Q_α values, W may be considered as a perturbation.

The Schrödinger equation for the system as a whole

$$H\,\Psi_i(r,Q) = \epsilon_i(Q)\Psi_i(r,Q) \tag{4}$$

with only the zeroth order term $V(r, 0)$ of eq 2 (i.e., neglecting the vibronic coupling) is

$$[H_r + V(r,0)]\varphi_k(r) = \epsilon_k'\,\varphi_k(r) \tag{5}$$

If by solving this equation we get a f-fold degenerate electronic term, $\epsilon_k' = \epsilon_0$, $k = 1, 2,..., f$, then, by including the linear terms of the vibronic coupling (eq 3) as a perturbation, we come to the secular equation of the order f in which the matrix elements of the linear terms $F_{Q\alpha}^{(\Gamma\Gamma')}Q_\alpha$ contains the linear vibronic coupling constant

$$F_{Q\alpha}^{(\Gamma\Gamma')} = \langle\Gamma|(\partial V/\partial Q_\alpha|\Gamma'\rangle \tag{6}$$

where $|\Gamma\rangle$ and $|\Gamma'\rangle$ are the wave functions of two states of the degenerate term (in fact we should denote the two degenerate states as Γ_γ and $\Gamma_{\gamma'}$, respectively;[1] the denotation in eq 6 is adapted to include the case of two nondegenerate terms as in the PJTE (sections II.C and II.D)).

The lack of extremum at $Q_\alpha = 0$ means that at least one of the vibronic constants of eq 6 is nonzero. On the basis of group-theoretical considerations, Jahn and Teller[44] proved that for any nonlinear molecule in a degenerate state there are such symmetry coordinates Q_α for which $F_{Q\alpha}^{(\Gamma\Gamma')} \neq 0$. The proof is given by checking all the point groups, one by one. On the other hand, the lack of extremum at the point $Q_\alpha = 0$ with respect to at least one coordinate means that there is no minimum in this point: the APES may have minima at other points $Q_\alpha \neq 0$, at which the nuclear configuration is distorted, or it has no minima. The quadratic terms of eq 3 produce further complications of the APES.[1−3]

Note that degenerate states occur mostly due to the high symmetry of the nuclear configuration: a doubly degenerate E term emerges when there is at least one 3-fold axis of symmetry. In these cases there is more than one equivalent minima of distorted configurations, and they complement each other to reestablish the reference symmetry.[1−3] If the degeneracy (conical intersection) is due to the compensation of electronic differences in atoms by distortions, mentioned in section I.A, the effect of equivalent multiminimum APES disappears.

With the vibronic coupling terms of eq 3 included in eq 5, the eigenvalues $\epsilon_k'(Q)$ are functions of the nuclear coordinates, and they may become different for the different states of the degenerate term, thus splitting the later in f branches. The real properties of the system are described by the Schrödinger equation (4) with the complicated branched potential for the nuclear motion. The rigorous formulation of the problem is to expand the full wave function of the system $\Psi(r,Q)$ over the set of solutions $\varphi_k(r)$

$$\Psi(r,Q) = \Sigma_k \chi_k(Q)\varphi_k(r,Q) \tag{7}$$

where the coefficients $\chi_k(Q)$ depend on the nuclear coordinates.

By substituting this expression into eq 4, we get the following system of coupled equations for the χ-(Q) functions

$$[H_Q + \epsilon_k(Q) - E]\chi_k(Q) + \Sigma_{m\neq k} A_{km}(Q)\chi_m(Q) = 0 \qquad k, m = 1, 2, ... \tag{8}$$

where $\epsilon_k(Q) = \epsilon_k' + W_{kk}(Q)$ while $A_{km}(Q)$ are the matrix elements of the so-called operator of nonadiabacity calculated with the $\varphi_k(r,Q)$ functions[1].

If the expansion in eq 7 is taken with the set of electronic functions $\varphi_k(r,0)$ obtained with fixed nuclei at $Q_\alpha^0 = 0$ (at which $W(r,0) = 0$), the expression for $A_{km}(Q)$ is simplified:[3] $A_{km}(Q) = W_{km}(Q)$. In this case, the equations in the system (eqs 8) are coupled via the operator of vibronic interactions $W(Q)$ given by eq 3. This version of the vibronic coupling equations seems to be physically more transparent and more appropriate with regard to the treatment of the many effects that emerge due to the vibronic interaction.

In particular, if the off-diagonal vibronic coupling W_{km} may be neglected, eqs 8 become decoupled; each of them describes the vibrational motions in a given electronic state. This is the *adiabatic approximation*. It was shown that in general this decoupling is

invalid if the electronic state as a solution of eq 5 is f-fold degenerate, $f > 1$. If the coupling of the degenerate states to the excited states can be neglected (see below), the infinite system of eqs 8 can be reduced to f-coupled equations, $k, m = 1, 2,..., f$. Thus, in degenerate electronic states, the electronic and nuclear motions cannot be separated in the adiabatic approximation.

The solution of eqs 8 is one of the most important computational aspects of the Jahn−Teller effect theory discussed in this paper. However, many manifestations of the JT effects can be evaluated from the form of the APES without solving eqs 8. For a degenerate electronic state at $Q_\alpha = 0$ obtained from eq 5, the dependence of the electronic state energies ϵ'_k, $k = 1, 2,..., f$, on nuclear displacements can be obtained by including the vibronic coupling terms $W(Q)$ as a perturbations. The latter splits the degenerate term and yields values ϵ_k^{v}, which together with the harmonic (nonvibronic part) nuclear interaction term[1] produce f branches of the APES that intersect at $Q_\alpha = 0$

$$\epsilon_k(Q_\alpha) = {}^1/_2\Sigma_\alpha K_\alpha Q_\alpha{}^2 + \epsilon_k{}^{\mathrm{v}}(Q_\alpha) \quad k = 1, 2,..., f \quad (10)$$

where K_α are the primary force constants (the force constant without vibronic coupling[1]) and $\epsilon(Q_\alpha)$, as above, is a function of all the active coordinates Q_α.

The APES of JT and PJT systems are very special. Their main features include multiminima branches, equipotential troughs, and conical intersection, including multiconical intersections and lines of conical intersections, etc.[1−3,27,45,46] The importance of conical intersections goes beyond the direct JT topic. A series of recent publications are devoted to this problem (see ref 47 and references therein). Further discussion of JTE related to conical intersections is given in sections II.B and II.E. For tensorial formulation of the JTE, see in ref 48.

B. Main JT Problems

1. Two-Fold Degenerate Electronic Terms E Interacting with a Two-Fold Degenerate E Vibration: the E⊗e Problem

This is one of the simplest and most widespread JT problems. An E term as a solution of eq 5 is the ground or excited state of any polyatomic system that has at least one axis of symmetry of not less than the third order. The smallest systems of this kind are triatomics X_3 (see examples in section III.B). If we denote the two electronic functions of the E term by their symmetry properties $|\theta\rangle$ and $|\epsilon\rangle$ (in the d function nomenclature $\theta \sim d_{z^2}$ and $\epsilon \sim d_{x^2-y^2}$), then the linear F_{E} and quadratic G_{E} vibronic coupling constants after eq 6 are

$$F_{\mathrm{E}} = \langle\theta|\ (\partial V/\partial Q_\theta)_0|\theta\rangle \quad (11)$$

$$G_{\mathrm{E}} = \langle\theta|\ (\partial^2 V/\partial Q_\theta \partial Q_\epsilon)_0|\epsilon\rangle \quad (12)$$

while

$$K_{\mathrm{E}} = \langle\theta|\ (\partial^2 V/\partial Q_\theta{}^2)_0|\theta\rangle \quad (13)$$

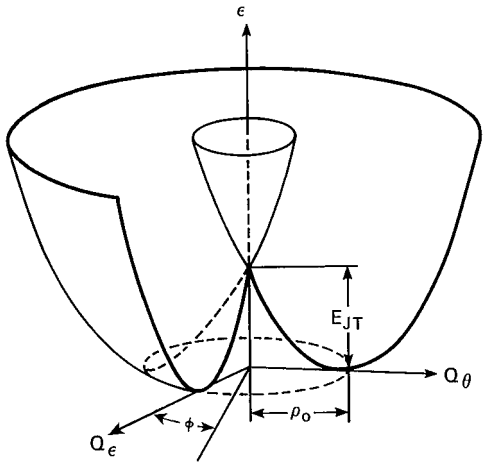

Figure 3. APES for a 2-fold degenerate E term interacting linearly with the 2-fold degenerate E-type vibrations described by Q_ϑ and Q_ϵ coordinates with a conical intersection at $Q_\vartheta = Q_\epsilon = 0$ (linear E⊗e problem, the "Mexican hat"). E_{JT} is the Jahn−Teller stabilization energy; ρ_0 is the radius of the trough. (Reprinted with permission from ref 25. Copyright 1996 John Wiley & Sons, Inc.)

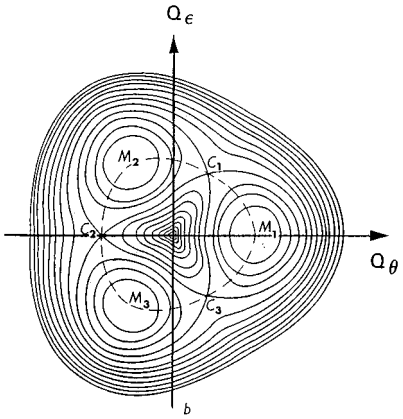

Figure 4. Equipotential sections of the lower sheet of the APES for the E⊗e problem with both the linear and quadratic vibronic interaction included. Three minima (M_1, M_2, M_3) and three saddle points (C_1, C_2, C_3) are linked by the dashed line of the steepest slope from the latter to the former. (Reprinted with permission from ref 25. Copyright 1996 John Wiley & Sons, Inc.)

is the primary force constant (see below). With these denotations, the APES after eq 10 in polar coordinates $Q_\theta = \rho \cos \phi$ and $Q_\epsilon = \rho \sin \phi$ is

$$\epsilon_\pm(\rho,\phi) = {}^1/_2K_{\mathrm{E}}\rho^2 \pm \rho[F_{\mathrm{E}}{}^2 + G_{\mathrm{E}}{}^2\rho^2 + 2F_{\mathrm{E}}G_{\mathrm{E}}\rho \cos 3\phi]^{1/2} \quad (14)$$

If the quadratic coupling is negligible, the APES (eq 14) becomes a surface of revolution with $\epsilon_\pm$ independent of ϕ, sometimes called "*Mexican hat*" (Figure 3). With nonzero quadratic coupling, this APES acquires three minima at $\phi = 0$, $2\pi/3$, and $4\pi/3$ divided by three saddle points at $\phi = \pi/3$, π, and $5\pi/3$ when moving along the bottom of the trough (*a tricorn*, Figure 4). The two wave functions corresponding to the two branches of the APES are

$$\Psi_- = \cos(\Omega/2)|\theta\rangle - \sin(\Omega/2)|\epsilon\rangle \quad (15)$$

and

$$\Psi_+ = \sin(\Omega/2)|\theta\rangle + \cos(\Omega/2)|\epsilon\rangle$$

where

$$\tan\Omega = (F_E \sin\phi - |G_E|\rho \sin 2\phi)/(F_E \cos\phi + |G_E|\rho \cos 2\phi) \quad (16)$$

It is seen that the wave function is not a product of one electronic and one nuclear function, as required by the adiabatic approximation; the latter thus does not hold.

Figures 5 and 6 illustrate the change of nuclear configuration in the *internal free rotation* (sometimes called *pseudo-rotation*) when the system moves along the bottom of the trough in a triangular and octahedral system, respectively, and the quadratic vibronic coupling is neglected. If the quadratic terms are large enough, the energy barrier between the minima δ becomes significant[1−3]

$$\delta = 4E_{JT}|G_E|/(K_E + 2|G_E|) \quad (17)$$

where E_{JT} is the JT stabilization energy (Figure 3)

$$E_{JT} = F_E^2/2(K_E - 2|G_E|) \quad (18)$$

and hindered motions (*pulsation*) take place instead of free rotations. Spectroscopically, this is reflected in *tunneling splitting* of the ground-state energy levels.

Note that eqs 17 and 18 are deduced under the assumption that $G_E < K_E$, i.e., the quadratic coupling is small. This means that approximate formula can be useful for estimation of parameters

$$E_{JT} \approx F_E^2/2K_E \quad (19a)$$

$$\rho_0 = F_E/K_E \quad (19b)$$

$$\delta \approx 4E_{JT}|G_E|/K_E \quad (19c)$$

In more widespread notations in dimensionless units with energy in $\hbar\omega$ units, time in ω^{-1}, length in $(\hbar/m\omega)^{1/2}$, and normal coordinates in mass-weighted length $(\hbar/\omega)^{1/2}$, eq 14 can be written in the following form

$$\epsilon_\pm(\rho,\phi) = {}^1/_2\rho^2 \pm \rho[k^2 + {}^1/_4g^2\rho^2 + kg\rho\cos 3\phi]^{1/2} \quad (20)$$

In this $K_E = 1$, $F_E = k$, $G_E/K_E = g/2$, $D = E_{JT}/\hbar\omega_E = k^2/2$, and $\delta/\hbar\omega_E = k^2g$, $g = {}^1/_2\delta/E_{JT}$.

In general, the totally symmetric displacements A (that do not lower the symmetry of the system but change proportionally some or all interatomic distances) are involved in the E⊗e problem, making it in fact E⊗(e + a). With the A displacements included, the APES, instead of eq 14, is[3]

$$\epsilon_\pm(\rho_A,\rho,\phi) = {}^1/_2K_A\rho_A^2 - F_A\rho_A + {}^1/_2K_E\rho^2 \pm \rho[F_E^2 + G_E^2\rho^2 + 2F_EG_E(\rho\cos 3\phi - 8^{1/2}\rho_A) + 4G_E^2\rho_A(2\rho_A - 2^{1/2}\rho\cos 3\phi)]^{1/2} \quad (21)$$

where ρ_A and K_A are the radial coordinate and force constant for the totally symmetric displacements A.

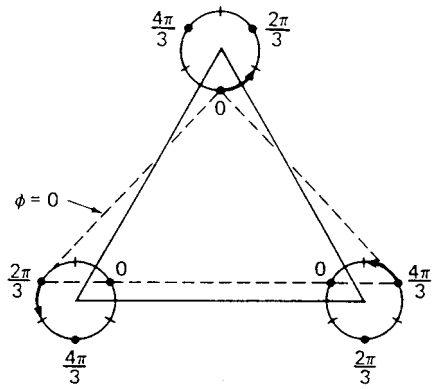

Figure 5. Distortions of a triatomic molecule X_3 by moving along the bottom of the trough of the lowest sheet of the adiabatic potential in the linear E⊗e problem. Each of the three atoms moves along a circle, their phases being concerted. The bold points indicate the minima positions when quadratic terms are taken into account. The dashed triangle corresponds to the point $\phi = 0$ in eq 14 ($Q_\epsilon = 0$, $Q_\theta = \rho$ in Figure 4), and the case of compressed triangles is shown; for the opposite sign of the vibronic constant the triangles are elongated.

In strongly coupled E⊗e problems, the totally symmetric (breathing) mode alters the absorption spectrum,[49] in particular, it quenches the so-called Slonczewski resonances.[1,2]

One of the important consequences of the presence of several equivalent minima on the APES with high enough barriers between them (Figure 4) is the tunneling phenomenon that results in splitting of the vibrational levels in each of the wells first considered in ref 50. Earlier developments of the theory of tunneling splitting in E⊗e problems are reviewed in refs 1−3, 8, and 51; further achievements are considered below in this and other sections.

An important development of the theory of the E⊗e problem emerged recently[52] when it was realized that the linear and quadratic coupling terms of the vibronic interaction W in eq 3 are described by rather independent constants, which means that the quadratic coupling is not necessarily small as compared with the linear coupling. If the quadratic coupling is sufficiently large, the form of the APES and all the consequent properties change essentially. As seen from eq 14, the two branches of the APES in this case intersect not only at $\rho = 0$ (central conical intersection), but also at $\rho = |F_E/G_E|$ and $\phi = \pi/3$, π, $5\pi/3$, i.e., along the three lines that include the saddle points on the APES.[53] Figure 7 shows one of these additional conical intersections in the cross section of the APES along the line containing the minimum M at $\phi = 0$, the saddle point S at $\phi = \pi$, and two conical intersections, the central one C and the additional one C' in this direction.

If g (or G_E) is small, the additional conical intersections are far away from the central conical intersections, the minima positions, and the saddle points, thus almost not affecting the main properties of the system. However, the quadratic coupling g may be sufficiently large, and then it dramatically affects the tunneling splitting and our general understanding of the problem.[52]

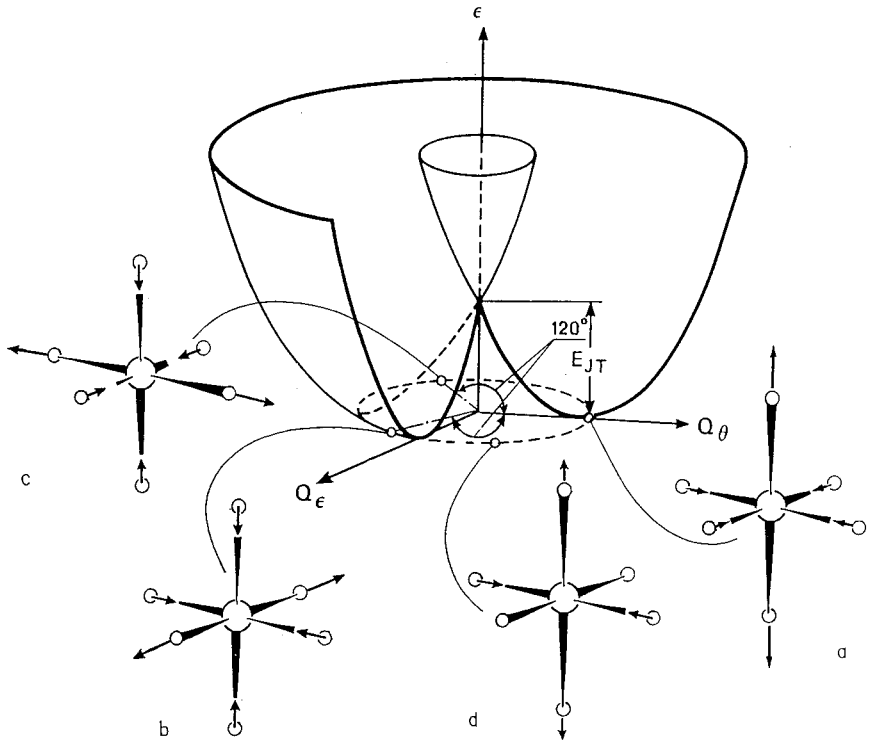

Figure 6. Distortions of an octahedral system ML_6 at different points along the bottom of the trough of the "Mexican hat" in the linear E⊗e problem. At the points $\phi = 0, 2\pi/3, 4\pi/3$, the octahedron is tetragonally distorted along the three 4-fold axes, respectively (a, b, c). Between these points the configuration has D_{2h} symmetry (d) and varies continuously from one tetragonal configuration to another. (Reprinted with permission from ref 25. Copyright 1996 John Wiley & Sons, Inc.)

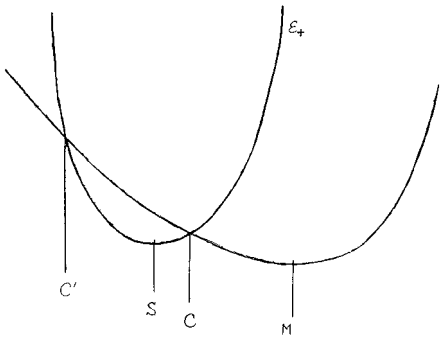

Figure 7. Cross section of the APES of a E⊗e system with linear and quadratic terms included with a plane containing one minimum M, the central conical intersection C, and a saddle point S. For sufficiently strong quadratic coupling, an additional conical intersection C′ emerges at $\delta = 2k/g$. There are three (equivalent) such additional conical intersections on the APES.

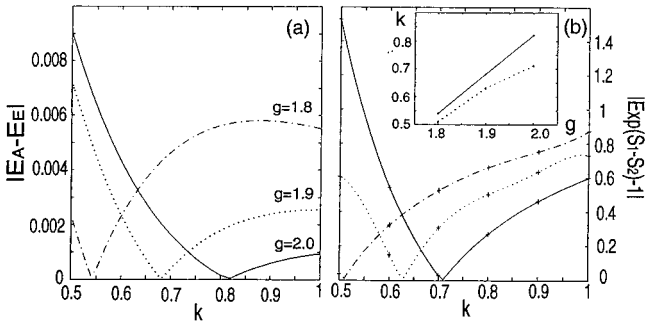

Figure 8. Absolute values of the energy difference $|E_A - E_E|$ between the lowest A and E levels (a), and the ratios of the tunneling rates via P_1 an P_2 paths (b) (plotted as $|\exp(S_1 - S_2) - 1|$) as functions of k for $f = 0.05$ and three values of g. Calculated points are indicated by "+", and polynomially interpolated curves for the $g = 2.0$, 1.9, and 1.8 values are depicted by solid, dotted, and dash−dotted lines, respectively. Inset: the g versus k values at the crossing points $E_A = E_E$ (solid line) and at $S_1 = S_2$ (dotted line). (Reprinted with permission from ref 52. Copyright 1999 American Physical Society.)

The most important (in some sense dramatic) conclusion from this (and some other, see below) work is that the long-standing belief (paradigm) that the ground vibronic state (a solution of eqs 8) has the same degeneracy and symmetry E as the initial electronic state (at the point of degeneracy) should be reversed. This paradigm emerged from many calculations (see refs 1−3, 10, 11, and 19), all performed for small g values, and has been misguiding for almost 40 years. By means of direct numerical calculations it was shown[52] that for sufficiently large quadratic coupling g, the first excited nondegenerate vibronic energy level A intersects the lower (ground) level E and remains the ground state for larger g values. Figure 8a shows the energy difference between these two levels as a function of the linear coupling k and quadratic coupling g. We see that for any g value (in the region of large enough g values) there is a k value for which the two levels intersect and the nondegenerate A level becomes the ground state. The constant f stands for the fourth-order terms.

The interpretation of this effect is that for sufficiently large g values the three additional conical intersections, mentioned above, approach the central conical intersection, thus creating an alternative pass for the tunneling between the near-neighbor minima (Figure 9). This additional pass goes around all four

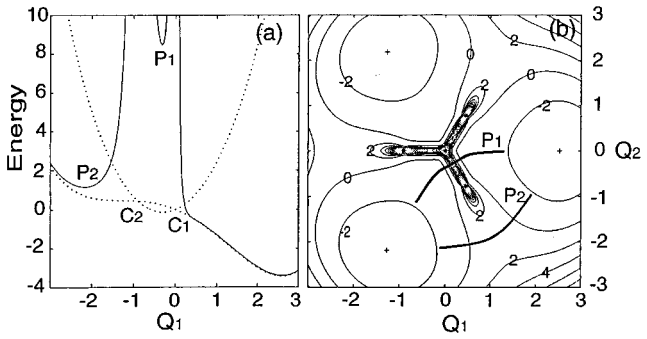

Figure 9. Adiabatic potential energy surface (APES) of a JT E⊗e system for parameter values $k = 0.9$, $g = 2$, $f = 0.05$: (a) Cross section with (solid line) and without (dotted line) the Born−Huang contributions at $Q_2 = 0$. C_1 and C_2 indicate conical intersections, while P_1 and P_2 indicate two saddle points. (b) Contour plot of the APES; "*" and "+" indicate a conical intersection and a minimum, respectively. The two steepest decent tunneling paths P_1 and P_2 are shown by thick lines. (Reprinted with permission from ref 52. Copyright 1999 American Physical Society.)

conical intersections instead of that for small g values which encircles only one, the central conical intersection.

In conjecture with the Berry phase problem (section II.E), this means that by encircling one conical intersection, the wave function changes sign, resulting in the ground state with a half-integer quantum number and double degeneracy. If the four conical intersections are encircled, the phase of the wave function does not change and a double degeneracy of the ground state is not required. The crossing of the two levels, A and E, and a nondegenerate ground-state A emerges when the tunneling path around all four conical intersections is lower in energy (Figures 8b and 9).

The change of the ground-state symmetry and degeneracy is most important in spectroscopy and low-temperature dynamics in the system (section III). It is particularly important for the theory of *vibronic reduction factors*,[1−3] which significantly simplifies the calculation of ground-state matrix elements that represent observable quantities. The theory of vibronic reduction factors is invalid if the symmetry of the ground vibronic energy level is different form that of the reference electronic state.

A more general conclusion from the works on tunneling splitting that lead to either degenerate or nondegenerate ground states as a function of the vibronic coupling parameter[50,52] (see also section III.B.3) is that the ground term orbital degeneracy is not necessarily related to the global symmetry of the system; it is rather dependent on internal interactions. A somewhat similar situation emerges in the so-called *spin crossover* (see, e.g., in ref 25) when in transition-metal complexes the ground term orbital and spin degeneracy change (from high-spin to low-spin configuration) as a function of the ligand field of the environment.

Somewhat related discussion of the topology of APES in triatomic system is given in ref 54. For other implications of JT symmetry breaking in such systems, see ref 55. Use of path-integral in multimode vibronic coupling is considered in ref 56a. The method of isostationary functions in multimode and multilevel JT problems is described in ref 56b.

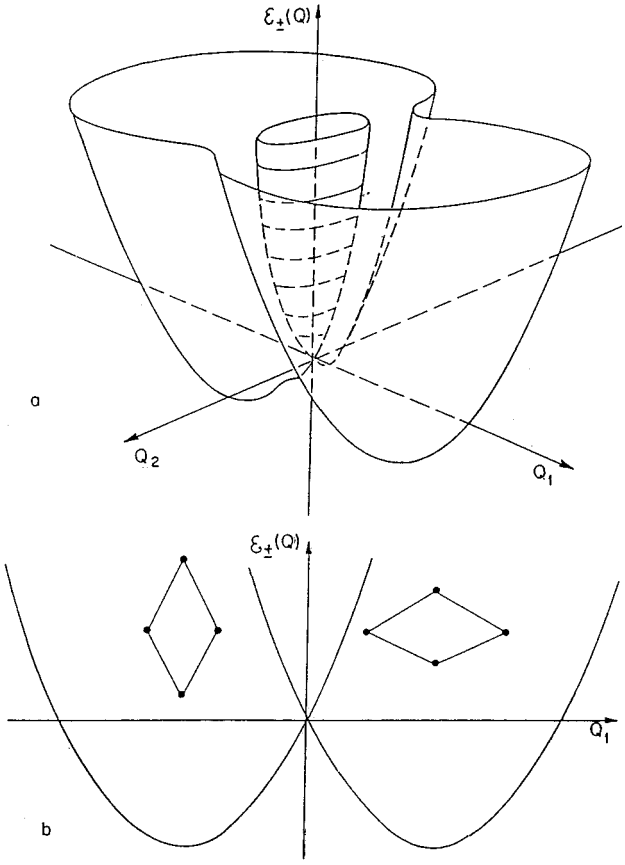

Figure 10. APES of a quadratic X_4 molecule in a E state linearly coupled to b_1 and b_2 displacement (E⊗(b_1 + b_2) problem) when $E_{JT}^{(1)} > E_{JT}^{(2)}$: (a) general view; (b) cross-section along the Q_1 coordinate with illustration of distortions of the square at the minimum points.

2. Two-Fold Degenerate E Tem Interacting with Two Independent Vibrations b_1 and b_2: The E⊗ (b_1 + b_2) Problem

This problem occurs when the system has a symmetry axis of the order multiple with four: $C_{4v(h)}$, S_4, $C_{8v(h)}$, $D_{8v(h)}$, etc. The simplest of them is a square-planar configuration X_4 (see the cyclobutadiene and cyclobutane examples in section III.C.1).

The b_1 distortion transforms the square into a rhombus, while under the b_2 displacements the square becomes a rectangle. Two linear and two quadratic constants describe the coupling to the two types of vibrations. If the linear coupling to one of them is stronger than to the other one, the APES has two minima with respect to the former and two saddle points in the direction of the latter. Figure 10 illustrates this case when the b_1 coupling is stronger. Upon taking into account the quadratic coupling terms, the saddle points may transform into minima and a coexistence of the two types of minima is possible.[1,57]

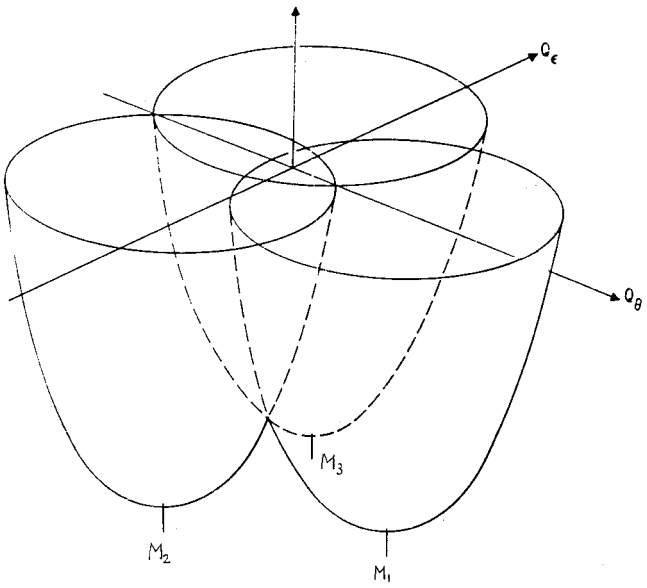

Figure 11. APES for the JT T⊗e problem. Three paraboloids intersect at $Q_\theta = Q_\epsilon = 0$. M_1, M_2, and M_3 are the three minima.

3. Triplet Terms Interacting with e and t_2 Vibrations: The T⊗(e + t_2) Problem

This problem emerges in systems with any kind of cubic and icosahedral symmetry (types T, O, and I point groups). Denote by ξ, η, and ζ the three electronic functions of the degenerate T term ($\xi \sim d_{xy}$, $\eta \sim d_{yz}$, $\zeta \sim d_{xz}$), by Q_ξ, Q_η, and Q_ζ the three t_2 type trigonal vibrational coordinates, and by Q_θ and Q_ϵ the two tetragonal vibrations of e type. The two types of active vibrations e and t_2 are described by two linear coupling constants

$$F_E = \langle\zeta|(\partial V/\partial Q_\theta)_0|\zeta\rangle$$

$$F_T = \langle\eta|(\partial V/\partial Q_\xi)_0|\zeta\rangle \qquad (22)$$

and four quadratic vibronic constants G_E(E × E), G_E-(T × T), G_T(T × T), and G_T(E × T). The APES in the space of the five coordinates above is rather complicated, but it can be relatively easily investigated in cross sections.

First, if the coupling to the e displacements is much stronger than to the t_2 one, the latter can be neglected in the zeroth approximation. The solution of the resulting T⊗e problem can be found directly. It consists of three equivalent intersecting paraboloids (Figure 11) with minima at the points (at which the system is tetragonally distorted): (Q_0^E,0), ($^1/_2Q_0^E$, ($^3/_4$)$^{1/2}Q_0^E$), and ($^1/_2Q_0^E$, −($^3/_4$)$^{1/2}Q_0^E$), where

$$Q_0{}^E = F_E/K_E \qquad (23)$$

and the JT stabilization energy (the depth of the minima read off the degeneracy point) is

$$E^E{}_{JT} = F^2{}_E/2K_E \qquad (24)$$

If, on the contrary, the coupling to the tetragonal displacement may be neglected, $F_E = 0$, the APES for the T⊗t_2 problem has four equivalent minima along the four trigonal axes C_3 of the cubic systems at the points ($m_1Q_0^T$, $m_2Q_0^T$, $m_3Q_0^T$), where the four sets of coefficients (m_1, m_2, m_3) are (1,1,1), (−1, 1, −1), (1, −1, −1), and (−1, −1, 1), respectively

$$Q_0{}^T = -2F_T/3K_T$$

$$E_{JT}{}^T = 2F_T{}^2/3K_T \qquad (25)$$

At the minima, the frequency of the t_2 vibrations ω_T splits into two

$$\omega_A = \omega_T,\ K_A = K_T$$

and

$$\omega_E = (^2/_3)^{1/2}\omega_T,\ K_E = {}^2/_3K_T \qquad (26)$$

In the general case when both types of vibrations are active in the JTE, the problem is more complicated and the results depend on the ratio between the vibronic coupling constants to e and t_2 vibrations and the JT stabilization energies. The APES has three types of extrema points: three tetragonal ones, which are qualitatively the same as in the T⊗e problem, four trigonal extrema points as in the T⊗t_2 problem above, and six orthorhombic points in which one tetragonal and one trigonal coordinate are displaced. The depth of the orthorhombic extrema points $E^0{}_{JT}$ is

$$E^0{}_{JT} = {}^1/_4E^E{}_{JT} + {}^3/_4E^T{}_{JT} \qquad (27)$$

If $E_{JT}{}^E > E_{JT}{}^T$, the tetragonal extrema points are absolute minima, the trigonal ones being saddle points. If, on the contrary, $E_{JT}{}^T > E_{JT}{}^E$, the trigonal points are absolute minima while the tetragonal ones are saddle points. If only the linear vibronic coupling is taken into account, the orthorhombic extrema points are always saddle points. However, if the quadratic coupling terms are taken into account, the orthorhombic saddle points become minima and there are whole regions of parameter values where different types of minima coexist[1,58] (see also ref 59). Figure 12 illustrates this statement based on calculations

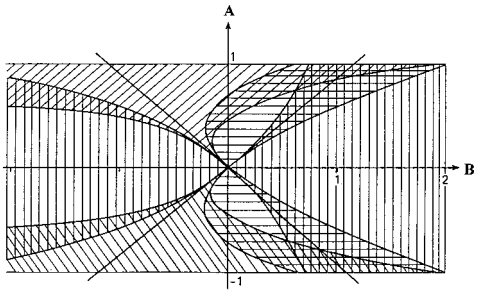

Figure 12. Areas of existence and coexistence of different types of minima of the APES for the quadratic T⊗(e + t_2) problem (in A and B coordinates); vertical, horizontal, and oblique shadings correspond to areas of existence of tetragonal, trigonal, and orthorhombic minima, respectively. Overlap shading shows areas of coexistence of corresponding minima (from ref 58).

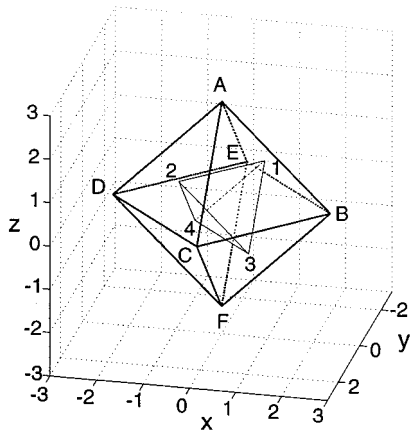

Figure 13. Schematic presentation of the positions of the six orthorhombic minima A, B, C, D, E, and F, and four trigonal minima 1, 2, 3, and 4 in the space of the *x*, *y*, *z* coordinates of the t_2 displacements in the T⊗t_2 problem. The vibronic coupling parameters used are $k = 1$, $g = 1.6$, and $f = 0.1$. (Reprinted with permission from ref 69. Copyright 2000 American Institute of Physics.)

for the case when only one (assumed most important) type of quadratic term of vibronic coupling

$$G = G_E(E \times T) = {}^1/_2\langle\xi|(\partial^2 V/\partial Q_\xi \partial Q_\eta)_0|\eta\rangle \quad (28)$$

is taken into account.

The two dimensionless constants in Figure 12 are $A = G(K_E K_T)^{-1/2}$ and $B = F_T G/F_E K_E$.

Evaluation of the possible minima of the complicated APES in JT problems is not always straightforward and may encounter difficulties. In this respect, the *epikernel principle* based on group-theoretical considerations may be helpful.[14]

A combined $(T_1 + T_2)\otimes(e + t_2)$ problem was considered recently.[60] The theory of tunneling splitting and vibronic reduction factors in systems with T terms was reviewed in refs 1−3 and further developed in a series of works.[61−66] For essential contribution to the theory of vibronic reduction factors, see in refs 67 and 68 and references therein.

As in the case of the E⊗e problem, significant progress has been reached recently by including strong quadratic and higher order vibronic coupling in the determination of the APES, energy spectra, and observable properties.[69] The complication of the APES produced by higher order vibronic coupling is most important because it changes the number and positions of conical intersections which, in turn, influence essentially the energy level ordering (similar to the case of the E⊗e problem, discussed above).

For the T⊗t_2 problem with quadratic and fourth-order vibronic coupling terms, there are four trigonal and six orthorhombic minima conventionally shown in Figure 13. They are separated by saddle points and conical intersections. Distinguished from the much more simple case of the E⊗e problem where the quadratic terms produce an additional (to the central one) three conical intersections (Figure 7), in the T⊗t_2 problem with quadratic coupling there are four lines of conical intersections between the trigonal minima that originate from the center of the tetrahedron (1, 2, 3, and 4 on Figure 13) and proceed along the four trigonal directions that cross the centers of its four faces (Figure 14) plus six lines of conical intersections that connect two of the four points as indicated in Figure 14.

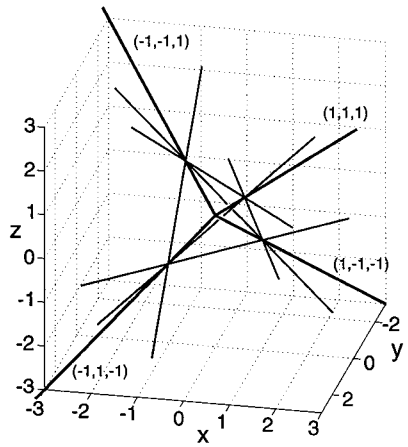

Figure 14. The 10 lines of conical intersection in the lowest potential energy surface of the T⊗t_2 problem. Four of them drawn by thick lines extend from (0, 0, 0) in the directions of (1, 1, 1), (1, −1, −1), (−1, 1, −1), and (−1, −1, 1). The other six lines connect two of the following four points: $(2k/3g, 2k/3g, 2k/3g)$, $(2k/3g, -2k/3g, -2k/3g)$, $(-2k/3g, 2k/3g, -2k/3g)$, and $(-2k/3g, -2k/3g, 2k/3g)$. The vibronic coupling parameters are $k = 1$, $g = 1.6$, and $f = 0.1$. (Reprinted with permission from ref 69. Copyright 2000 American Institute of Physics..

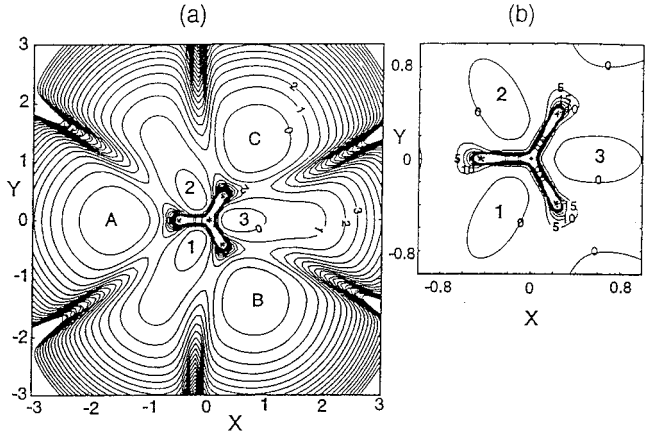

Figure 15. Cross sections of the lowest APES in the $X-Y$ plane: (a) at the trigonal minima ($Z = 0.157$) for $k = 1$, $g = 1.6$, and $f = 0.1$. The letters A, B, and C denote three orthorhombic minima, while 1, 2, and 3 denote the trigonal minima. Conical intersections are located at $(X, Y) = (0,0)$ and -0.45 $[\cos(2n\pi/3), \sin(2n\pi/3)]$, $n = 0, 1, 2$; (b) around $(X, Y) = (0, 0)$, enlarged; asterisk indicates the position of conical intersections. (Reprinted with permission from ref 69. Copyright 2000 American Institute of Physics.)

An easier way to visualize this rather complicated topology is to look into cross sections. Figure 15 brings one of such cross sections perpendicular to one of the lines of conical intersections showing the energy contours around the three original minima, 1, 2, and 3, and three orthorhombic minima, A, B, and C, and the central conical intersection plus three lateral conical intersections. The six additional conical intersections between the orthorhombic minima are outside the picture in the well-seen directions.

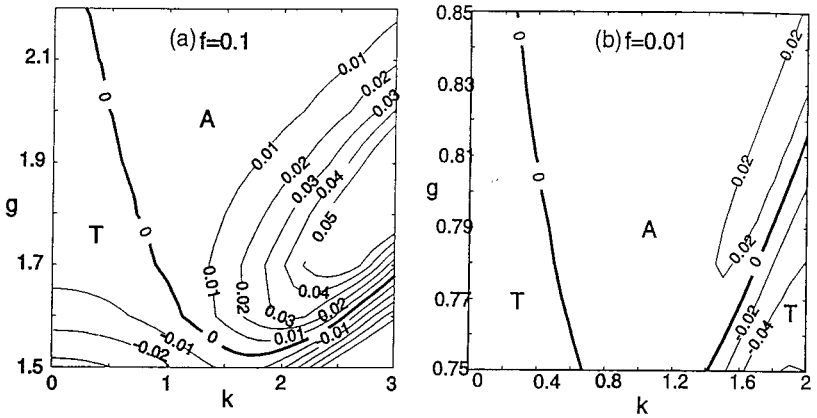

Figure 16. Energy difference between the lowest T and A vibronic states for $f = 0.1$ (a) and $f = 0.01$ (b) as a function of k and g. Thick lines are zero contour lines. The letters T and A denote the regions of T and A ground states, respectively. (Reprinted with permission from ref 69. Copyright 2000 American Institute of Physics.)

The positions of minima and conical intersections depend on the parameter values. For strong linear coupling and weak quadratic coupling, only trigonal minima are important and only the four lines of conical intersections that originate from the center (Figure 14) are significant in formation of the energy spectrum. By increasing the quadratic coupling, the orthorhombic saddle points become minima and the six additional lines on the conical intersection become significantly involved. As a result, similar to the E⊗e case, a new tunneling path occurs which encircles an even number of conical intersections. For parameter values for which this path is lower, the nondegenerate A state becomes the ground state. Figure 16 illustrates some of these results.[69] For large quadratic coupling, a fourth-order term presented by the parameter $f \neq 0$ should be included in the calculations to stand for the stability of the system.

4. Higher Order Degeneracy in Icosahedral Systems: The T⊗h, G⊗(g + h), and H⊗(g + h) Problems

The latest achievements in the preparation and studies of icosahedral systems (fullerenes) stimulated further intensive and extensive investigation, although the first work[70] on the JT effect in such systems was published before the discovery of fullerenes. Essential contribution to the development of the JTE theory in application to icosahedral system was made in a series of works[27,70−97] partly reviewed in ref 27.

In icosahedral systems, there are 4-fold (G) and 5-fold (H) orbitally degenerate electronic terms in addition to the E and T terms that are present also in systems with lower symmetry (with Kramers spin degeneracy included, cubic systems have 4-fold G terms, too). The typical JT problems here are T⊗h (a T term interacting with 5-fold degenerate nuclear h displacements), G⊗(g + h) (a G term interacting with 4-fold g and/or 5-fold h vibrations; do not confuse the g displacements in icosahedral systems with the quadratic coupling constant in the JT problems above), and H⊗(g + h) (an H term interacting with g and/or h vibrations). Figure 17 illustrates the possible JT distortions of an icosahedron with I_h symmetry as a result of vibronic coupling to the corresponding symmetrized nuclear displacements.[2,27]

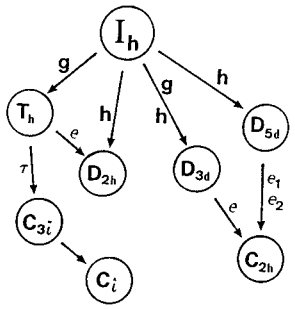

Figure 17. Possible distortions (symmetry reduction) of an icosahedral system with I_h symmetry in degenerate states under g and h modes (displacements) and further distortions of the lower symmetry configurations under e and t_2 modes; all modes are even as required by the JT theorem; "i" means inversion. (Reprinted with permission from ref 2. Copyright 1972 John Wiley & Sons, Inc.)

For obvious reasons of higher complexity, the JT problems in icosahedral systems are less studied than those in the simplest systems discussed above, although the number of publications on the JTE in fullerens is significant and is increasing continuously.

The T⊗h problem[27,70−72,77] is somewhat similar to the particular case of T⊗(e + t_2) when the vibronic coupling to the e and t_2 vibrations and their frequencies are the same (cf. the T⊗d problem[1]). In the linear approximation with respect to the vibronic coupling to the five symmetrized displacements, the APES has a continuum of equipotential minima points which form a two-dimensional trough on the five-dimensional surface, somewhat similar to the one-dimensional trough in the E⊗e problem (section II.B.1). Denoting the two coordinates of distortion by the angles θ and ϕ, we can illustrate the motion along the bottom of the trough as an internal free rotation of quadrupole distortions of a sphere as show in Figure 18. Present the 3-fold degenerate electronic state by three atomic states and assume that the initial state is p_z-like with the spheroidal distortion along the Z axis, $\theta = 0$. By moving along the trough, the sphere remains quadrupolly distorted but the direction of distortion is gradually changing along the (θ, ϕ) directions. Note that as in other JT pseudorotation, an internal rotation of the distortion but not a rotation of the system as a whole takes place.

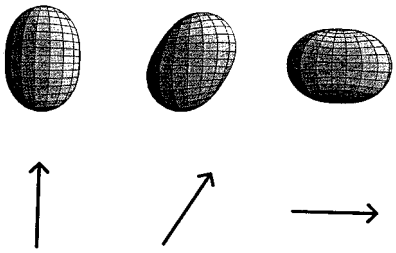

Figure 18. Three orientations in the pseudo-rotation of a quadrupole-distorted spherical surface. The principal axis of the associated electronic p state is shown below each distortion. (Reprinted with permission from ref 27. Copyright 1997 Princeton University Press.)

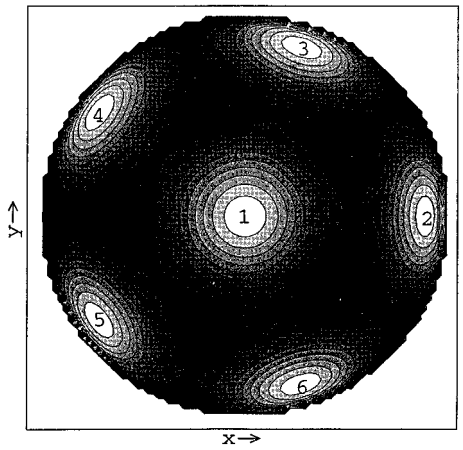

Figure 19. Illustration of the D_{5d}-type minima on the spherical surface of a icosahedral system with a JT T⊗h problem which occupy the vertexes of the icosahedron, while the maxima are at the vertexes of the dodecahedron. Changing the sign of the quadratic coupling interchanges the maxima and minima. (Reprinted with permission from ref 27. Copyright 1997 Princeton University Press.)

The system is thus performing free internal rotation along the bottom of the trough at which its symmetry is lower than icosahedral. If the quadratic terms of vibronic coupling are taken into account, warping of the trough takes place (again, similar to the E⊗e case) and minima, maxima, and saddle points occur when moving along it. All these extrema points are complementary to each other so that the system regains its icosahedral symmetry. Figure 19 illustrates this case.[27]

The six D_{5d}-type minima on the spherical surface are at the vertexes of the icosahedron, the 10 D_{3d} maxima are at the vertexes of a dodecahedron, and the 15 D_{2h} saddle points are at the centers of the edges of either polyhedron. Changing the sign of quadratic coupling interchanges the minima and maxima leaving the saddle points where they are. Dependent on the coupling strength, these minima may be deep enough to quasi-localize the distorted configuration. In this case, the system performs hindered rotations—tunneling transitions between the minima via the lowest barriers at the saddle points (sections II.B.1 and II.B.2)

The G⊗(g + h) problem[70−74,76,82] is more complicated since it involves 4 + 5 = 9 degrees of freedom in JT distortions with two types of vibronic coupling constants to g and h displacements. The approach to the problem is to consider the cases when the coupling to one of the two types of vibrations is much stronger than that to the other one, which allows one to ignore the weaker coupling in the zeroth order approximation and to take it into account as a perturbation afterward. Another approach can be employed when the two types of couplings are of approximately the same magnitude, which would allow one to ignore their difference.

Table 1. Positions (g, θ, α, β) of the Five Minima of an Icosahedron with a Linear G⊗g JT Problem[a]

	g	θ	α	β
min 1	g_0	$\pi/4$	$3\pi/2$	$\pi/2$
min 2	g_0	$\pi/4$	$7\pi/10$	$9\pi/10$
min 3	g_0	$\pi/4$	$3\pi/10$	$\pi/10$
min 4	g_0	$\pi/4$	$11\pi/10$	$17\pi/10$
min 5	g_0	$\pi/4$	$19\pi/10$	$13\pi/10$

[a] $g_0 = (9h/2\omega_g)^{1/2}k_g$, where k_g is the coupling constant.[27]

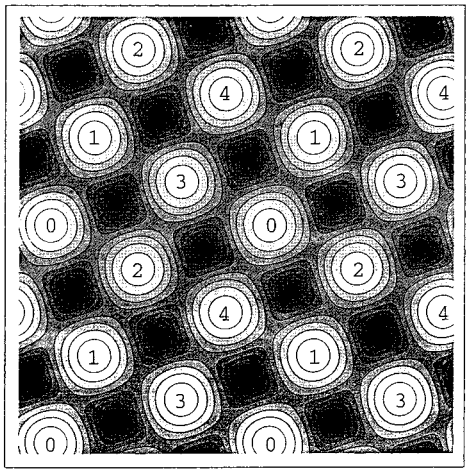

Figure 20. Energy contours for the lowest APES in the G⊗g problem plotted on an (α, β) surface with α horizontal. The range of α and β is (0, 4π), $\theta = \pi/4$, and g is constant. The minima are numbered to show how each one recurs with a period of 2π in each direction. The projections of the saddle points onto this surface are midway between neighboring minima. (Reprinted with permission from ref 27. Copyright 1997 Princeton University Press.)

For the G⊗g problem, the four coordinates of g type may be chosen with the following angular dependence (similar to polar coordinates): $g_1 = g \sin\theta \sin\alpha$, $g_2 = g \sin\theta \cos\alpha$, $g_3 = g \cos\theta \sin\beta$, and $g_4 = g \cos\theta \cos\beta$, where $0 \le g < \infty$, θ is similar to the usual polar angle, $0 \le \theta \le \pi/2$, while $0 \le \alpha < 2\pi$, $0 \le \beta < 2\pi$. In terms of these coordinates, the APES of the G⊗g system has five minima of tetrahedral T_h symmetry listed in Table 1, where g_0 depends on the vibronic coupling constant and the vibrational frequency ω_g (or the force constant K_g). In the five-dimensional space of the APES as a function of the four coordinates, it is difficult to visualize the positions of these minima.

Figure 20 gives some impression of the minima and saddle point positions projected on the plane (α, β). The five minima form a square mesh, each of them having the other four as neighbors in equivalent positions, so that the five equidistant points (with the same distance from the origin) form a four-dimensional analogue of a tetrahedron. There are 10 saddle points of D_{3d} symmetry at the midpoint between the

Table 2. Four Types of Extrema Points in the Icosahedral JT G⊗g and G⊗h Problems and Their Energies in the Linear Coupling Approximation[27] (k_g is given in units where $\hbar\omega = 1$)

symmetry	E(G⊗g)	E(G⊗h)
D_{3d} (I)	$-{}^3/_2 k_g{}^2\hbar\omega_g$	$-{}^3/_2 k_h{}^2\hbar\omega_h$
D_{2h} (II)	$-{}^1/_4 k_g{}^2\hbar\omega_g$	$-4k_h{}^2\hbar\omega_h$
D_{3d} (III)	$-{}^1/_6 k_g{}^2\hbar\omega_g$	$-{}^{25}/_6 k_h{}^2\hbar\omega_h$
T_h (IV)	$-{}^9/_4 k_g{}^2\hbar\omega_g$	0

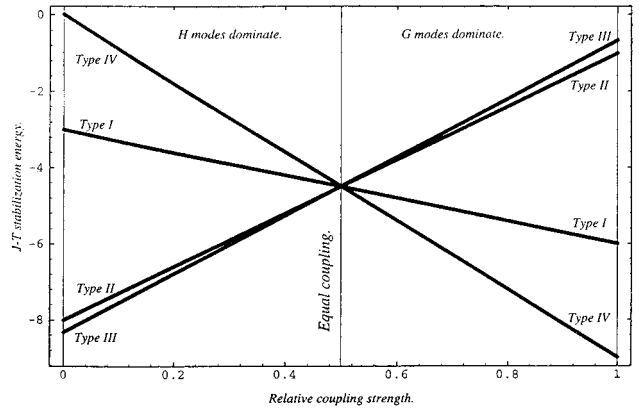

Figure 21. JT stabilization energies of the four types of minima in the linear G⊗(g + h) problem (Table 2) as a function of the coupling constant. If the coupling to the H modes dominates, the D_{3d} minima are the lowest, whereas if the G modes dominate, the T_h minima are lower. (Reprinted with permission from ref 27. Copyright 1997 Princeton University Press.)

minima on the (α, β) plane but with slightly different g and θ values. Table 2 lists some additional information about this APES.

The G⊗h problem is very similar to the G⊗g one, and it has features that are similar to the T⊗h problem, considered above. The APES has 10 D_{3d} minima which are also possible minima in the T⊗h problem, but distinguished from the latter, the six D_{5d} points are not stationary points but lines of degeneracy. There are also (other than in the T⊗h problem) 15 D_{2h} saddle points near the shortest path between pairs of minima which form the lowest energy barrier between them. Table 2 gives some additional information.

In the general case of the G⊗(g + h) problem, some complications emerge, but in the linear approximation with respect to the vibronic coupling the solution of this problem can be essentially reduced to that obtained for the particular cases of G⊗g and G⊗h. Indeed, it can be shown that in this approximation the APES has the same number and kind of extrema points as in the two particular cases shown in Table 2. If the coupling to the g vibrations predominates, the minima are of T_h type and the path of lowest energy between them is via the D_{3d}(I) saddle point. Conversely, if the h coupling is stronger, the minima are of D_{3d}(III) type and the intermediate saddle points are of D_{2h} symmetry. All the above points coincide in energy when $k_g{}^2\hbar\omega_g = 2k_h{}^2\hbar\omega_h$ (the equal coupling regime). The energy plot in Figure 21 shows how the minima and saddle points of one type gradually change to that of the other type when moving from one predominant type of coupling (i.e., h) to the other one (g).

The linear H ⊗(g + h) problem was considered in a most general way in ref 73 (see also in ref 27). It was shown that since H × H = A + G + 2H, there are two types of JT-active h displacements that influence the main features of the APES (in the first work on the H⊗h problem,[70] only one type of h displacement was considered). If you denote the two h distortions by H_a and H_b, then the corresponding JT stabilization energies from interactions with G, H_a, and H_b displacements can be denoted by $E_{JT}{}^G$, $E_{JT}{}^{Ha}$, and $E_{JT}{}^{Hb}$, respectively. The average value $E°$ is

$$E° = (4E_{JT}{}^G + 5E_{JT}{}^{Ha} + 5E_{JT}{}^{Hb})/14 \qquad (29)$$

(the coefficients stand for the corresponding degeneracy). Another parameter E' characterizes the difference in strengths of the two distortions

$$E' = {}^5/_{56}(4E_{JT}{}^G + 5E_{JT}{}^{Ha} - 9E_{JT}{}^{Hb}) \qquad (30)$$

Similar to the G⊗(g + h) problem, three types of stationary points on the APES were found in this approximation: pentagonal D_{5d}, trigonal D_{3d}, and two sets of D_{2h} points. If $E' > 0$, the D_{5d} points are minima, whereas the D_{3d} points are minima in case of $E' < 0$. The D_{2h} stationary points are always saddle points in this approximation: one set yields isolated points, while the other is situated on continuous curves in the phase space. Figure 22 illustrates the energy level splitting of the 5-fold degenerate H term in the two types of distortions that lead to pentagonal and trigonal minima.

Thus, despite their complexity, the icosahedral JT problems G⊗(g + h) and H⊗(g + h) are in fact reduced to two-mode problems when the interactions with one of the modes is independent of the interaction with the other one and they compete just in forming the absolute minima. This situation is similar to that of the T⊗(e + t_2) problem (in the linear approximation) where either tetragonal or trigonal minima occur dependent on the predominant coupling to either e or t_2 vibrations, respectively, while the intermediate orthorhombic extrema points are always saddle points (section II.B.3).

However, as stated above, in the T⊗(e + t_2) problem the quadratic terms of the vibronic coupling change the APES topology essentially. In particular, with quadratic terms included, the orthorhombic saddle points become minima and there are a variety of different types of coexisting minima.[1,58,59] To my knowledge, so far nobody has tried to include the quadratic vibronic coupling in the consideration of icosahedral problems. It can be expected that similar to the E⊗e, T⊗t_2, T⊗(e + t_2), etc., JT problems, the quadratic terms significantly alter the topology of APES, thus essentially influencing the tunneling splitting and other properties.

An interesting development in the JTE theory of these systems was reached when it was shown[80] that in the H⊗h problem with linear vibronic coupling, the vibronic ground state becomes nondegenerate for large enough values of the coupling constants. This result shattered the long-stayed belief that in JT problems the ground vibronic state has the same

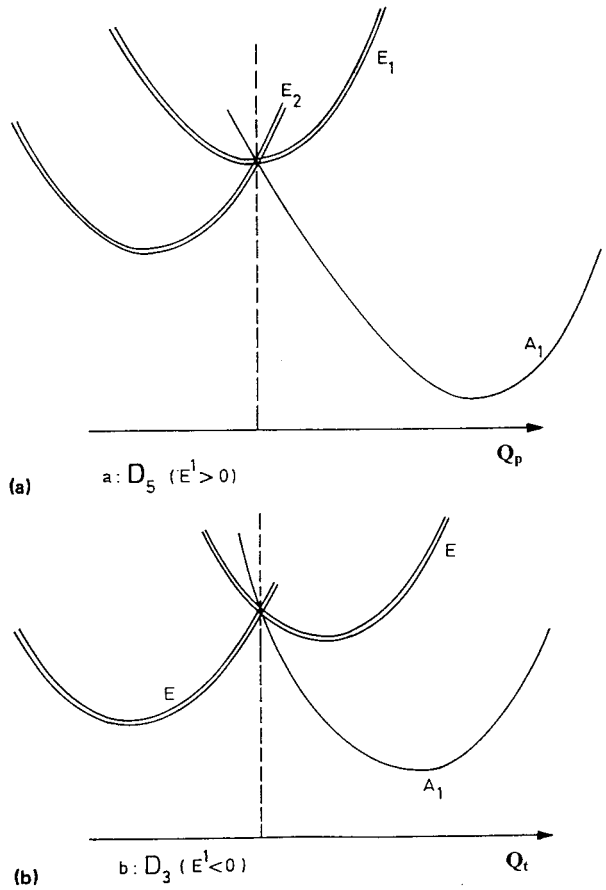

Figure 22. Splitting of the electronic 5-fold degenerate state under pentagonal Q_p (a) and trigonal Q_t (b) distortion coordinates in the linear H⊗(g + 2h) problem. (Reprinted with permission from ref 73. Copyright 1990 American Institute of Physics.)

symmetry and degeneracy as the initially degenerate electronic term. The ground vibronic level H is found indeed for small coupling constants. However, it crosses the next nondegenerate A level at larger couplings, the latter thus becoming the ground state. Somewhat similar to the situations in the E⊗e and T⊗t_2 problems, discussed above (sections II.B.1 and II.B.3), the H−A level crossover as a function of the vibronic coupling takes place because of the change of the lowest tunneling paths between the minima.

C. The Pseudo JT and Renner–Teller (RT) Effects

1. Pseudo-Jahn–Teller Effect

Among the vibronic coupling effects (JTE, PJTE, and RTE), the PJTE occupies a special place. The assumption that the vibronic coupling between the ground and excited states $W_{km}(Q)$ is sufficiently small and that the system of eqs 8 can be decoupled from the excited states is not valid in many cases. In general, the system of coupled eqs 8 should include the excited states to which the vibronic coupling is not small enough. *The effects originating from the vibronic mixing of two (or several) electronic states under nuclear displacements are called the pseudo-JT effect.* This notion comes from the two-level problem, ground and excited: sufficiently strong vibronic coupling to the excited state leads to the ground-state instability, which is similar to the JT instability. The effect as a whole can be regarded as emerging from avoided JT crossing.

Note that the term "second-order JT effect" sometimes used for this purpose may be misleading: *there are no first-order (JT) and second-order (PJT) effects*, the two effects are described by two different and independent vibronic coupling constants, and the pseudo-JT effect may be very strong when the proper JT effect is zero.

With the PJTE included, there are no a priori exceptions from the vibronic coupling effects and the presence of electronic degeneracy is just an important special case of vibronic coupling. Moreover, as shown earlier,[1,25,98,99] the smallness of the energy gap to the excited state is not a crucial condition of pseudo-JT instability of the ground state. For the simplest two-level problem of vibronic coupling (nondegenerate ground-state coupled to a nondegenerate excited state), the condition of pseudo-JT instability[1−3]

$$\Delta < |F_Q^{(1,2)}|^2/K_Q^{(0)} \tag{31}$$

involves, in addition to the energy semi-gap Δ, the vibronic coupling constant $F_Q^{(1,2)}$ after eq 6 (Q is the coordinate of distortion), and the primary force constant in the Q direction in the ground state (it is assumed that the first derivative $<1(\partial V/\partial Q)_0|1) = 0$)

$$K_Q^{(0)} = \langle 1|(\partial^2 V/\partial Q^2)_0|1\rangle \tag{32}$$

Numerical calculations[25,98,99] show that the inequality in eq 31 takes place even for very large Δ values (tens of eV) due to large vibronic coupling constants and/or small $K^{(0)}$ values.

A general expression for the force constant K can be obtained in the second-order perturbation theory as follow[100] (the subscript Q is omitted)

$$K = K^{(0)} + K^{(v)} \tag{33}$$

where $K^{(0)}$ is given above and

$$K^{(v)} = -2\Sigma_j |F_Q^{(1j)}|^2/\Delta_{1j} \tag{34}$$

For the ground state this expression for $K^{(v)}$, the vibronic contribution to K, is always negative; it stands for the partial "relaxation" of the electronic cloud to the displaced nuclei that lowers the force constant. If $|K^{(v)}| > K^{(0)}$, then $K < 0$ and the system is unstable with respect to Q displacements. Hence, the vibronic coupling to the excited state may produce the instability of the ground state, which is somewhat similar to the JT instability. However, distinguished from the latter, the selection rules for the matrix element $F^{(1j)} = \langle 1|\partial V/\partial Q)_0|j\rangle$ that determines the symmetry of the coordinate of instability Q may be quite different from the JT ones, in which the functions $|1\rangle$ and $|j\rangle$ are from the same degenerate term and span the same symmetry. In particular, for systems with inversion centers, the JT effect allows for even distortions only (no dipole moment formation) whereas the pseudo-JT effect may create both even and odd distortions.[3] Usually one to several excited states contribute significantly to the distor-

tion of the ground state in eq 34, and different excited states may contribute to different symmetrized distortions (see calculations in section III.E.1). There are other distinctions between a JT and pseudo-PJT effect.[1−3] In particular, while the JT distortions emerge due to uncompensated forces in the low-symmetry charge distribution in any of the degenerate states, the PJT distortion is due to the formation of new covalence in the low-symmetry configuration.[3,25]

Of particular interest is the case of combined JTE and PJTE. A widespread example emerges in many systems with relatively close-in-energy E and A states with the JTE in the E state plus the PJT mixing of the E and A states. For earlier solutions, see, e.g., refs 101 and 102; many other examples are cited in section III.

An important development of the pseudo-JT effect theory emerged when it was shown that the nonvibronic contribution $K^{(0)}$ to the force constant K is always positive,[1,98,99,103] $K^{(0)} > 0$. For high-symmetry systems, the proof of this inequality is based on some general properties of the second derivatives of Coulomb potentials V in eq 32 and on numerical calculations in other systems. If $K^{(0)} > 0$, then the inequality $K < 0$ can be obtained due to and only to $K^{(v)} < 0$ and $|K^{(v)}| > K^{(0)}$. In other words, if the polyatomic system in the high-symmetry configuration (when $\langle 1|(\partial V/\partial Q)_0|1\rangle = 0$) is unstable with regard to nuclear displacements Q (configurational instability), there should be excited states, the vibronic coupling to which causes this instability. In this presentation, *any configurational instability of polyatomic systems is of JT vibronic (JT, PJT, or RT) origin. The JT vibronic effects are thus the only source of instability of high-symmetry configurations.*

This conclusion may serve as a tool to the study of a variety of effects in molecules and crystals (section III). Qualitatively, the expected distortion of the ground state due to the vibronic coupling to the excited state may be determined directly from the symmetry properties of the mixing states: the symmetry of the expected distortions (its symmetrized coordinate Q) should be among those of the direct product of the symmetry representations of the two mixing states (otherwise $F_Q^{(12)} = 0$). However, only numerical estimates of the parameter values in the inequality in eq 31 allow one to check its validity and the possibility that the system becomes unstable with respect to Q displacements. If the inequality in eq 31 does not hold, the system will be just softened in the Q direction but not unstable. Computational issues with regard to eq 34 are discussed in ref 104. Section III provides many examples of applications of this general PJTE theory.

2. The Renner−Teller Effect (RTE)

As indicated above, linear molecules are exceptions from the JT theorem but they too are subject to similar instabilities in their degenerate or pseudo-degenerate states[1−3] called the Renner effect (after the first publication[105]) or Renner−Teller effect. The difference between JTE and RTE is in that the JTE in nonlinear molecules takes place in the first order of perturbation theory with respect to the linear vibronic coupling (eq 3) whereas for linear systems the linear coupling terms (linear in bending distortions) do not split the degenerate level and do not produce instability. However, in these systems the splitting and consequent instability takes place when quadratic and higher order terms of the vibronic coupling are included. The RTE theory, first suggested for a triatomic system[105] (see also ref 106), was afterward extended to four-atomic systems,[109] higher order interactions,[107,108] etc. For reviews of the RTE theory and applications, see, e.g., refs 1−3, 6, and 110−113 as well as section III.

D. Orbital Vibronic Coupling

For the sake of completeness of the picture of the most interesting aspects of the JTE and PJTE theory, especially with regard to useful applications in chemistry, the notion of *orbital vibronic coupling* presented by *vibronic molecular orbitals* (MO) and *orbital vibronic constants* should be mentioned.[3] The idea is that the vibronic coupling constant in eq 6 can be presented as a sum of MO contributions. Indeed, the operator of electron−nuclear (Coulomb) interactions in a system with n electrons $V(r,Q)$ is additive with respect to the electronic (and nuclear) coordinates, and hence, we can present it as

$$V(\mathbf{r},Q) = \Sigma_k V_k(\mathbf{r}_k) \tag{35}$$

where

$$V_k(\mathbf{r}_k) = -\Sigma_\alpha e^2 Z_\alpha/|\mathbf{r}_k - \mathbf{R}_\alpha| + (1/n)\Sigma_{\alpha,\beta} e^2 Z_\alpha Z_\beta/|\mathbf{R}_\alpha - \mathbf{R}_\beta| \tag{36}$$

Here the second, nuclear−nuclear interaction term is independent of the electronic coordinates, and it is divided between all the n electrons for convenience. Now, if the wave function of states $|\Gamma\rangle$ and $|\Gamma'\rangle$ in eq 6 are taken, for simplicity of proof, in an one-determinant presentation formed by one-electron MO $|i\rangle$ and $|j\rangle$, then we have[3] (cf. eq 6)

$$F_Q^{(\Gamma\Gamma)} = \sum_i q_i^\Gamma f_Q^{(ii)} \tag{37a}$$

and

$$F_Q^{(\Gamma\Gamma')} = f_Q^{(ij)}, \Gamma \neq \Gamma' \tag{37b}$$

where q_i^Γ is the occupancy of the ith MO in the Γ term and $f^{(ij)}$ is the linear orbital vibronic constant

$$f_Q^{(ij)} = \langle i|(\partial V_i/\partial Q)_0|j\rangle \tag{38}$$

and it is assumed that the excited state is formed from the ground one by the one-electron excitation $i \rightarrow j$.

In other words, in this approximation the (integral) vibronic coupling constants are an additive function of the orbital vibronic constants calculated by one-electron MO's with the one-electron potential operator V_k in eq 36. This presentation is useful in many applications where charge transfers change the JTE and PJTE (e.g., in chemical activation,[114,115] in spec-

tra of mixed-valence compounds,[116] in determining the intramolecular forces in molecules and crystals,[117] in calculation of vibronic coupling in superconductivity,[118] etc.)

E. Berry Phase Implications

An interesting development in this field, often called the Berry phase problem,[119] became widespread recently, although it emerged from the solution of the JT E⊗e problem long ago.[120] The phase problem in JT systems is directly related to conical intersections on the APES.[45−47,122−138] Conical intersection, as mentioned above, takes place in almost all JT systems. For one of the simplest problems, E⊗e (section II.B.1), it is illustrated in Figure 3.

Consider the electronic wave functions as a function of the nuclear coordinates for the linear E⊗e problem given by eqs 15, in the linear approximation $G_E = 0$ and $\Omega = \phi$. It can be easily shown that *these wave functions are not single-valued*: when moving at the bottom of the trough in Figure 3 along ϕ from $\phi = 0$ to $\phi = 2\pi$ (i.e., coming to the same starting point), the wave functions in eqs 15 change sign! Since the total wave function should be single-valued, a phase factor $e^{im\phi}$ should be attached to the electronic wave functions in eqs 15 (or to their nuclear counterparts) with half-integer values of m. In the case under consideration, the total wave function for the lower surface in the adiabatic approximation is[1−3]

$$\psi_{nm}(r,\rho,\phi) = \psi_{-}(r,\phi)\chi(\rho)e^{im\phi} \qquad (39)$$

$$E_{nm} = \hbar\omega_E(n + {}^1/_2) + m^2(\hbar\omega_E)^2/4E_{JT} - E_{JT} \qquad (40)$$

$$n = 0, 1, 2,...; m = \pm{}^1/_2, \pm{}^3/_2, \pm{}^5/_2,...$$

where $\chi_n(\rho)$ is the vibrational function.

Since the energy is a function of m^2, all energy levels, including the ground state, are doubly degenerate.

Thus, the singularity of the conical intersection produces a very strong effect, making the ground and excited states doubly degenerate (some of these degeneracies in the excited states are removed by quadratic coupling[1−3]). Berry[119] generalized this fact by showing that similar phase problems occur in many other physical circumstances and may lead to novel observable effects.

To illustrate some consequences of this phase problem, consider the equation of nuclear motions in the adiabatic approximation, i.e., when the total wave function can be presented as a product of the electronic and nuclear wave functions: $\Psi(r,Q) = \psi(r,Q)\chi(Q)$. Conventionally, a general expression for this equation for Q vibrations can be presented as follows[121]

$$[{}^1/_2M(-i\partial/\partial Q + A_Q)^2 + \epsilon(Q)]\chi(Q) = E\chi(Q) \qquad (41)$$

where in addition to the usual terms of the ordinary Hamiltonian a gauge potential A is added

$$A_Q = \int \psi^*(r,Q)(\partial\psi/\partial Q)dr \qquad (42)$$

If the electronic functions can be chosen (single-valued) and real, then $A = 0$ and eq 41 acquires its usual form for nuclear motions with the potential energy $\epsilon(Q)$. However, in the presence of conical intersections, the electronic function has an attached phase factor which makes it essentially not real and $A \neq 0$. On the other hand, the gauge potential A is nonzero in the presence of a magnetic field. Therefore, the implication of a conical intersection is equivalent to that of an additional magnetic field. *The conical intersection acts as a fictitious magnetic field that makes all the energy levels doubly degenerate*.

An important feature of the Berry phase implications in JT problems is that the peculiar phase factor that changes the sign of the electronic wave functions occurs only when one or an odd number of conical intersections are encircled while it retains the same sign if an even number (including zero) are encircled.[122] In fact, the phase factor is $n\pi$, where n is the number of conical intersections encircled; for $n = 0, 2, 4,...$, the sign of the wave function does not change.

With regard to the JTE theory, the Berry phase implications are most important in determining the ground-state vibronic energy levels. As shown above, in the E⊗e problem the quadratic vibronic coupling increases the number of significant conical intersections from one to four. Similar complications occur in the T⊗t_2 and other JT problems. In sections II.B.1, II.B.3, and II.B.4 the influence of the Berry phase factors on the ground vibronic (tunneling) energy levels are considered. In general, the Berry phase problem is presently developed into a separate trend with many applications to a variety of physical and chemical phenomena.[45−47,119,120,122−141]

III. Molecular Geometry and Spectra

Increased computer power allows for sufficiently accurate calculations of adiabatic potential energy surfaces (APES) of small to moderate molecular systems and determination of their absolute minima, which are necessary to determine the molecular geometry. In many cases and for many electronic states, ground and excited, the APES are rather complicated: there are several (equivalent) minima and they do not correspond to the high-symmetry configuration, which one may expect from a (general) classical point of view. Instead, complicated anharmonicity, conical intersections, and lines of conical intersections occur.

On the other hand, as it follows from the previous sections, the JT vibronic effects are the only sources of instability of high-symmetry configurations. Therefore, the vibronic effects may serve as a fundamental basis for understanding (rationalizing) the results of quantum-chemical computations. In this section we discuss many examples that illustrate this statement as well as experimental confirmation of various vibronic effects. Citing numerical data from different papers, we try to keep the form of presentation and units of the original work where possible.

A. Linear Configurations of Simple Molecules

For the purpose of vibronic coupling effects investigation it is convenient to classify the molecular systems on their reference high-symmetry configu-

ration,[1] i.e., on the configuration from which the JT, PJT, and RT distortions start. We emphasize that without a reference configuration there is no way to formulate the JT vibronic coupling effects. In this respect it is important to follow the terminology below: the electronic ground state in the high-symmetry configuration means the calculated ground state of the system when it is *fixed* in this configuration. If this state is degenerate, the nuclear configuration is unstable and the ground state of the stable (APES minimum) configuration may differ from the ground state of the reference configuration.

Obviously, in some cases the choice of reference configuration may be somewhat ambiguous. For instance, a strongly distorted flattened tetrahedron may be regarded also as a distorted square-planar configuration. The choice of the reference configuration in such cases may be conventional, but all possibilities should be tried.

In this section we consider molecular systems that are linear in the high-symmetry configuration but may be unstable with regard to RT and PJT bending.

1. Linear Triatomic Systems

The configurations of presumably linear triatomics have been of special attention to researchers beginning with the dawn of quantum mechanics (see refs 105−113 and 142 and references therein). According to the RTE theory (section II.C), the linear configuration of any molecular system is unstable with respect to bending if its electronic state is degenerate. This explains directly why the NH_2 radical is bent in the ground-state H−N−H configuration (one unpaired π electron forms a doubly-degenerate Π term in the linear configuration) and linear in the excited nondegenerate state. Similarly, AlH_2, BH_2, HCO, H_2O^+, NO_2, etc., are bent in the ground state and linear in the lowest excited state.[110,143,144] On the contrary, CO_2 is linear in the ground nondegenerate state and bent in the excited state.[105,145] The radical CH_2^+ is bent in the ground state and becomes linear upon light absorption.[146−148]

More recent numerical calculations[113] confirm the earlier qualitative assignments and allow one to predict the distortions quantitatively in agreement with experimental data. Ab initio calculations of the NH_2 radical[149] result in the unstable linear configuration in the degenerate $^2\Pi_u$ ground state and in the bent ground $^2B_1$ and excited $^2A_1$ states with angles H−N−H of 103° and 143°, respectively, in the stable configurations. Figure 23 illustrates the calculated bending potentials of these two states in comparison with that derived from spectroscopic data.[150]

For BH_2, the $^2\Pi_u$ state of the reference linear configuration is unstable too; the stable ground state $^2A_1$ is bent with an angle H−B−H of 129°, while the excited state $^2B_1$ is linear.[151] Several examples of ab initio calculation are given in Table 3. The C_3, NCO, and BO_2 molecules seem to be linear in the degenerate ground state, which may be explained by very weak RT coupling (calculations of vibronic coupling constants are not reported). The RT bending of the tetraatomic linear $C_2H_2^+$ [165] and $B_2H_2^+$ [166] radicals are considered based on the theoretical work[90] on four-atomic systems.

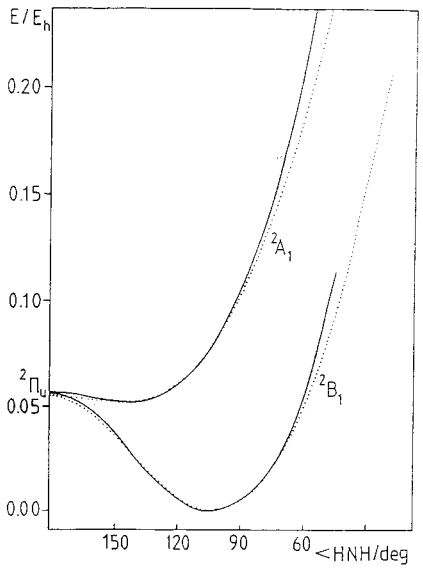

Figure 23. Comparison of ab initio calculated effective bending potential curves for the $^2B_1$ and $^2A_1$ states of NH_2 (solid lines)[149] with the counterparts derived by fitting experimentally observed vibronic band positions (dotted lines).[150] (Reprinted with permission from ref 113. Copyright 1995 Kluwer Academic Publishers.)

In free molecules, the RT-type distortions, similar to the JT ones, result in an essentially anharmonic APES which influence all the properties, first of all their spectra. However, the RTE is not the only source of bending of the linear configuration of molecules. Another important bending force arises from the PJT mixing of the electronic state under consideration with other states (of appropriate symmetry) under the bending distortion. Similar to other cases, bending configurations in linear molecules in nondegenerate states may occur as a result of the PJT effect. For a linear system, the bending displacements are of doubly degenerate Π symmetry. This means that if this system is in a nondegenerate Σ state, the bending may occur due to the vibronic coupling to the excited state of Π symmetry ($\Sigma \times \Pi = \Pi$), provided the coupling is strong enough and the inequality in eq 31 holds. The same is true for the PJT mixing of two excited states.

Although the bending produced by the PJT $\Sigma-\Pi$ mixing is geometrically the same, as in the RTE for degenerate terms, in fact these two distortions are somewhat different in nature and result in significant differences in the observable effects. In the PJT case there is an additional parameter Δ, the energy gap between the mixing states, which is significant in forming the APES (involving also the totally symmetric displacements[1]). Most important, the PJT distortions may be linear in the bending coordinate[167] whereas the RT ones are always quadratic. The result is that the APES in these two cases is different, the PJT one being more complicated because of anharmonicity and conical intersections.

Note that if the linear system with more than two atoms has a center of inversion, the PJT vibronic mixing between electronic states of opposite parity (i.e., Σ_g with Σ_u) may remove the center of inversion and form a dipole moment in the minima leaving the linear configuration intact. The RTE does not

Table 3. Calculated ab Initio Renner–Teller Distortions of Linear Configurations of Triatomic Molecules ABA and ABC[113]

system	linear ground state	stable state	∠A–B–A or ∠A–B–C	ref
BH_2	$^2\Pi_u$	$^2A_1$	129	151
		$^2B_1$	180	151
CH_2^+	$^2\Pi_u$	$^2A_1$	141	147, 148
		$^2B_1$	180	147, 148
CH_2	$^1\Delta_g$	$^1A_1$	103	152
		$^1B_1$	137	152
NH_2^+	$^1\Delta_g$	$^1A_1$	108	153
		$^1B_1$	155	153
NH_2	$^2\Pi_u$	$^2B_1$	103	149
		$^2A_1$	143	149
OH_2^+	$^2\Pi_u$	$^2B_1$	109	154
		$^2A_1$	180	154
AlH_2	$^2\Pi_u$	$^2A_1$	118	155
		$^2B_1$	180	155
SiH_2^+	$^2\Pi_u$	$^2A_1$	119	156
		$^2B_1$	180	156
PH_2	$^2\Pi_u$	$^2B_1$	91	157, 158
		$^2A_1$	122	157, 158
SH_2^+	$^2\Pi_u$	$^2B_1$	93	159
		$^2A_1$	128	159
HNO^+	$^2\Pi$	2A′	125	160
HNF	$^2\Pi$	2A″	101	161
		2A′	123	161
C_3	$^1\Pi_u$	$^1B_1$, $^1A_1$	180	162
NCO	2Π	2A′	180	163
BO_2	$^2\Pi_g$	$^2B_2$, $^2A_2$	180	164

produce this kind of dipolar distortion.

The study of PJT distortions in linear systems is at its beginning, although the first investigations were carried out more than two decades ago.[167] In this work the authors derived the general Hamiltonian of such $\Sigma-\Pi$ vibronic coupling in linear systems and applied it to the linear to bent transition in HCN and DCN to explain their photoelectron spectra. The solution of the PJT problem of vibronic coupling between the Σ and Π states with energies E_σ and E_π, respectively, including the two bending coordinates Q_x and Q_y ($\rho^2 = Q_x^2 + Q_y^2$) and one totally symmetric coordinate Q_g with frequencies ω and ω_g, respectively, yields the following three branches of the APES (in conventional units[167])

$$V_\pi = -E_\pi + {}^1/_2\omega\rho^2 + {}^1/_2\omega_g{}^2Q_g{}^2 + 2^{1/2}k_\pi Q_g \qquad (43)$$

$$V_\pm = -{}^1/_2(E_\pi + E_\sigma) + {}^1/_2\omega\rho^2 + {}^1/_2\omega_g{}^2Q_g{}^2 + 2^{1/2}(k_\pi + k_\sigma)Q_g \pm \{[{}^1/_2(E_\pi - E_\sigma) + 2^{1/2}(k_\pi - k_\sigma)Q_g]^2 + 2\lambda^2\rho^2\}^{1/2} \qquad (44)$$

where k_π and k_σ are the constants of vibronic coupling of, respectively, the Π and Σ states to the Q_g vibrations and λ is the constant of the $\Sigma-\Pi$ PJT coupling.

It is seen from these equations that one of the branches (V_π) is not affected by the bending while the distortion in the other two depends on the value of Q_g. Figure 24 illustrates this effect for the cationic states of HCN that are most important in the photoelectron spectra. For $Q_g = 0$ (note that this read-off of the totally symmetric coordinate is conventional) and $4\lambda^2 > |E_\sigma - E_\pi|$, the lower branch of the potential V_- is unstable at the point $\rho = 0$, which corresponds to the linear configuration. It has a continuum of minima forming a circle at the bottom of a trough at which the configuration of the system

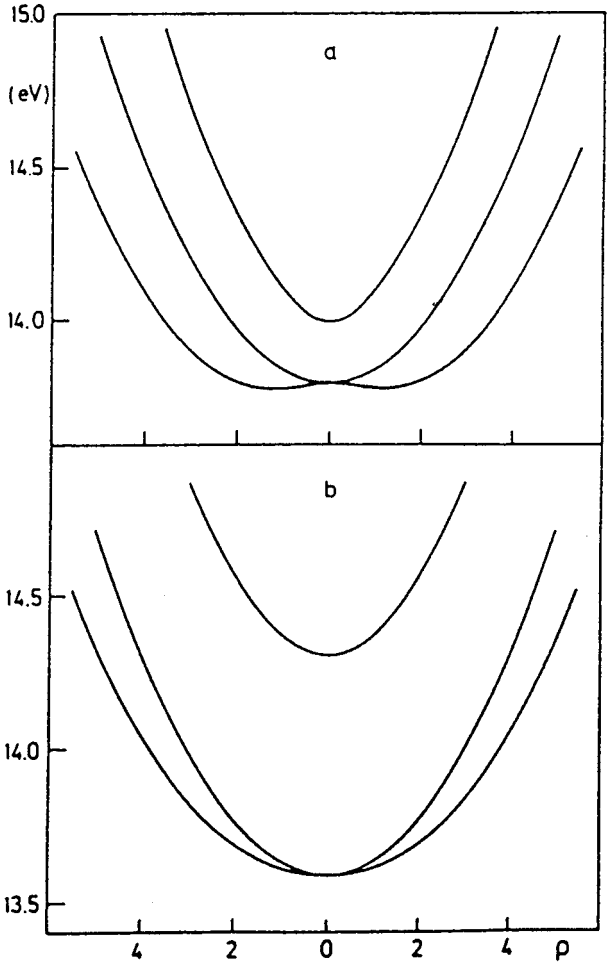

Figure 24. Adiabatic potential energy curves for the lowest cationic states of HCN as functions of the bending coordinate $\rho = (Q_x^2 + Q_y^2)^{1/2}$ for (a) $Q_g = 0$ and (b) $Q_g = -1.26$. The three curves represent (from top to bottom) V_+, V_π, V_- in eqs 43 and 44. (Reprinted with permission from ref 167. Copyright 1979 Elsevier Science Publishers.)

is bent. In the linear HCN molecule, the totally symmetric displacement Q_g involves H–C and C–N stretching, which play a significant role in the $\Sigma-\Pi$ PJT coupling and formation of the APES.

The two sets of curves in Figure 24 (a and b) should be regarded as two cross sections along the totally symmetric coordinate Q_g illustrating the complexity of the fully anharmonic APES in which the different kinds of vibrations are nonseparable. By means of numerical calculations taking into account this complex APES, the authors[167] succeeded in explaining the origin and vibronic structure of the first photoelectron band at 14 eV and the excitation band at ~9 eV. The RTE in the excited (cationic) Π state is also important, but by itself it cannot explain the origin of the vibronic structure of the spectra.

An interesting APES with a conical intersection in the excited state was obtained by electronic structure calculations of the HCO molecule.[168] Figure 25 illustrates a part of the complicated APES of this molecule. It confirms that conical intersections with consequent vibronic coupling effects take place more often than it seems at first sight. By means of numerical calculations carried out for the four lowest electronic states of HCO, the authors[168] explained the

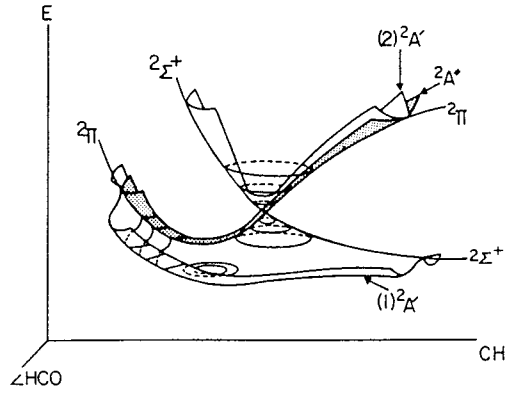

Figure 25. Schematic presentation of the APES of the lowest three states of HCO (the CO bond length is kept fixed). (Reprinted with permission from ref 168. Copyright 1979 American Institute of Physics.)

origin of several important features of this molecule. In particular, it was shown that the A bands in the hydrocarbon flame are due to electronic transitions from the strongly bent configuration of the $\tilde{B}^2A'$ state to the ground state $\tilde{X}^2A'$.

Further work on this radical may be found in refs 113 and 169−171. Ab initio calculations of ground and excited states confirm the presence of several conical intersections and avoided (PJT) crossing with bent configurations in the excited states due to the RTE and PJTE coupling. A full interpretation of the spectroscopic data for this system seems to remain a difficult task.

For the main APES features that determine the geometry, qualitative results can be obtained with much less effort than in the above-mentioned investigations. Consider, for example, the series of six molecular systems, two triatomics Ag_3 and I_3 and their positive (Ag_3^+, I_3^+) and negative (Ag_3^-, I_3^-) ions.[172] There are several works devoted to these systems in which theoretical calculations[173−176] combined with femtosecond spectroscopy[177,178] and X-ray measurements[179] allow one to conclude that Ag_3^- and I_3^- are linear while the neutral molecules and their positive ions are bent and have the configuration of mostly an isosceles triangle; Ag_3^+ is an equilateral triangle, while Ag_3 is not equilateral because of its degenerate electronic ground state resulting in the JTE (Figure 26, see also section III.B.1).

Starting with the high-symmetry linear configuration, one can determine approximately its electronic structure and estimate the numerical values of the PJTE parameters and the curvature of the adiabatic potential with respect to the PJT-active displacements.[172] The electronic structure of the linear configuration of all six systems under consideration was calculated[172] by means of the semiempirical extended Huckel method including self-consistency with respect to the atomic charges and electron configurations and the intramolecular electrostatic effects. The method itself is not very reliable when getting exact numbers to be compared with the experimental data. However, in the case under consideration, the question is about large effects of orders of magnitude which provide for a general understanding of the problem and allow one to make qualitative and semiquantitative predictions, especially when series of related systems are considered.

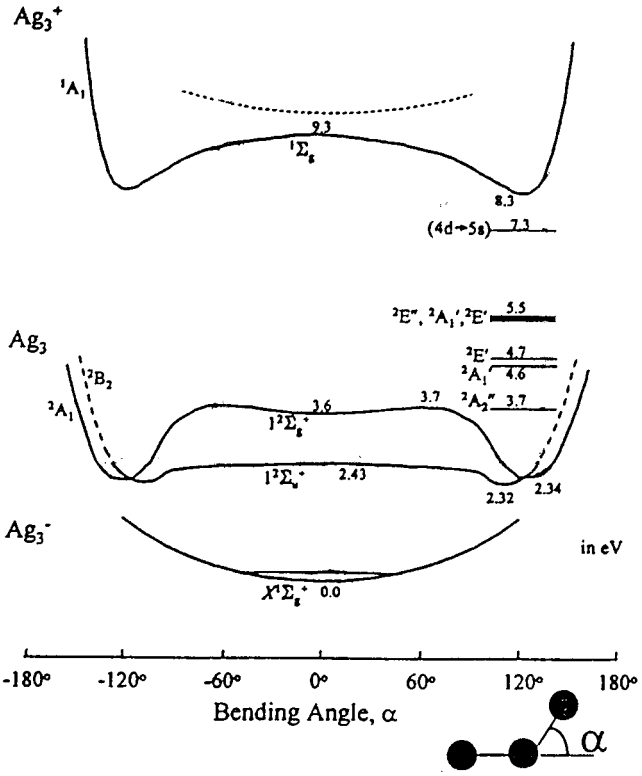

Figure 26. Schematic potential energy curves for Ag_3^-, Ag_3, and Ag_3^+ along the bending coordinate. The energies indicated are drawn form a multiplicity of sources and represent the best present knowledge of this system. (Reprinted with permission from ref 178. Copyright 1997 American Chemical Society.)

Table 4. Contributions of the PJT Coupling to the Excited States Π_u (formed by one-electron excitation $i \rightarrow \alpha$) in the Ground-State Force Constant for Ag_3^n Systems ($n = -1, 0, +1$)[a]

$i \rightarrow \alpha$	Ag_3^-	Ag_3	Ag_3^+
$3\alpha_g \rightarrow 2\pi_u$	−7.56	−6.87	−5.08
$2\sigma_u \rightarrow 3\pi_g$	−4.43	−1.44	
$1\pi_g \rightarrow 2\sigma_u$		−1.13	−1.72
$2\pi_g \rightarrow 2\sigma_u$		−0.42	−0.79
$K^{(v)} = \Sigma_i K_i^{(v)}$	−11.99	−9.86	−7.59
$K = K^{(0)} + K^{(v)}$	1.55	−0.47	−2.17

[a] All values are in mdyn/Å (from ref 172).

With the calculated MO's and taking the excited states as one-electron excitations $i \rightarrow \alpha$ from the occupied MO to the virtual one, the authors[172] estimated the constants of PJT vibronic coupling $F_Q^{(ij)}$ from eq 6, where Q is the bending coordinate and $|i\rangle$ and $|j\rangle$ are the ground and excited states, the primary force constant $K^{(0)}$ from eq 32, the vibronic contribution to the curvature of the adiabatic potential energy from eq 34, and the full curvature with respect to Q displacements (bending distortions). Some results are shown in Tables 4 and 5.

From Table 4, it can be seen that all the excited states that contribute to the bending of the linear configuration are of $\sigma \Leftrightarrow \pi$ type, which confirms the general explanation[1,3,25] of the origin of the PJT instability: in the linear configuration the overlap of σ and π orbitals is zero, while in the bent geometry this overlap becomes nonzero, thus producing additional covalent bonding. The two main vibronic contributions arising from the PJT mixing of the

Table 5. Contriburions of the PJT Coupling to the Excited States Π_u (formed by one-electron excitation $i \rightarrow \alpha$) in the Ground-State (A_g) Force Constant for I_3^n Systems ($n = -1, 0, +1$)

$i \rightarrow \alpha$	I_3^-	I_3	I_3^+
$1\pi_g \rightarrow 3\sigma_u$	−0.44	−0.38	−0.38
$1\pi_u \rightarrow 3\sigma_g$		−2.62	−4.96
$2\pi_u \rightarrow 3\sigma_g$		−0.58	−0.89
$K^{(v)} = \Sigma_i K_i^{(v)}$	−0.44	−3.58	−6.23
$K = K^{(0)} + K^{(v)}$	3.13	−2.71	−7.90

All values are in mdn/Å (after[172]).

ground state with two low-lying excited states Π_u (one formed by one-electron excitation $3\sigma_g \rightarrow 2\pi_u^*$ and the other formed by $2\sigma_u \rightarrow 3\pi_g$) decrease when passing along the series Ag_3^-, Ag_3, and Ag_3^+. The decrease of the former contribution is due to some increase of the energy gap between the ground and excited states, while for the latter it is due to the decrease of the occupation number of the $2\sigma_u$ MO (2 in Ag_3^-, 1 in Ag_3, and 0 in Ag_3^+). Note that these two main contributions come from the excited states associated with an electron density transfer from occupied σ- to the vacant π-orbital. For Ag_3 and Ag_3^+, significant contributions also come from the vibronic mixing to the two Π_u excited states formed by one-electron excitations from the occupied d shell to the $2\sigma_u$ MO ($1\pi_g \rightarrow 2\sigma_u$ and $2\pi_g \rightarrow 2\sigma_u$ excited states) which is partly occupied in Ag_3 and unoccupied in Ag_3^+. As a whole, the resulting negative vibronic contribution $K^{(v)}$ decreases from Ag_3^- to Ag_3^+ but more slowly as compared with the decrease of the positive $K^{(0)}$ values.

As a result, the value of the curvature of the ground-state adiabatic potential with respect to the bending displacements is positive for Ag_3^- and negative for Ag_3 and Ag_3^+ and the increase of instability along this series will be stronger when the contribution of the 5s electron density (which is omitted in the estimation of $K^{(0)}$) is taken into account. The not very large value of K for Ag_3 is in agreement with ab initio calculations of its APES, which yields the $^2B_2$ ground state and bent nuclear configuration in the minima.[173] The excited $^2\Sigma_u^+$ state with linear geometry is close in energy to the $^2B_2$ state, and the bent $^2B_2$ minima were found to be shallow.

For I_3, in contrast to the silver series, the negative vibronic contribution to the curvature increases in absolute value from I_3^- to I_3 and I_3^+ (Table 5). This is due to the fact that in I_3 and I_3^+ there are two new (as compared with I_3^-) excited π_u states for which the vibronic mixing to the ground state gives a significant contribution to the K value. These excited states are formed by one-electron excitations from the occupied $|\pi_u\rangle$ and $|2\pi_u\rangle$ MO's to the MO $|3\sigma_g\rangle$, which is singly occupied in I_3 and unoccupied in I_3^+.

Note that the vibronic mixing to the excited Π_u state formed by the one-electron excitation $1\pi_g \rightarrow 3\sigma_u$ which exists in all three iodine systems gives a relatively small contribution to the K value. Since, moreover, the positive nonvibronic contribution decreases in this series, the whole value of curvature K decreases essentially when passing from I_3^- (for which it is positive) to I_3 and to I_3^+ (for which it is negative). The contribution of the 5s-electron density at the nuclei omitted in the estimation of $K^{(0)}$ just increases all these values by approximately the same amount. All the excited states of π_u symmetry, active in the PJTE, are associated with an electron density transfer from occupied π to the not fully occupied σ bonds, which explains the new covalence bonding created by distortion.[1,3,25]

2. "Quasilinear" Molecules

We call the system quasilinear if it has a linear framework in the high-symmetry configuration with additional hydrogen atoms that make it nonlinear. This definition is conventional, suited here for JT vibronic coupling problems (see the remark at the beginning of section III.A), and it may not coincide with other definitions. An interesting example of combined JT and PJT effects in a simple seven-atom quasilinear system is the allene radical cation $C_3H_4^+$, the final state of photoelectron spectrum of allene. In its high-symmetry D_{2d} geometry, $C_3H_4^+$ has a 2-fold degenerate ground-state ^2E term, the next term being $^2B_2$.[180−183] The system has a total of 15 vibrational modes from which 11 modes, $3A_1 + B_1 + 3B_2 + 4E$, are JT and PJT active. Since $\{E \times E\} = A_1 + B_1 + B_2$, three totally symmetric A_1 plus four B type, $B_1 + 3B_2$, are JT active in the distortion of this system in its electronic ^2E state. The vibronic mixing of this latter with the first excited $^2B_2$ state takes place under E vibrations ($E \times B = E$). The authors[180] calculated the APES using a polarized valence triple-ζ basis set with MP2 perturbation theory for correlation effects and determined the linear vibronic coupling constants.

The numerical data for the constants of coupling to all the 11 types of vibrational modes and their vibrational frequencies are given in Table 6. It is seen that, as expected, the ^2E term is coupled to all the three A_1- and four B-type modes, while the four degenerate E modes participate in the PJT mixing of the ^2E and ^2B states. The JT distortions with regard to A_1 and B_2 displacements are illustrated in Figure 27. These results are essential for interpretation of the photoelectron spectra[180,181] and provide a nice demonstration of the importance of the PJTE in the spectra of even relatively small molecules such as allene.

Table 6. Constants of Linear Vibronic Coupling of the ^2E and $^2B_2$ States to A_1 Displacements ($k_A(^2E)$ and $k_A(^2B)$, respectively), the ^2E State to B-Type Displacements ($k_B(^2E)$), the $^2E \otimes ^2B_2$ Mixing ($k(^2E \otimes ^2B_2)$), and the Harmonic Vibrational Frequencies ω in Its Ground State $^1A_1$ for the 11 JT- and PJT-Active Modes ν_i, $i = 1, 2, ..., 11$, in $C_3H_4^+$ (all quantities in eV)[180]

	$\nu_1(A_1)$	$\nu_2(A_1)$	$\nu_3(A_1)$	$\nu_4(B_1)$	$\nu_5(B_2)$	$\nu_6(B_2)$	$\nu_7(B_2)$	$\nu_8(E)$	$\nu_9(E)$	$\nu_{10}(E)$	$\nu_{11}(E)$
$k_A(^2E)$	0.321	0.294	0.180								
$k_B(^2E)$				0.103	0.308	0.114	0.371				
$k_A(^2B_2)$	−0.165	−0.445	−0.005								
$k(E \otimes B_2)$								0.245	0.237	0.133	0.044
ω	0.3945	0.1846	0.1359	0.1110	0.2944	0.2529	0.1782	0.4055	0.136	0.1069	0.0446

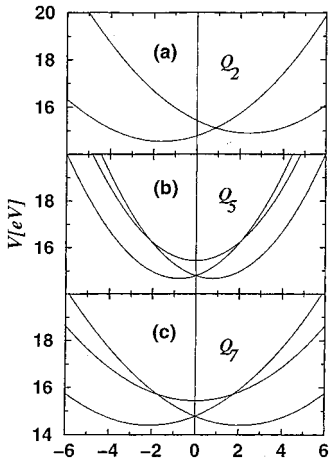

Figure 27. Potential energy of the $\tilde{A}^2E$ and $\tilde{B}^2B_2$ electronic states of the allene radical cation ($C_3H_4^+$) as a function of the dimensionless normal coordinates (a) Q_2 (A_1 symmetry), (b) Q_5 (B_2 symmetry), and (c) Q_7 (B_2 symmetry). The equilibrium geometry of allene in its electronic ground state ($^1A_1$) corresponds to $Q = 0$. (Reprinted with permission from ref 180. Copyright 1999 American Institute of Physics.)

Note that this molecule has D_{2d} symmetry in its ground state, in contrast to cumulenes with an even number of carbons which belong to D_{2h} symmetry. This seemingly small difference in symmetry is very important from the point of view of the JT and PJT effects: the D_{2d} molecules possess 2-fold degenerate electronic E states and e vibrations, whereas D_{2h} symmetry has no degenerate representations. However, the E states of the D_{2d} molecules do not interact with the e vibrations. Similar to D_{4h}, D_{4d}, D_{8h},..., groups, the JT active coordinates are b_1 and b_2 ($[E \times E] = A_1 + B_1 + B_2$) instead of e in trigonal and cubic groups (see section II.B.2), so the JT problem is $E \otimes (b_1 + b_2)$ instead of $E \otimes e$. However, the degenerate e vibrations may be very significant in PJT mixing of E terms with nondegenerate A or B states.

The final states in the photoelectron (PE) spectrum of allene are those of $C_3H_4^+$, which in the D_{2d} configuration has the ground term $\tilde{X}^2E$ followed by the terms $\tilde{A}^2E$ and $\tilde{B}^2B_2$ (formed by one-electron excitation from the 2e, 1e, and $3b_2$ valence orbitals, respectively), the latter two being rather close in energy. The PE band of transitions to the $\tilde{X}^2E$ state (around 10 eV) was shown to be JT active with respect to the b_1 vibrations (the $E-b_1$ problem),[184] but a more elaborate theoretical consideration[182,183] shows that one of the (three) b_2 vibrations is also involved significantly.

The spectrum produced by transitions to the $\tilde{A}^2E$ and $\tilde{B}^2B_2$ terms (the $\tilde{A}^2E/\tilde{B}^2B_2$ system) is more complicated. First, a small peak between the $\tilde{X}^2E$ band and the $\tilde{A}^2E/\tilde{B}^2B_2$ system at 12.7 eV, initially considered as a correlation peak, was reconsidered[181] and shown to (possibly) be due to the strong vibronic coupling between two excited states, the higher component of the JT split $\tilde{X}^2E$ state and the lower component of the $\tilde{A}^2E$ state that intersect at the dihedral angle of 144°, and a non Franck−Condon transition to this mixed state.

The $\tilde{A}^2E/\tilde{B}^2B_2$ system was subject to a much more elaborate investigation.[180] In a three-state vibronic

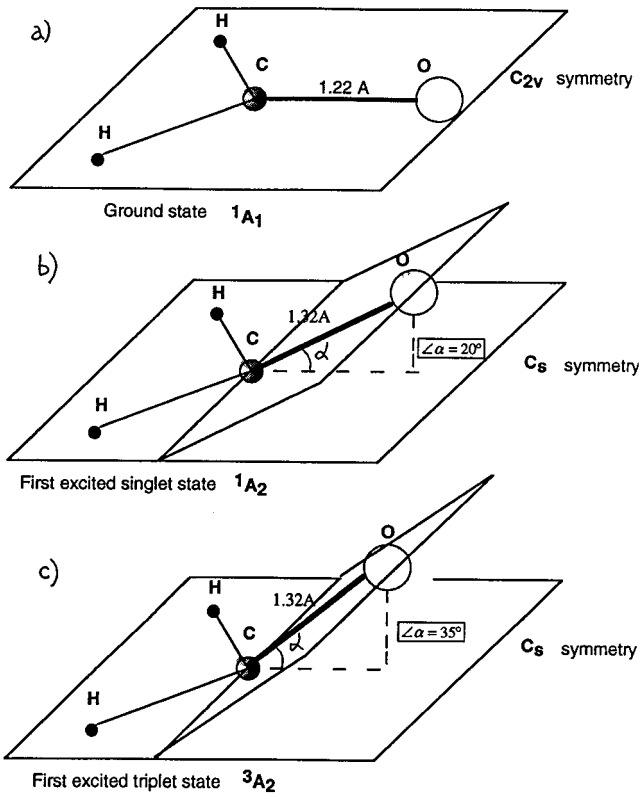

Figure 28. Geometry of H_2CO in the ground $^1A_1$ and first excited singlet $^1A_2$ and triplet $^3A_2$ states.

Hamiltonian, using the mentioned above ab initio determined vibronic coupling parameters and numerical calculations of the vibronic energy levels and transition probabilities they took into account both the JTE in the $\tilde{A}^2E$ state and the PJT coupling between this state and the $\tilde{B}^2B_2$ one by the degenerate e-type vibrations. The multimode (15 mode) problem was simplified by introducing effective modes (see also ref 1). The results explain this part of the PE spectrum and show that while the lower energy part of it follows relatively well the yield of earlier calculations of the $\tilde{A}^2E$ band as being due to the JT $E \otimes b$ coupling, the higher energy part of the spectrum is essentially determined by the PJT coupling between the $\tilde{A}^2E$ and $\tilde{B}^2B_2$ states which significantly affects both the vibronic energy level positions and the intensities of transitions. This part of the spectrum cannot be understood, even roughly approximate, without involving the PJTE.

Another example with another kind of PJT treatment is provided by formaldehyde in excited states. Formaldehyde H_2CO is planar in the ground state, but it is nonplanar in the two lowest excited states $^1A_2$ and $^3A_2$, and has an elongated C−O bond (1.32 Å instead of 1.2 Å in the ground state) with an angle between the C−O bond and the H−C−H plane of 20° in the $^1A_2$ and 35° in $^3A_2$ states[185] (Figure 28). The PJTE qualitatively and semiquantitatively explains the origin of these peculiar geometries.[186]

According to the theory (section II.C), the planar configuration of H_2CO in a given electronic state may become unstable with respect to the out-of-plane bending of the CO bond if (and only if) there are such excited (higher in energy than that under consider-

ation) states, the vibronic coupling to which is strong enough to produce the inequality in eq 31. To compare the instabilities of two excited states, singlet and triplet, a more detailed consideration of the interelectron interaction as it affects the parameters in eq 31 is given.[186]

In the single-transition approximation (STA), the excited singlet and triplet states are obtained by one-electron excitations $\alpha \rightarrow m$ from the occupied Hartree−Fock (HF) states to the corresponding unoccupied ones. In this approximation the energies $E^{s}_{\alpha\rightarrow m}$ ($E^{T}_{\alpha\rightarrow m}$) for singlet (triplet) excited states can be presented as follows

$$E^{s}_{\alpha\rightarrow m} = E_0^{HF} + \epsilon_m - \epsilon_\alpha + 2(m\alpha|m\alpha) - (mm|\alpha\alpha) \quad (45)$$

$$E^{T}_{\alpha\rightarrow m} = E_0^{HF} + \epsilon_m - \epsilon_\alpha - (mm|\alpha\alpha) \quad (46)$$

where E_0^{HF} is the HF ground-state energy, ϵ_m and ϵ_α are the one-electron energies in unoccupied (m) and occupied (α) MO's, respectively, and $(ij|kl)$ are the usual interelectron interaction integrals calculated with the one-electron MO's. The Greek and Latin letters are used here to denote, respectively, occupied and unoccupied MO's in the ground HF state.

Passing from integral vibronic constants F to *orbital vibronic constants*[3] (see section II.D)

$$f_\Gamma^{(ij)} = \langle i|(\partial V(r)/\partial Q_\Gamma)_0|j\rangle \quad (47)$$

where $V(r)$ is the one-electron component of the electron−nuclear plus nuclear−nuclear interactions (see eqs 35 and 36), the authors[186] find directly for the diagonal vibronic constants (eq 37a)

$$F_Q(\alpha \rightarrow m) = f_Q^{(mm)} - f_Q^{(\alpha\alpha)} \quad (48)$$

The off-diagonal contributions to the force constant in the singlet state are

$$K_\Gamma(^1A_2) = -2|f^{mn}|^2/[\epsilon_n - \epsilon_m + 2(K_{n\alpha} - K_{m\alpha}) - (J_{n\alpha} - J_{m\alpha})] \quad (49)$$

while for the triplet states

$$K_\Gamma(^3A_2) = -2|f^{mn}|^2/[\epsilon_n - \epsilon_m - (J_{n\alpha} - J_{m\alpha})] \quad (50)$$

Here $K_{m\alpha} = (m\alpha|m\alpha)$ denotes the exchange integral (not to confuse with the force constant) while $J_{m\alpha} = (mm|\alpha\alpha)$ is the Coulomb integral.

In the case of configuration interaction with single and double excitations, these expressions are modified accordingly and become linear combinations of the configurations involved.[186]

The calculation of the excited singlet and triplet states of H_2CO for the planar configuration were performed with a simple basis set STO-6G which proved to be satisfactory for this problem. In the ground state, the molecule is planar with C_{2v} symmetry and the following interatomic distances are found, R(C−O) = 1.216 Å, R(H−H) = 1.8497 Å, R(C−H) = 1.093 Å, and R(O−H) = 2.0308 Å. With this symmetry, the numerical data for the one-electron MO energy levels and wave functions were obtained.

The CI included all the configurations produced by single and double excitations form the HOMO $2b_2$ to the lower four MO $2b_1(\pi_2^*)$, $6a_1(\sigma_2^*)$, $3b_2$, and $7a_1$ that remain unoccupied in the ground state; higher MO's are neglected. The energies and wave functions of the excited singlet and triplet states obtained in the STA and CI approximations show that the lowest excited singlet $^1A_2$ and triplet $^3A_2$ states are mainly formed by the electron excitation from the HOMO $2b_2(n_{2p}O)$ to the LUMO $2b_1(\pi_2^*)$, while the next excited states may be more implicated in the CI approximation.

With these data, using eqs 45−50 above, the ratio $K_{B1}(3A_2)/K_{B1}(^1A_2)$ of the PJT contributions to the instability of the planar configuration (B_1 distortions) in the exited states $^1A_2$ and $^3A_2$ was estimated as being approximately equal to 1.20 in the STA approximation and 1.31 in the CI approximation.

Thus, the essentially nonplanar geometry of the formaldehyde molecule in two excited states, singlet $^1A_2$ and triplet $^3A_2$, as compared with the planar configuration in the ground state is due to the vibronic PJT mixing of these states with higher excited states of appropriate symmetry: $^1B_2(2b_2 \rightarrow 6a_1)$ and $^1B_2(2b_2 \rightarrow 7a_1)$ and $^3B_2(2b_2 \rightarrow 6a_1)$ and $^3B_2(2b_2 \rightarrow 7a_1)$, respectively. This vibronic coupling produces the B_1 distortion of the planar configuration as predicted by the general theory. It is shown also that the elongation of the C−O bond in the excited A_2 states as compared with the ground state is due to the change of the corresponding diagonal orbital vibronic constants in eq 48 resulting from the one-electron excitation.[186]

B. Trigonal Molecular Systems

1. Triatomics X_3

Equilateral triangular triatomics X_3 are the simplest systems with a 3-fold axis of symmetry that allow for 2-fold degenerate E terms, ground or excited. In these states, if the only linear coupling is taken into account, the JT distortions result in the Mexican-hat-type APES with a conical intersection in the center (section II.A.1, Figure 3). With the quadratic coupling terms included, the APES acquires three equivalent minima becoming a "tricorn" (section II.A.1, Figure 4); at each of these minima the equilateral triangle is distorted to an isosceles one.

For triangular H_3, the topography of the APES was shown[187] to have these "tricorn" features with instability and dissociation to H_2 + H along the three minima (see also refs 188−193 and references therein). The presence of the upper branch of the Mexican hat and the Berry phase factor (section II.D) essentially influence the reactive scattering process of this system and its isotopomers.[194−196] Since triangular H_3 is stable in some excited states, most important are the implications of this topography in the emission spectra.

The optical emission spectra of Rydberg-excited (n = 3) H_3 and D_3 was calculated[194−196] taking into account the JTE in the ground state (2p)1E′. In the excited-state components (3d)1E″ and (3d)3E′ (separated by about 200 cm^{-1}), which give the largest

Table 7. Some Numerical Data for Li_3, Na_3, and K_3 in Their Minima (obtuse triangular) and Saddle-Point (acute triangular) Configurations (from 197)

extrema	parameter	Li_3	Na_3	K_3
minima	D_e	0.64	0.38	0.38
	R	5.3	6.0	7.5
	θ	73	80	77
saddle point	D_e	0.64	0.35	0.36
	R	5.1	5.8	7.2
	θ	52	50	41

[a] R is the smallest interatomic distance (in a.u.), D_e is the dissociation energy (in eV), and θ is the apex angle (in degrees).

contribution to the spectrum, the JTE is very weak and hence the emission band shape is expected to be "two-humped"[1−3] due to the JT APES in the ground state. Using the time-dependent wave packet method and the vibronic coupling theory, the authors[194] calculated the expected emission spectra in good agreement with the experimental data.

The alkali trimers Li_3, Na_3, and K_3 are stable and possess an electronic ground-state E term in the regular triangular configuration. Quite a number of papers are devoted to the JTE in these systems (see refs 197−216 and references therein). The first calculations of their APES beyond the HF approximation were carried out in the DFT approach (LSD approximation) using pseudo-potentials for the contribution of core electrons[197] (see references in ref 197 for earlier attempts). In all three cases the equilateral triangular D_{3h} configuration is unstable with a conical intersection in this point (as in Figures 3 and 4 in section II.A) and extrema points at the three obtuse (isosceles with the apex angle larger than 60°) and three acute triangles.

In Li_3, all these extrema points have approximately the same energy, so there is a trough along which the system performs free rotations (more precisely, pseudo-rotations) as illustrated in Figure 5 (section II.A.1). This means that the quadratic coupling is very weak to negligible (at least in this approximation of the calculations). For Na_3, the obtuse configurations are minima while the acute ones are saddle points that form a potential barrier between the minima of about 1kcal/mol. The K_3 system APES is qualitatively the same as that in Na_3 with some different interatomic distances and angles in the distorted triangle. The ionized systems, the cations, Li_3^+, Na_3^+, and K_3^+, are regular triangles in the ground state, as expected for the nondegenerate electronic states.

Some numerical data for alkali X_3 geometry are given in Table 7. Vibronic coupling constants and other JT parameters estimated based on the APES geometry and spectroscopic data are given in Table 8 for several of the systems with a 3-fold axis of symmetry and an electronic degenerate E state discussed below in this and later sections. They include the dimensionless JT stabilization energy $D = E_{JT}/h\omega_E$, the vibronic coupling constants k and g (section II.B.1, eqs 19 and 20), as well as the JT-active ω_E and totally symmetric ω_A vibrational frequencies, where available. Because of the complicated topology with conical intersections, minima, and saddle points and approximations used in their evaluation, not all data in this table seem to be sufficiently reliable.

Among the triangular JT X_3 systems, Na_3 is the most studied both theoretically and experimentally. The reason is in its relatively simple electronic structure and existence in the vapor phase that allows one to use jet-cooled supersonic beam expansion and optical−optical double resonance with high-resolution resonant two-photon ionization techniques.[200] This molecule may be regarded as a probe system serving to better understand the implications of the JT and PJT effects which can be used as a base for the treatment of more complicated systems.

To explain the high-resolution two-photon ionization spectrum of Na_3, the authors[200] attributed the so-called B band (600−625 nm) to transitions to the excited electronic state, which is an E state too. Figure 29 illustrates their identification of the spectral lines. From the experimental spectrum we see, first, a long progression composed of nearly equally spaced doublet lines at $\omega_\rho \approx 128$ cm^{-1} which can be attributed to the higher frequency radial vibrations in the trough along the ρ coordinate (section II.B.1, Figures 3 and 4, eq 19b), plus a series of more closely spaced lines that represent the pseudo-rotation energy levels. A series of weaker lines was attributed to the totally symmetric harmonic vibrations with $\omega_a = 137$ cm^{-1}. Ignoring the latter and considering the pseudo-rotations to be free rotations (i.e., neglecting the energy barrier between the minima along the ϕ coordinate), these energy levels may be approximated by the following equation

$$E_{n,j} = (n + {}^1/_2)\omega_\rho + Am^2 \qquad (51)$$

where n is the quantum number of the high-frequency ω_ρ vibrations, $A = h^2/2I$ is the constant of internal rotations with the moment of inertia $I = M\rho_o^2$, M is the reduced mass of Na_3, ρ_o is the distortion amplitude (see eq 19b), and m is the half-integer quantum number that emerges from theoretical treatment (eq 40).

By fitting the experimental line positions with this formula and with the constants of the Hamiltonian, eq 20, the authors[200] got a reasonable estimation of the constants of the JT linear coupling, $k = 4.04$, and quadratic coupling, $g = 0.012$, the JT stabilization energy $E_{JT} = 1050$ cm^{-1}, the barrier between the minima $\delta = 26$ cm^{-1}, and the tunneling splitting $\Delta E \approx 3-5$ cm^{-1}. The authors claim that these results are the first manifestation of the half-integer quantum numbers for the pseudo-rotation in the exited state of Na_3 predicted by the theory (section II.E, eq 40).

However, this identification of the B band in the Na_3 spectrum has been contested in a series of consequent papers.[204,208,209] First, ab initio calculations by the GVB CI method[201] revealed that the linear vibronic coupling in the excited $^2E'$ state is weak but there is a very close in energy $^2A_1$ state above the $^2E'$ state which affects essentially the electronic transition to the latter (the E−A energy gap $\Delta \leq 100$ cm^{-1}). The pseudo-JT $^2E-{}^2A_1$ mixing of these two states (see section II.C) was fully considered in ref 208 with the result that the origin of the

Table 8. Dimensionless JT Stabilization Energies $D = E_{JT}/\hbar\omega_E$, Linear k and Quadratic g Vibronic Coupling Constants, and Frequencies (in cm^{-1}) of E-Type and Totally Symmetric A-Type Vibrations for the JT E⊗e Problem in Some Small Molecules with a Three-Fold Axis of Symmetry

system	$D = E_{JT}/\hbar\omega_E$	k	g	ω_E	ω_A	ref
Li_3	1.92	1.96 ± 0.33	0.22 ± 0.07	278 ± 61		214
Li_3	2.53	2.25 ± 0.24	0.14 ± 0.06	250 ± 41		197
Na_3	4.50	3.00 ± 0.08	0.20 ± 0.03	97 ± 5		199
Na_3	7.56	3.89 ± 0.22	0.21 ± 0.06	98 ± 9		197
K_3	21.98	6.63 ± 2.48	0.44 ± 0.53	34 ± 11		197
$Cu_3(^2E')$	2.27	1.86	0.223	137	269.5	221
$Cu_3(^2E')$	2.48	2.23	0.154	224		217
$Cu_3(X^2E')$	11.99	4.90 ± 1.41	0.35 ± 0.19	94 ± 27		219
$Cu_3(X^2E')$	1.22	1.56	0.274	132	270	198
$Cu_3(^2E'')$	0.04	0.273	0.127	138.7		198
$Ag_3(^2E')$	1.86	1.93	0.25	99	121	227
$Ag_3(^2E')$	3.72	2.73		134		218
$Ag_3(^2E'')$	0.02	0.19	0.02	96	158.2	227
$Ag_3(A^4E')$	0.29	0.757	3.86	61.9	179.7	230
VF_3	0.306	0.78	0.044	784	692	233
$C_3H_3^-$	2.10	2.04 ± 0.04	0.02 ± 0.02	1410 ± 51		238
$C_3(CH_2)_3$	3.79	2.75 ± 0.03	0.04 ± 0.01	701 ± 13		241
MnF_3	3.10	2.490	0.896	810	758	234

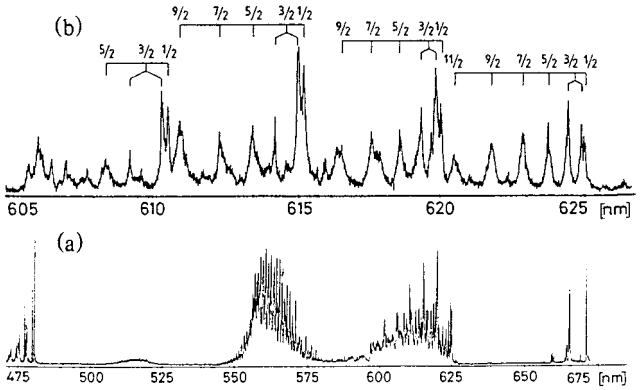

Figure 29. (a) Resonant two-photon ionization spectrum of Na_3 in the visible region. Spectra in different regions are not rigorously normalized to variation in dye laser parameters. (b) Expanded spectrum of the region 600−625 nm. State labels correspond to assignment given in ref 200. (Reprinted with permission from ref 200. Copyright 1986 American Physical Society.)

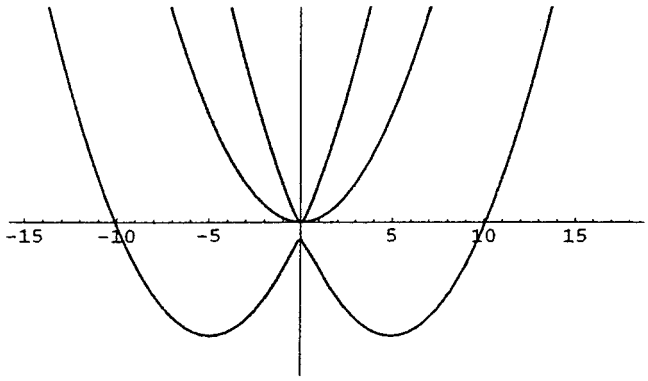

Figure 30. Schematic presentation of the cross section of the APES in case of a E−A PJTE along one of the E coordinates (quadratic terms are neglected). The whole APES is cylindrically symmetrical and allows for free pseudo-rotation of the distorted configuration.

individual transitions in the B series should be reconsidered. The authors[208] solved the combined problem for two models: (1) JT model in which the PJT E−A coupling constants, linear λ and quadratic f, are neglected and (2) PJT model in which the JT coupling is neglected ($k = g = 0$) (in both cases the E−A energy separation $\Delta = 0$). By fitting the first 19 energy levels to those observed experimentally, it was shown that the PJT model with $\lambda/\omega = 3.07$ and $f/\omega = 0.0045$ ($\omega = 127$ cm^{-1}) is considerably better than the JT model (the root-mean-square error in the former is 1.7 cm^{-1} as compared with 2.3 cm^{-1} in the latter).

The lowest branch of the APES in this PJT system in the space of the two E type vibrations is a trough, similar to the JT E⊗e problem one, but with a different behavior at the intersection (Figure 30). Hence, there are pseudo-rotations along the bottom of the trough. If we neglect the rather weak quadratic PJT coupling ($f = 0$), the energy levels follow the equation[208]

$$E_{n,j} = (n + {}^1/_2)\omega_\rho - (\lambda^2/\omega) + (\omega^3/4\lambda^2)j^2 \quad (52)$$

where λ is the PJT linear coupling constant and $j = 0, 1, 2,...$, is the quantum number of the free pseudo-rotation which, distinct from the JT case, is an integer: in the PJTE there is no wave function sign change upon encircling the origin and no superimposed condition of half-integer j values, no fractional quantization.

The PJT model was confirmed by more elaborate calculations of the relative intensities of the individual lines in comparison with the experimental values. To get the vibronic states, the ground electronic state E′ data were re-estimated for the best fit to the APES and then refined for the PJT spectrum. The obtained parameter values are $k = 5.350$, $g = 0.076$, $\omega_\rho = 82.2$ cm^{-1}, $\omega_\phi = 49.7$ cm^{-1}, and $\delta = 199$ cm^{-1}. The comparison of intensities obtained in the JT and PJT models confirm, again, that the latter fits the experimental data better.

An even more unambiguous experimental confirmation of integer (not fractional) quantization of the vibronic energy levels in the excited state of the B site of the Na_3 spectrum was obtained from the analysis of the rotational structure of and Coriolis interaction in the spectral bands.[204] For a triangular X_3 (symmetric top) molecule, the rotational energy

is given by the following approximate expression[142]

$$E = BJ(J+1) - (B-C)K_c^2 \pm 2C\zeta K_c \quad (53)$$

where B and C are the rotational constants (the C axis is perpendicular to the X_3 plan), J and K_c are the rotational quantum numbers of a symmetric top, and the last term describes the Coriolis interactions with the Coriolis constant ζ. For strong JTE or PJTE, the effective Coriolis constant can be taken to be equal to the quantum number of pseudo-rotation j.[142]

It emerges from eq 53 that the Coriolis splitting for different K_c values and integer j values will differ essentially from those for half-integer j. Moreover, the ground vibronic state with $j = 0$ should not be split by the Coriolis interaction whereas is should be split in the state with fractional quantization where $j = 1/2$. The analysis of the high-resolution rotational structure of the optical transitions[204] confirms the integer quantization model. For $j = 0$, only one P and one R branch of nonsplit lines are observed, while for nonzero j values, both the P and R lines are split, the splitting being approximately equal to $4CK_cj$. A total of 106 transitions for $n = 1$, 2 and $j = 0$, 1, 2, 3, 4, and 5 were assigned in this way. This assignment based on rotation and pseudo-rotation interaction (rovibronic coupling) was further refined taking into account more sophisticated theoretical consideration[209] and the influence of quadratic coupling which makes the pseudo-rotation not free but hindered.

With these works the spectrum of the Na_3 system gets one of the most detailed interpretations known so far for JT and PJT systems.

Another detailed interpretation of high-resolution spectra with essential JT implications has been performed on Li_3.[211,212] This molecule is similar to Na_3 but has less electrons (meaning advantages in ab initio calculations) and a smaller mass (meaning a larger rotational constant that allows for a better resolution of the rovibronic transition single lines). The authors used two-photon ionization of $^{21}Li_3$ with continuous wave lasers and mass-selective detection of Li_3^+ to record rotationally resolved spectra of the electronic $A^2E'' \leftarrow X^2E'$ transition. The spectra were analyzed by optical double-resonance techniques in combination with accurate ab initio calculations of the APES and rovibronic energy levels of both electronic states. The APES of the E state was shown[212] to have the JT stabilization energy $E_{JT} = 502$ cm^{-1} and the barrier between the minima $\delta = 72$ cm^{-1} in the $\tilde{X}(1^2E')$ electronic state yielding a ground-state tunneling splitting of $\Delta E = 36$ cm^{-1}, while in the $\tilde{A}(1^2E'')$ state $E_{JT} = 787$ cm^{-1}, $\delta = 156$ cm^{-1}, and $\Delta E = 5$ cm^{-1} (for Na_3 the tunneling splitting for these two states are 9.017 and 0.003 cm^{-1}, respectively[211,215]). The ΔE values give the splitting between the lowest E and next A pseudo-rotation states.

Using an effective rovibronic Hamiltonian,[216] the authors[212] analyzed the rotational structure of the rovibronic spectra and, after a series of corrections, reached an accuracy of 0.001cm^{-1}. The results confirm that the ground vibronic state is E in accordance with the Berry phase requirement and the rovibronic

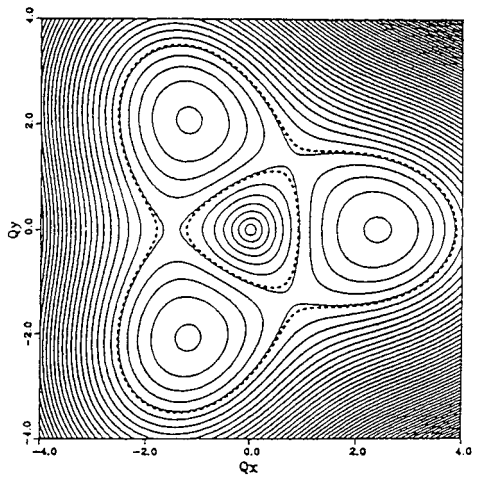

Figure 31. Lower APES for the $^2E'$ state of Cu_3 obtained from the experimental spectra.[221] Contour spacing equals 27.4 cm^{-1}. Dashed contours correspond to the classical turning points of the zero-point level. (Reprinted with permission from ref 221. Copyright 1986 American Chemical Society.)

energy levels are described well by an effective pseudo-rotation Hamiltonian with five parameters: three rotational constants for the system in the minimum C_{2v} configuration plus the vibronic and Coriolis coupling constants.

For Cu_3, calculations[198,217−220] yield a Mexican-hat-type APES in the ground state with three minima and three saddle points in accordance with general theory (section II.B.1). At the minima, the configuration Cu1−Cu2−Cu3, similar to the alkali metals, is an obtuse isosceles triangle: $R(1-2) = R(1-3) = 4.474$ au, $R(2-3) = 5.035$ au. At the saddle points the triangle is acute: $R(1-2) = R(1-3) = 4.753$ au, $R(2-3) = 4.383$ au.[217,218] The JT stabilization energy is estimated as $E_{JT} = 555$ cm^{-1} with a barrier between the minima $\delta = 171$ cm^{-1}. In another estimation,[220] $E_{JT} = 280$ cm^{-1} and $\delta = 59$ cm^{-1}.

The parameters of the APES can also be determined from comparison of the vibronic energy level positions with those extracted from absorption, emission, two-photon ionization, and photoelectron spectra.[198,217,221,222] In particular, by fitting the calculated energy levels obtained from numerical diagonalization of the Hamiltonian (eq 20), the authors[221] obtained the APES shown in Figure 31 with the numerical values of the linear vibronic coupling constant $k = 1.86$, $g = 0.223$, and $\omega_E = 137$ cm^{-1} in the D_{3h} configuration (the totally symmetric vibration frequency is estimated as $\omega_A = 269.5$ cm^{-1}). Using more accurate relations between these parameters than in section II.B.1, they estimated the JT stabilization energy $E_{JT} = 305$ cm^{-1} and the barrier between the minima $\delta = 111$ cm^{-1}. With the zero-point vibrations at 118 cm^{-1}, the authors[221] concluded that there are no localized states in the minima in this system and the JT distortions perform hindered pseudo-rotations along the bottom of the trough of the Mexican hat.

The strong JT distortions in the ground state $^2E'$ of the copper trimer Cu_3 (Figure 31) and its obtuse triangular configurations in the C_{2v} minima was confirmed by the ESR measurements of copper

isolated in an adamantane matrix.[223] The spin density was found to be localized mainly on the two terminal atoms. However, the interpretation of the nature of the excited state that participates in the electronic transition observed at 5397Å in two-photon ionization and fluorescence[224,225] was subject to controversial discussion.[222] The first assignments of this spectrum as due to $^2E'' \longleftrightarrow {}^2E'$ transitions was questioned[222] based on a more detailed comparison with the $^2A_1' \leftarrow {}^2E'$ transition in the fluorescence spectrum, especially on the selection rules for vibronic transitions from the vibrationally excited $^2A_1'$ levels. More work on intensities may be useful to further elucidate this problem.

The APES of Ag_3 in the ground state is similar to that of Cu_3. Ab initio calculations[218] (see also refs 226 and 227) show that at the minima the regular triangle configuration is distorted to an obtuse isosceles triangle, $R(1-2) = R(1-3) = 5.119$ au and $R(2-3) = 5.810$ au, while at the saddle points the triangle is acute, $R(1-2) = R(1-3) = 5.452$ au and $R(2-3) = 5.054$ au, with $E_{JT} = 498$ cm^{-1}, $\delta = 108$ cm^{-1}, and $\omega_E = 134$ cm^{-1}. The corresponding vibronic constants together with data obtained by other authors are listed in Table 8.

The absorption spectrum of Ag_3 was interpreted[228] as being due to the electronic transitions $^2E'' \leftarrow {}^2E'$ with a strong JTE in the ground state $^2E'$ ($k = 1.93$, $g = 0.25$) and a much weaker JTE in the excited state $^2E''$ ($k = 0.19$, $g = 0.02$). These parameters give a good fit of the calculated vibronic level positions with those observed experimentally in the lower part of vibrational energies. However, at higher energies the calculations predict fewer bands than observed. The authors[228] assume that inclusion of spin–orbital interactions quenched by vibronic reduction factors[1-3] may resolve the problem. No full calculations of this kind have been performed so far.

In the series of Ag_3^-, Ag_3, Ag_3^+ discussed above (section III.A.1), the first system, Ag_3^-, is linear, Ag_3 is a JT distorted triangle, while Ag_3^+ is a regular triangle (Figure 26). This sequence of configurations was confirmed by experimental studies of ultrafast dynamics using a charge reversal technique based on femtosecond spectroscopy.[178] It can be understood qualitatively by means of JTE-based argumentation: Ag_3^+ has a nondegenerate ground state and remains in a regular triangle configuration, while in Ag_3 the additional electron occupies the 2-fold degenerate $^2E'$ state in the triangular configuration resulting in the JT distortion with an obtuse triangle and the electronic state $^2B_2$ at the APES minimum. The next electron in Ag_3^-, if occupying the same E′ orbital, enhances the distortion of the triangle resulting in a more stable linear configuration in the state $^1\Sigma_g'$.

For Au_3,[226,227,229-231] in the ground state $^2E'$ the APES is qualitatively similar to Cu_3 and Ag_3 but the quadratic coupling is very weak,[229] $E_{JT} = 561$ cm^{-1} and $\delta = 45$ cm^{-1}, so the system is assumed to perform almost free pseudo-rotations. The distortions at the minima are $R(1-2) = R(1-3) = 5.021$ au and $R(2-3) = 5.469$ au, while at the saddle points $R(1-2) = R(1-3) = 5.287$ au and $R(2-3) = 4.932$ au. Recent relativistic coupled cluster calculations[231] confirmed the low-energy barrier between the minima.

A complicated vibronic spectrum, the so-called $\tilde{A} \leftarrow \tilde{X}$ system (13300−14000 cm^{-1}) observed in Au_3 by means of resonant two-photon ionization technique,[230] is assigned as a spin-forbidden doublet ($S = {}^1/_2$) to quartet ($S = {}^3/_2$) transition, $\tilde{A}^4E' \leftarrow \tilde{X}^2E'$, in which both states are JT active. The assignment is based on fitting 25 vibronic levels of the excited $\tilde{A}$ state taking into account the linear JT coupling plus spin–orbital interaction and significant anharmonicity. The combined effect of spin–orbit coupling and anharmonicity in the JT problem is considered seemingly for the first time in this paper.[230]

2. MX_3 Systems

There are a series of JT MX_3 systems with M as a transition metal and X as a halogen or hydrogen (see refs 232–237 and references therein). CuF_3 is one of many examples. In the ground singlet state ^1E of the planar D_{3h} configuration, this system has the outer electron configuration $(e'')^4(a_1')^2(e')^2$ (note that only one of the 2-fold degenerate e orbitals is occupied by two electrons). At the minima of the JT E⊗e APES within the planar configuration, CuF_3 is almost T-shaped with C_{2v} symmetry and the following interatomic distances:[232a] R_1(Cu−F1) = 1.7305 Å, R_2(Cu−F2) = R_3(Cu−F3) = 1.7148 Å and ∠F1CuF2 = ∠F1CuF3 = 95.4°. The E_{JT} value and saddle-point positions are not reported. The lowest triplet excited state $^3A'_2$ has undistorted D_{3h} symmetry.

VF_3 has a $^3E''$ ground state in the D_{3h} configuration[232b] and three equivalent C_{2v} minima on the APES, one of them at R_1(V−F1) = 1.768 Å, R_2(V−F2) = R_3(V−F3) = 1.748 Å, and ∠F2VF3 = 129°. At one of the saddle points, these parameters are 1.744 Å, 1.761 Å, and 112°, respectively. The JT stabilization energy is estimated as $E_{JT} = 270$ cm^{-1} with the barrier between the minima $\delta = 24$ cm^{-1}.

Similar to CuF_3, the MnF_3 molecule has a strong JTE in the ground $^5E'$ state of the planar D_{3h} symmetry with a Mn−F distance $R = 1.754$Å.[233] At the minima of the APES, the molecule remains planar with a nearly T-shaped C_{2v} symmetry: R(Mn−F1) = 1.735Å, R(Mn−F2) = R(Mn−F3) = 1.753Å, and ∠F2MnF3 = 145.2°. At the saddle point these parameters are 1.777 Å, 1.734 Å, and 105.2°, respectively. The JT stabilization energy is rather large, $E_{JT} = 2515$ cm^{-1}, with $\delta = 726$ cm^{-1}.

In another work[234] on MnF_3, similar data obtained by both gas-phase electron diffraction and quantum-chemical calculations are reported. The system has three equivalent C_{2v} minima with a distorted planar configuration and R(Mn−F1) = 1.728 ± 0.014 Å, R(Mn−F2) = R(Mn−F3) = 1.754 ± 0.008 Å, and ∠F2MnF3 = 143.3 ± 2.0°. The JT stabilization energy is calculated as 25 kJ/mol on the CASPT2 level with the barrier between the minima $\delta = 6.4$ kJ/mol. Similarly, three minima with equivalent T-shaped configurations and an energy barrier of 3.6 kcal/mol between them were found in AuF_3 by means of electron diffraction and electronic structure calculations.[235] However, correctly attributing the distortions to the JTE, the authors[235] did not reveal the

degenerate E state of the D_{3h} configuration that causes this effect: they refer to the state $^3A'$ at 46 kcal/mol (above the bottom of the minimum) and $^1A'$at 13 kcal/mol higher, both nondegenerate; these states do not produce the JTE.

Relativistic calculations for AuH_3, AuF_3, and $AuCl_3$ are reported in ref 236a. Other MF_3[236b] and MH_3[236c] systems with M = N, P, As, Sb, and Bi were studied with regard to the barrier of inversion, slightly involving the JTE and PJTE in the interpretation of the results.

Several MH_3 systems were calculated,[237] showing degenerate excited states with small JT distortions. Vibronic coupling in the radiationless decay of the $^2E'$ state of NO_3 is considered in ref 238.

3. Other Systems with a Three-Fold Symmetry Axis

Systems with a 3-fold axis of symmetry which have more than three atoms possess the same E terms and E⊗e JT problems as X_3 but their quantitative consideration is complicated by the presence of more vibrational modes and more than one e-type vibration. The rigorous treatment of such JT systems should involve *the multimode JT problem*.[1−3] However, in some cases the motions of the atoms outside the main triangular framework can be considered as separated from (or, alternatively, completely incorporated in) the latter, thus not participating essentially (individually) in the JT vibronic coupling (see ref 1 for possible reduction of the multimode problem to an ideal one-mode one).

Examples of this kind are triangular $C_3H_3^-$ [239] and isoelectronic $N_3H_3^{2+}$.[240] The calculations of the latter reveal several interesting features that emerge due to the JTE in the ground $^1E'$ state of the D_{3h} configuration and the PJT vibronic coupling of this state to the excited $^1A'_1$ state. Both the JT E⊗e and PJT (E′ + A′$_1$)⊗e vibronic coupling contribute to the E-type distortions that make the initial equilateral triangle isosceles.

APES ab initio calculations of $N_3H_3^{2+}$ with $\sigma-\pi$ CI and a basis set of double-ζ quality including polarization functions yield $R(N_1-N_2) = R(N_1-N_3) = 1.622$ Å for the long and $R(N_2-N_3) = 1.279$ Å for the short sides of the triangles. The authors[240] also explored the out-of-plane bending of the hydrogen atoms (pyramidalization of the nitrogen atom). The strongest pyramidalization takes place at the distinct nitrogen N_1 with the angle $\phi_1 \approx 75°$ between the N_1-H bond and the $N_1N_2N_3$ plane, the pyramidalization of the two other nitrogens being much weaker ($\phi_2 \approx -3°$). The nonplanarity was attributed to the PJT $\pi-\sigma$ mixing of the ground and corresponding excited states. This work was one of the first to explicitly involve the PJTE for the explanation of the origin of the distortions of the high-symmetry configuration of small molecules. Similar PJT explanation of out-of-plane distortions of organic compounds is given in different subsections of this section (see, e.g., puckering in section III.D.2).

At the saddle points the triangle is obtuse with $R(N_1-N_2) = 1.375$ Å and $R(N_2-N_3) = 1.675$ Å and angles of pyramidalization $\phi_1 = 3.6°$ and $\phi_2 = -51°$.

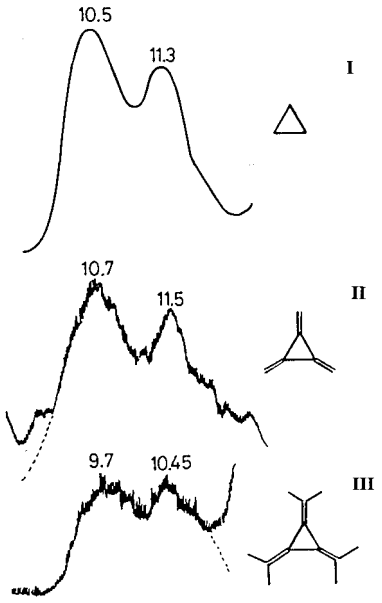

Figure 32. JT splitting of the $^1A'_1 \rightarrow {}^2E'(\sigma)$ band in the photoelectron spectra of C_3H_3 (I), $C_3(CH_2)_3$ (II), and $C_3(C_3H_5)_3$ (III) (numbers in eV). (Reprinted with permission from ref 242. Copyright 1978 Wiley-VCH Verlag GmbH.)

The energy barrier between the minima is rather high, $\delta = 8165$ cm^{-1}, which means very strong quadratic coupling with all the (not explored so far) consequences for the vibronic energy spectra discussed in section II.B.1. The JT stabilization energy is $E_{JT} \approx 20390$ cm^{-1}, seemingly the highest reported so far for JT systems. Together with the large δ value, this makes the $(NH)_3^{2+}$ system one of the strongest influenced by the JT E⊗e-type distortions. Similar strong vibronic coupling has been found in the isoelectronic $C_3H_3^-$.[239]

The two-photon absorption spectra of cyclopropane-h_6 (I) and cyclopropane-d_6 (II) were interpreted as being due to electronic transitions to the JT 3sE′ state.[241] The JTE in the latter was considered in a model with linear coupling to two active e modes, v_{10} for the carbon ring deformation and v_{11} for the methylene wag mode. The linear coupling constants that fit the spectra are $k_{10} = 1.38$ and $k_{11} = 2.45$ for I and $k_{10} = 1.48$ and $k_{11} = 2.59$ for II, the corresponding frequencies of the two modes being $\omega_{10} = 436$ cm^{-1} and $\omega_{11} = 690$ cm^{-1} for I and $\omega_{10} = 415$ cm^{-1} and $\omega_{11} = 610$ cm^{-1} for II. Thus, the JT distortions in the excited E′ state are significant, while there is no barrier of pseudo-rotation (in this model). However, the two kinds of pseudo-rotations (corresponding to the two e modes) seem to be correlated.

In the cyclic configuration of a regular triangle of C_3H_3 (I), $C_3(CH_2)_3$ (II), and $C_3(C_3H_5)_3$ (III), the ground state $^1A'_1$ is nondegenerate while the ionized ground state is doubly degenerate $^2E''$ followed by excited states $^2E'$ and $^2A''_2$. According to the JTE theory,[1−3] the band for the A → E transition in the photoelectron spectrum, in general, should be double-humped. The JT split two-humped bands for $^1A'_1 \rightarrow {}^2E''(\pi)$ and $^1A'_1 \rightarrow {}^2E'(\sigma)$ were observed in the photoelectron spectrum.[242] Figure 32 shows the second band $^1A'_1 \rightarrow {}^2E'(\sigma)$ for all three compounds mentioned above. This assignment is confirmed by MINDO/3 calculations.

Table 9. JT Stabilization Energy E_{JT} and E-Type Vibration Frequencies in Molecular XCH_3-, XCD_3-, and XCF_3-Type Systems with a JT E⊗e Problem (in cm^{-1}) (see Tables 10−14 for more details on OCH_3)

system	E_{JT}	ω_E	ref
OCH_3	255.6	1065	32
OCD_3	165	825	32
SCH_3	41.1	913	32
OCF_3	20.9	465	32, 246
SCF_3	76.8	320	32, 246
$MgCH_3$	17.9	633	253, 32
$CaCH_3$	15.3	767	249, 32, 247
$ZnCH_3$	37.5	749	247, 32
$CdCH_3$	14.2	710	248, 32

Three equivalent JT minima were obtained in an earlier work[243] on a somewhat similar system, $Au(CH_3)_3$, by means of extended Hückel calculations.

The JTE in combination with spin−orbital coupling in a series of trigonal molecules with C_{3v} symmetry and general formula CX_3Y was considered in a series of papers.[32,244−254] They include the methoxy family CH_3O, CH_3S, CF_3O, and CF_3S and organometallic monomethyl radicals $MgCH_3$, $CaCH_3$, $ZnCH_3$, and $CdCH_3$. All these systems have E terms, ground or excited, $\tilde{X}^2E$ in the ground state of the methoxy family and $\tilde{A}^2E$ in the excited state of the organometallics, and three totally symmetric a_1 and three doubly degenerate e vibrations. In the organometallic series, only one of the latter, v_6, seems to be significant in the JTE while the spin−orbital coupling is rather weak, except for $CdCO_3$. In the methoxy family, the JTE is much stronger. Table 9 provides some of the parameters obtained from fitting the spectroscopic data. For more details, see the recent review in ref 32 as well as refs 244−254 and references therein.

Recently a rather full theoretical investigation of the JTE in the methoxy radical CH_3O was carried out using high-level ab initio (CASSCF + MRCI) calculations including all the three active e-type JT modes and three totally symmetric (a total of all nine) vibrations and anharmonicities[254] (for earlier calculations, see the references in refs 250−252). This is seemingly the first multimode JT problem solved in full by ab initio calculations without adjustable parameters. Tables 10−14 list some of the results on vibrational frequencies without and with the vibronic coupling included (both at the minima and saddle points), the geometry parameters, the vibronic coupling constants, and anharmonicity. In this full calculation of the JT five-atomic system, there are nine vibrational constant, three linear coupling constants k_i, $i = 4, 5, 6$, to the three JT-active E coordinates, six quadratic constants, three diagonal g_{ii}, $i = 4, 5, 6$, for coupling to the three E-type coordinates, and three off-diagonal g_{ij}, $ij = 45, 46, 56$, that represent mixed E coordinates, nine bilinear constants that stand for the terms of mixed A and E coordinates (three A coordinates mix with three E coordinates; see eq 21 for the E⊗(e + a) problem in section II.B.1), and three anharmonicity constants f_i, $i = 1,2,3$, for the totally symmetric vibrations. It emerges from the JT stabilization energies that the mode ω_6 is most involved in the JTE, the other two E modes being less effective. In this full ab initio calculation, the authors reached an agreement with the experimental data within 10% for some vibronic energy levels.

The APES in Al_3 and Al_3H was considered in ref 255.

Al_3O is a E⊗e JT system in the ground state.[256−259] High-level UB3LYP/6-31+G* calculations[259] yield the following Al−O interatomic distances in the base triangle with the oxygen atom in the center: R_1 = 1.992 Å and $R_2 = R_3$ = 1.835 Å with the unique angle Al2−O−Al3 ϕ_1 = 163° at the minima (R_1 = 1.780 Å and $R_2 = R_3$ = 1.950 Å with ϕ_1 = 91.9° at the saddle points), the energy barrier between them being δ = 2.71 kcal/mol. Note that different methods of calculation yield significantly different numerical values of these parameters.[256−259] A rather large value of the JT stabilization energy E_{JT} = 26.4 kcal/mol is reported[256] (MP2/6-31G level of ab initio calculations), but the authors are not sure in this number. For Al_3O^- in the same approximation the above parameters are R_1 = 2.012 Å, $R_2 = R_3$ = 1.835 Å at the minima, and R_1 = 1.735 Å, $R_2 = R_3$ = 1.987 Å at the saddle points.[256]

For the treatment of the JTE in the hydronium ion H_3O^+, see ref 260.

An example on how the origin of observed geometry of small molecular systems can be explained as being due to the PJT distortion of high-symmetry configurations is provided by the calculations for molecular ammonia NH_3.[98]

The JTE in the 2E′ state of SO_3^+ was analyzed[210] in a model of linear coupling to two E modes, ω_3 and

Table 10. Geometry Parameters of CH_3O in the Undistorted High-Symmetry C_{3v} Configuration and in the JT-Distorted Minima and Saddle Points of the APES (distances in Å, angles in degrees)[254]

CH_3O	R(C−O)	R*(C−H_b)	R(C−H_a)	∠H_bCO	∠H_aCO	∠H_aCH_b
undistorted, C_{3v}	1.3934	1.0892	1.0892	109.975	109.975	109.975
distorted, C_s minimum	1.3934	1.0923	1.0876	105.3	112.3	107.9
distorted, C_s saddle point	1.3934	1.0867	1.0904	113.4	108.3	110.3

Table 11. Vibrational Harmonic Frequencies (in cm^{-1}) of A (ω_1, ω_2, ω_3) and Two-Fold Degenerate E (ω_4, ω_5, ω_6) Symmetry in the Undistorted Configuration and at the JT Minima and Saddle Points of CH_3O (under the distortion the e vibration splits into a′ and a″ but ω_4 does not split; the imaginary ω_6(a″) indicates the saddle point)[254]

CH_3O	ω_1	ω_2	ω_3	ω_4(a′)	ω_4(a″)	ω_5(a′)	ω_5(a″)	ω_6(a′)	ω_6(a″)
undistorted C_{3v}	3065	1470	1070	3153	3153	1509	1509	1116	1116
JT-distorted C_s minimum	3065	1470	1070	3145	3147	1544	1512	1003	896
JT-distorted C_s saddle point	3065	1470	1070	3144	3144	1482	1542	1180	799i

Table 12. Linear (k_i, i = 4, 5, 6) and Quadratic (g_{ii} and g_{ij}) Vibronic Coupling Constants and Anharmonicity Constants (f_i) for CH_3O (in cm^{-1})[254]

	i						*ij*		
	1	2	3	4	5	6	45	46	56
k_i				−55.4	−216.6	−617.0			
g_{ii}				8.0	27.2	−80.3			
g_{ij}							5.4	−16.9	40.9
f_i	178	141	569						

Table 13. Bilinear Constants b_{ij} that Couple Different Displacements in the Quadratic Approximation of the JT E⊗e Problem in CH_3O (in cm^{-1})[254]

b_{14}	b_{24}	b_{34}	b_{15}	b_{25}	b_{35}	b_{16}	b_{26}	b_{36}
−8.1	−26.7	3.7	−15.3	106.5	−54.1	31.1	−35.5	−128.5

Table 14. Dimensionless JT Stabilization Energies D_i and Interminima Barriers δ_i in CH_3O for Three JT-Active Displacements i = 4, 5, 6 (from ref 254)

D_4	D_5	D_6	δ_4	δ_5	δ_6
0.00016	0.01063	0.15716	0.00514	0.03589	0.14579

ω_4. By fitting the corresponding calculated frequencies and intensities of the electronic transitions to the experimentally determined band shapes of the photoelectron spectrum of SO_3, the authors[210] determined that the JT stabilization energies for each of the two modes are $D_3 = E'_{JT}/h\omega_3 = 0.06$, $D_4 = E''_{JT}/h\omega_4 = 0.35$, the total being thus $E_{JT} = E'_{JT} + E''_{JT} = 230.4$ cm^{-1} ($\omega_3 = 1390$ cm^{-1} and $\omega_4 = 420$ cm^{-1}).

A generalized view of energy contour plots for chemical reactions, multiple reaction paths, and transition-state theory for small clusters of the X_3Y type is given in ref 261.

C. Distorted Square-Planar and Tetrahedral Geometry

1. Cyclobutadiene, Cyclobutane, and Tetrahedrane Radical Cations

Cyclobutadiene radical cation $C_4H_4^+$ is one of the simplest systems with a square -planar D_{4h} geometry in the high-symmetry configuration and a doubly degenerate ^2E_g term resulting in a JT $E\otimes(b_1 + b_2)$ problem (section II.B.2). Geometry optimization of this system has been reported in several papers.[262−267] Qualitatively, the possible JT and pseudo-JT distortions of this system are shown in Figure 33.[262]

According to the general theory,[1−3] JT-active coordinates are of either B_{1g} or B_{2g} symmetry resulting in D_{2h} configurations of a rhombus or rectangle, respectively (section II.B.2). These configurations are not final because the PJTE may produce further distortions. In particular, if there is a sufficiently strong (in the sense of inequality eq 31) vibronic coupling of the ground state $^2B_{3g}$ of the rectangular configuration to the excited $^2B_{3u}$ state, an A_u distortion (puckering) of this configuration takes place ($B_{3g} \times B_{3u} = A_u$). Similar puckering of the rhombus (b_{1u} distortion) is produced by strong pseudo-JT coupling to its $^2A_{2u}$ excited state. However, if the PJT coupling to the $^2A_{1u}$ state is strong (in the rectangle), the distortion b_{3u} leads to a trapezium configuration which may also be subject to further puckering due to the influence of an excited $^2A_1$ state. The rhombus can also be distorted to a kite (b_{3u} distortions), and the latter may be puckered by $B_1 \times A_1$ vibronic coupling. Quadratic coupling terms may also be important.

The energy differences between these configurations may be small. Therefore, only a very high level of correlated ab initio calculation may be able to reveal the real minima and saddle points. Figure 34 illustrates the optimized geometries obtained[262] in the RMP2/6-31G(2d,p) level of ab initio calculations (RMP2/6-31G* for the puckered parallelogram). The energy differences between those configurations are given in Figure 35 together with the results obtained with other methods. The best results show that the puckered rhombus gives the absolute minimum energy (Figure 34), while the planar rectangle is also a minimum, which is 2.5 kcal/mol higher in energy than the puckered rhombus. The puckered parallelogram is a transition state (saddle point) between

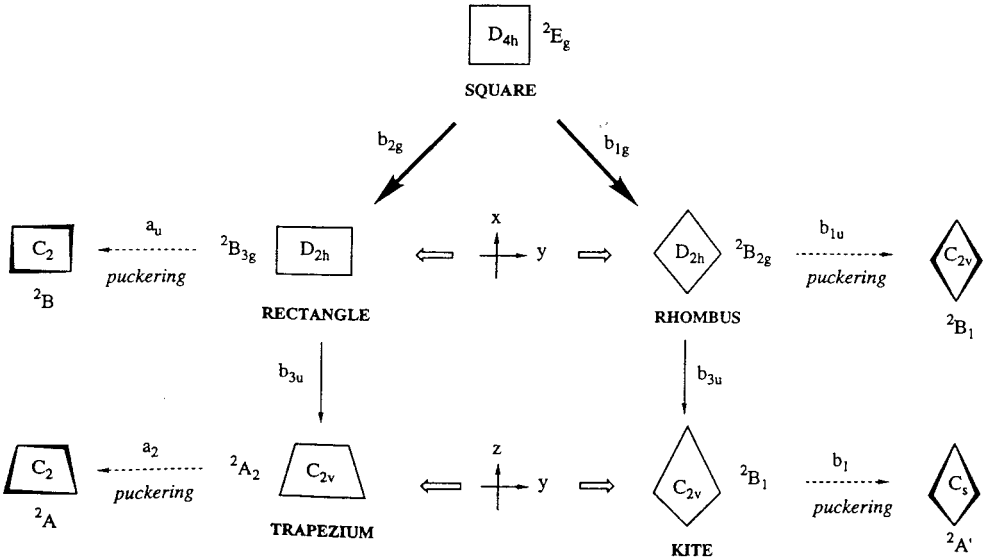

Figure 33. Possible JT and PJT distortions of a square-planar configuration in an electronic E state. (Reprinted with permission from ref 262. Copyright 1995 Elsevier Science Publishers.)

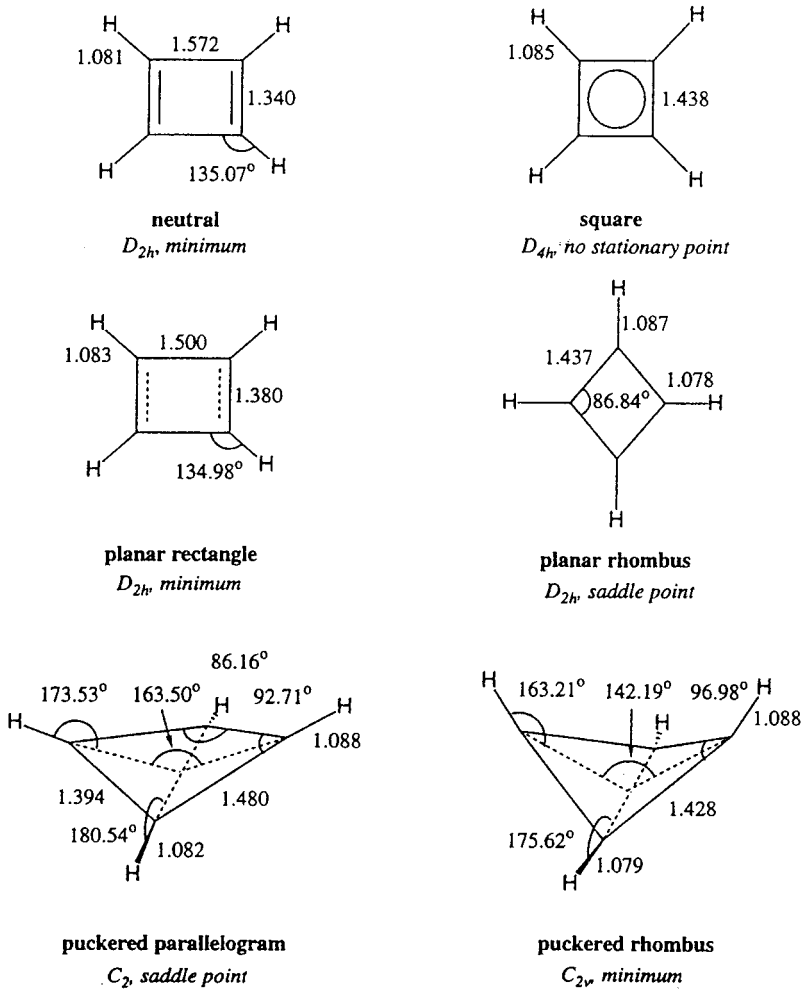

Figure 34. Ab initio calculated geometry of neutral cyclobutadiene and its radical cations. (Reprinted with permission from ref 262. Copyright 1995 Elsevier Science Publishers.)

these two minima at 4.6 kcal/mol higher than the absolute minimum.

From symmetry considerations, there are two planar-rectangle minima (two directions to elongate the square into rectangle). The calculations show that they are $E_{JT}(B_{2g}) = 5.9$ kcal/mol lower in energy than the square-planar geometry; the energy barrier between them is $\delta = 4.2$ kcal/mol. The system is a planar rhombus at the saddle point (at the top of the barrier). For these parameters, similar values of $E_{JT} = 7.0$ kcal/mol and $\delta = 1.0$ kcal/mol were obtained in a simpler calculation at the CI/STO-3G level.[263] Further distortion shown in the last row of Figure 33 did not emerge from these calculations.

By comparison of these results with those expected from the JT effect theory, one gets an understanding of the origin of the calculated geometries. In particular, we see that the linear vibronic coupling to B_{2g}-type nuclear displacements is significant in distorting the square-planar $C_4H_4^+$ system to a planar rectangle with a stabilization energy of about 6 kcal/mol (~2100 cm^{-1}). The coupling to the B_{1g} displacements is weaker, making the planar rhombus geometry a saddle point of the APES, in full accord with the theory (in the case of strong quadratic coupling, the rhombic saddle points become minima too[57]). Thus, the JT effect only does not explain the origin of the calculated absolute minima.

By including the pseudo-JT coupling of the ground state $^2B_{2g}$ of the planar rhombus to the $^2B_{2u}$ excited state via b_{1u} displacement, we get a puckering distortion, which makes this geometry the absolute minimum. There is no pseudo-JT energy gain in puckering of the planar rectangle configuration, but the latter serves as the lowest transition state from the planar rectangle to the puckered rhombic minima. Unfortunately, the authors[262] have not calculated the excited states, which would allow them to estimate vibronic coupling constants and the direction of the PJT distortions.

Note that adiabatic potentials cannot be observed directly. With the complicated APES obtained by numerical calculations, the nuclear dynamics should be evaluated by solving the system of coupled eqs 8. In this way, a true energy spectrum and observables can be predicted. However, as mentioned above, the APES allows one to make reasonable qualitative predictions for many of such observables. The authors[262] estimated the scaled SCF zero-point energies which reduce the effective energy difference between the minima and saddle points to about 0.54 kcal/mol, making the APES almost flat to the corresponding pseudo-rotations.

Directly related to the cyclobutadiene radical cation is its isomer, the tetrahedrane (TH) cation $C_4H_4^+$ with an initial tetrahedral symmetry. Distinguished from

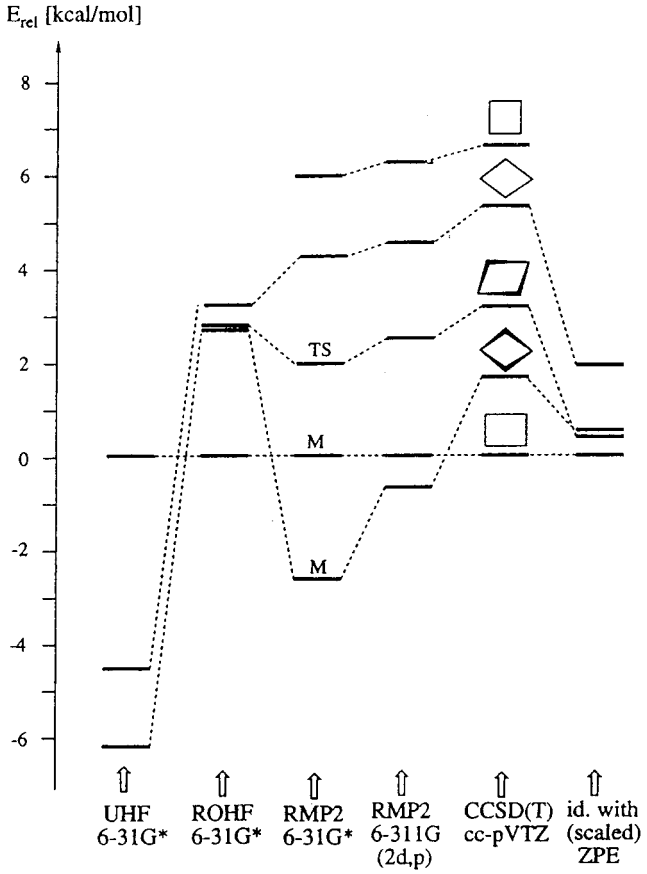

Figure 35. Relative energies of the cyclobutadiene radical in different geometry calculated by the ab initio methods indicated. M and TS denote minima and transition state, respectively. (Reprinted with permission from ref 262. Copyright 1995 Elsevier Science Publishers.)

the cyclobutadiene (CB) cation, the doubly degenerate electronic state of TH^+ in the configuration of a regular tetrahedron leads to a JT E⊗e problem (instead of E⊗($b_1 + b_2$) in CB^+). Numerical calculation[268] allowed the authors to reveal the stationary points of the APES illustrated in Figure 36. By comparison with analytical eqs 17− 20 in the general theory of the JT effect (section II.B.1), they estimated the JT stabilization energy E_{JT} and the linear F_E and quadratic G_E vibronic coupling constants as well as the primary force constant K_E and the barrier between the minima δ. At the UQCISD/6-31G* level, $E_{JT} = 25.07$ kcal mol^{-1}, $\delta = 5.62$ kcal mol^{-1}, $K_E = 5.04 \times 10^2$ kcal mol^{-1} Å^{-2}, $F_E = 1.45 \times 10^2$ kcal mol^{-1} Å^{-1}, $G_E = 0.32$ kcal mol^{-1} Å^{-2}.

The authors[268] also calculated the transition steps from the less stable JT minimum TH1 (Figure 36) of the tetrahedron to the more stable minimum of the rectangular cyclobutadiene cation CB^+ (Figure 34), which show that this isomer interconversion reaction is driven by the JT distortion of the TH^+ configuration (see JT- induced reacitivity in refs 3 and 25). Such JT-driven (triggered) reactions take place rather often. Other examples of PJT driven transformation are given in refs 269 and 270, where different rearrangements of systems such as *syn*-tricyclooctadiene, cyclooctatetraene, etc., radical cations are considered, and below in section II.C.2.

Similar numerical calculations of the APES and analysis of the JT and PJT distortions were performed on the cyclobutane radical cation $C_4H_8^+$.[271−277] The results obtained depend significantly on the level of calculations involved. The ESR spectra for this system are consistent with a puckered rhomboidal structure[278] (Figure 33). This corresponds to the absolute minimum found by means of the most accurate (so far) account for correlation effects in ab initio calculations on the QCISD(T)/6-31G*//UMP2/6-31G* level of theory.[271] In the majority of other works on this system that employ a lower level of calculations,[273] the planar trapezoidal geometry was found as the global minimum and it was suggested that the observed by ESR rhomboidal structure might be reinterpreted in terms of rapidly interconverting equivalent trapezoidal structures.

As mentioned above, observable properties cannot be obtained directly from the APES, although some specific features of the later may be very useful as qualitative indications of possible properties. With regard to ESR spectra there is a special theory developed of what can be expected as a result of vibronic coupling and multiminima APES.[1−3,8] In particular, if as a result of the solution of the system of eqs 8 the ground vibronic state has the same degeneracy and symmetry as the initial electronic state in the point of degeneracy (see, however, section II.B.I), the vibronic reduction factors allow for a reliable and reasonable prediction of the ESR spectra. There is not enough physical meaning in comparison of the observed spectra with the calculated minima positions on the APES without involving the theory of ESR with vibronic coupling.

Note that the neutral cyclobutane system C_4H_8 is not planar either (Figure 37), its nonplanarity being confirmed by both electron diffraction experiments[279] and ab initio calculation.[271] The out-of-plane distortion of the reference square-planar configuration might be a good example of the pseudo-JT effect, the proof of which requires knowledge about the corresponding B_{1u}-type excited states.

In the cyclic system $C_4(CH_2)_4$ with D_{4h} symmetry, the transition from the nondegenerate ground state $^1A_{1g}$ to the ionized ground state ^2E_g in the photoelectron spectrum is not split by the JTE in the ^2E_g state because in this case there is no E⊗e problem. Indeed, as in the case of square-planar $C_4H_4^+$, the JT problem for an ^2E_g term here is ^2E_g⊗($b_{1g} + b_{2g}$), where the vibronic coupling to the b_{1g} and b_{2g} displacements toward a rhombus and rectangle, respectively, are described by two different coupling constants (section II.B.2). If the coupling to one of them is much stronger than to the other one, the problem is reduced to E_g⊗b_{1g} or E_g⊗b_{2g}. For any of them the band of the A−E transition is singly peaked.[1−3] The equal coupling to both kind of vibrations (provided their frequencies are equal too) would convert the problem to E⊗e with a two-humped band of the A−E transition. The calculations in the MINDO/3 approximation[280] allowed the authors to estimate the JT stabilization energies for the two kinds of distortions as 7.5 and 20.1 kcal/mol, respectively.

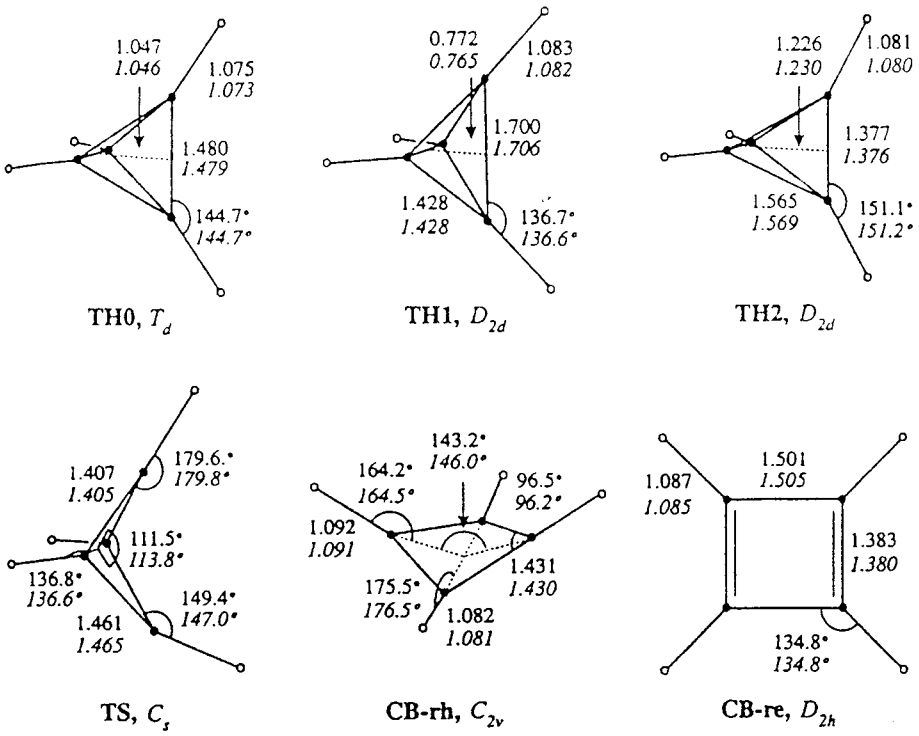

Figure 36. Geometry of $C_4H_4^+$ at stationary points calculated by ab initio QCISD (indicated by normal font) and B3LYP methods (italic). TH and CB denote tetrahedrane and cyclobutadiene radical cations, respectively. TH0 is neutral TH. TH2 and TS are saddle points; all other structures are energy minima. (Reprinted with permission from ref 268. Copyright 1997 American Chemical Society.)

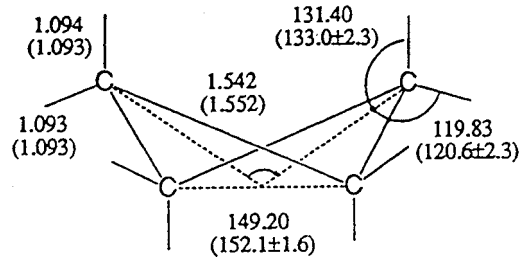

Figure 37. Ab initio (MP2/6-31G*) optimized structure of cyclobutane.[271] Values in parentheses are from the recent electron diffraction study.[279] (Reprinted with permission from ref 271. Copyright 1993 American Chemical Society.)

2. Tetrahedral MX4 and X4 Systems

The methane radical cation CH_4^+ is another example of the simplest systems. The ground state of this cation is triply degenerate in the regular tetrahedron configuration leading to the $T\otimes(e + t_2)$ JT problem (section II.B.3). In this case, if only linear terms of vibronic coupling are significant, the theory predicts either tetragonal or trigonal minima with orthorhombic saddle points. If the quadratic coupling is strong enough, the orthorhombic saddle points become minima too and there is a range of parameters when different kind of minima coexist.[1,3,58,59]

There were several works reported aimed at calculating the APES of this system (see refs 281−292). Ab initio calculations in the MRSDCI (multireference singles and doubles configuration interaction) approximation with a 6-31G** basis set[281] show that the six equivalent global minima are at C_{2v} symmetry with two C−H distances at $R_1 = 1.155$ Å and an angle between them $\phi_1 = 53°$ and the other two C−H distances at $R_2 = 1.075$ Å with $\phi_2 = 127°$, the remaining four angles H−C−H being the same and equal to $\phi_3 = 113°$ (Figure 38). The saddle points between these minima are by 3.1 kcal/mol higher and have C_s symmetry with the four C−H distances, respectively, at (in Å) 1.147, 1.100, 1.117, and 1.117 and angles $\phi_1 = 140.8°$, $\phi_2 = 142.3°$, $\phi_3 = \phi_4 = 104.8°$, and $\phi_5 = \phi_6 = 85.8°$. The C_{2v} ground-state symmetry in the minima is seemingly consistent with ESR experimental data.[293] In relation to the general theory, the C_{2v} minima are "orthorhombic" (the term comes from octahedron distortions) in which one E-type vibration (leading to D_{2d} symmetry) and one T_2-type vibration (leading to C_{3v} symmetry) are displaced. This means that the quadratic coupling is sufficiently strong. In view of the novel achievements in tunneling splitting theory (sections II.B.1 and II.B.3), this system may be an interesting test example.

As mentioned above, the JT distortions in molecular systems are definitively important in chemical reactions[3]. Some examples of JT-driven transformations[268−270] were mentioned in section III.C.1. Reactions with CH_4 participation may serve as further examples. The hydrogen abstraction from CH_4 (or CD_4) by oxygen in its triplet state $O(^3P)$ was shown[294] to have an intermediate system OCH_4 in a doubly degenerate ^3E state, the JT distortion of which influences the consequent transformations. In another process,[295] the impact of a proton on CH_4 abstracts an electron resulting in the ^2T state of CH_4^+, discussed above. This determines the energy-transfer and charge-transfer reaction mechanisms.

The results of calculations[296−300] of the JTE in SiH_4^+ are less illustrative. Different authors give

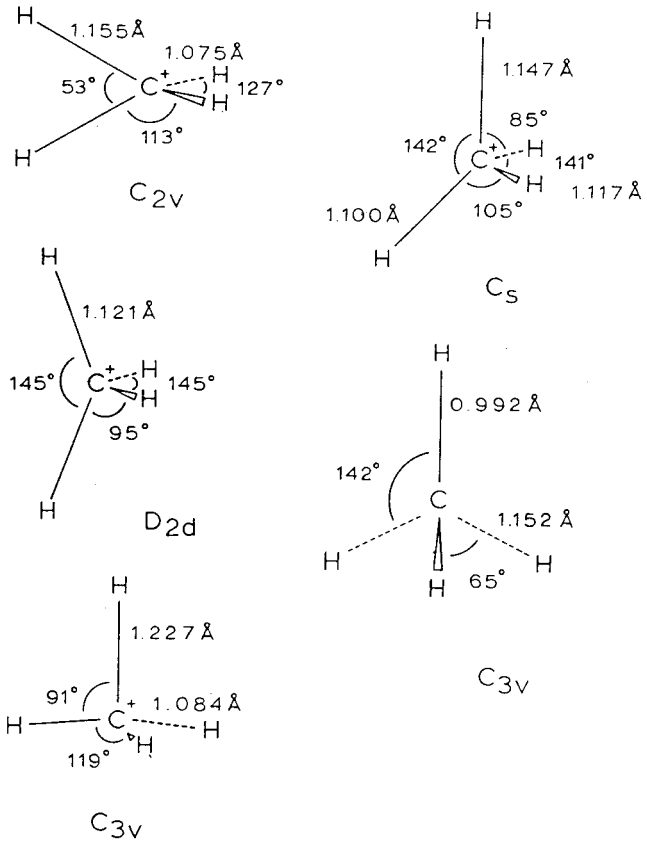

Figure 38. Geometry of CH_4^+ at different symmetry points. The energy minimum is at C_{2v} with the C_s saddle points between them. The C_{3v} configuration (left) has a nondegenerate ground electronic state, whereas at C_{3v}' the ground state is degenerate. (Reprinted with permission from ref 281. Copyright 1988 American Institute of Physics.)

different ground-state symmetries in the minima from C_{3v} to C_{2v} to C_s. The latest more elaborate calculations[296,300] seem to indicate that the lowest in energy configuration corresponds to C_s symmetry with the geometry of a van der Waals complex $SiH_2^+ + H_2$ and with $R_1 = R_2 = 1.4590$ Å, $R_3 = 1.9730$ Å, $R_4 = 1.9240$ Å, $\phi_1 = 120.2°$, $\phi_2 = 22.1°$, $\phi_3 = \phi_5 = 33.405°$, $\phi_4 = 99.292°$. This geometry can be considered as emerging from the C_{2v} symmetry of the $T_2 \otimes (e + t_2)$ JT effect plus a PJT influence of the corresponding excited state. However, such a possibility has not been explored as yet.

For DFT calculations of the JTE in CCl_4^+, see ref 303.

The system H_4^+ was shown by calculations[304−306] to be unstable in both high-symmetry configurations, tetrahedral T_d and planar D_{4h}, in accordance with the JTE for their ground T_2 and E states, respectively. Ab initio QCISD calculations with a 6-211G** basis set yield a planar C_{2v} ground state like $H_3^+ + H$[306] (H_3^+ is an isosceles triangle).

Three tetrahedral systems, P_4, As_4, and Sb_4, have a doubly degenerate ^2E term in the final ionized states P_4^+, As_4^+, and Sb_4^+ of the photoelectron spectra. These systems are thus JT unstable and subject to the $E \otimes e$ problem.[307−309] By solving the vibronic coupled eqs 8 using direct diagonalization of the Hamiltonian with a two-dimensional oscillator

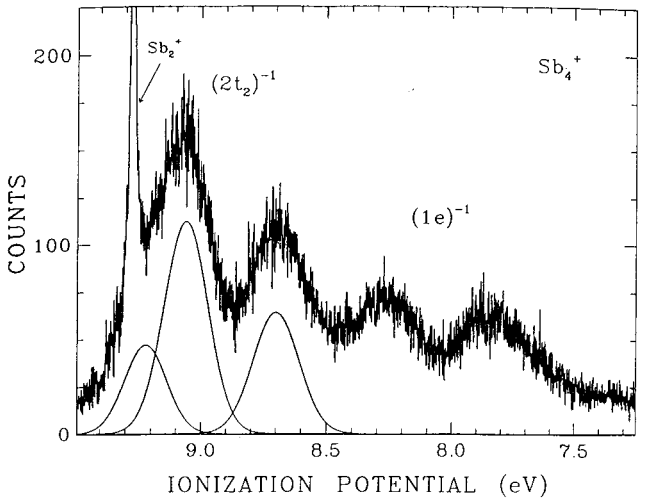

Figure 39. The $(1e)^{-1}$ and $(2t_2)^{-1}$ bands of the P_4^+ photoelectron spectrum. Three component functions are drawn to show the three components in the $(2t_2)^{-1}$ bands. (Reprinted with permission from ref 308. Copyright 1990 American Institute of Physics.)

basis set, the authors[307] revealed the parameters of vibronic coupling for P_4^+ by comparison of the results of expected photoelectron transitions to this state with the experimental data. In this way, they obtained (in eV) $E_{JT} = 0.65$, $k = 0.22$, $g = 0.0004$. For As_4^+ and Sb_4^+ in the linear coupling approximation, the JT stabilization energies are 0.84 and 1.4 eV, respectively.

Alongside with the ^2E ground state, the next one $^2T_2$ (formed by ionization of the $2t_2$ orbital) is important in the photoelectron spectrum of these X_4^+ systems.[308] Figure 39 shows the general band system in the region of transitions from the nondegenerate $^1A_1$ state of neutral P_4 to the ground state $^2E(1e^{-1})$ of P_4^+ and to its excited state $^2T_2$ $(2t_2^{-1})$. The band shapes directly follow the predictions of the JTE theory:[1−3] the band of the $A_1 \rightarrow E$ transition is two-humped, while that of the $A \rightarrow T$ transition has three humps. The separations between the component bands are directly related to the strengths of the JT coupling.

However, much fuller information is contained in the high-resolution spectrum.[308] For the ^2T state, as distinguished from the E state, the spin−orbital interaction may be important. It was shown[308] that, as expected, the spin−orbital interaction is most significant in Sb_4^+ and less effective in P_4^+. Note that the JTE reduces the spin−orbital interaction by the vibronic reduction factors.[1−3] However, there is no full treatment of the combined JT and spin−orbital interaction in these systems as yet.

The P_4^+ system was reconsidered[309] taking into account that the excited $^2T_2$ state in the tetrahedral configuration is close in energy to the ground ^2E state and contributes significantly to the distortion of the system in the ground state via the PJTE. Ab initio SCF calculations performed on this system[309] reveal a rather complicated APES with a variety of conical intersections. The P_4^+ ^2E term JT parameters from eq 20 are (in eV) are $k = 0.24$, $g = -6.6 \times 10^{-3}$, and $\omega_E = 0.045$ (the latter is taken from experimental data). For the $^2T_2$ term ($T \otimes (e + t_2)$ problem), the

Table 15. Bond Angles (degrees) and Bond Lenths (Å) for MX_4 Polyhedra in cat [MX_4], where cat = *p*-Xylylene Bis(triphenylphosphonium)$^{2+}$ (from ref 16)

system	$Co(NCS)_4^{2-}$	$Ni(NCS)_4^{2-}$	$Cu(NCS)_4^{2-}$	$CuBr_4^{2-}$
ϕ_1	113.9	115.6	135.0	134.5
ϕ_2	116.1	126.3	139.5	136.9
$\phi_3 = \phi_4 = \phi_5 = \phi_6$	106 ± 1	103 ± 2	97 ± 1	98 ± 2
R(M−X)	1.96	1.93	1.92	2.39

linear vibronic coupling constants to e and t_2 vibrations are $\mu_e = 0.005$ and $\mu_t = 0.14$, respectively, with $\omega_t = 0.0577$. The authors[309] also included the coupling to the totally symmetric vibrations (section II.B.1), which yields the coupling constants $k_g^E = -0.09$ and $k_g^t = -0.05$. The pseudo-JT $^2E-^2T_2$ mixing between the two JT terms (making the overall problem $(E + T)\otimes(a + e + t_2)$) emerged with the vibronic coupling constant $v = 0.12$, which is of the same order of magnitude as the JT coupling with the e and t_2 manifold separately. It was shown[309,310] that with these parameters, dynamical calculations using a large basis set of harmonic oscillator states explain the observed photoelectron spectra of P_4 well. While the gross features of the band shape can be explained by the simpler model of the JT coupling, considered above,[307,308] the PJT vibronic mixing of the ^2E and ^2T electronic states contributes substantially to the fine structure of the spectrum.

In contrast to the CH_4^+ cation, the JTE in tetrahedral CuX_4^{2-} yields E-type minima at which the system has D_{2d} symmetry (see refs 15 and 16 and references therein). For instance, the tetrahedron clusters of $CuCl_4^{2-}$ in Cs_2CuCl_4 are considerably flattened $\phi_1 = \phi_2 = 129°$ with $F_E = 4500$ cm^{-1} Å^{-1}.[311,312] In the tetrahedral VCl_4, the APES for the ground-state ^2E was calculated using DFT methods[313] (for earlier attempts, see references in ref 313). The JT distortion is rather small, $E_{JT} = 52$ cm^{-1} and $\delta = 12$ cm^{-1}, which corresponds to the following constants in eq 14: $F_E = 1311 \pm 6$ cm^{-1} Å^{-1}, $G_E = 1260 \pm 50$ cm^{-1} Å^{-2}, $K_E = 19084 \pm 100$ cm^{-1} Å^{-2} and $\rho \cong F_E/K_E = 0.068$ Å. For the excited-state $^2T_2$, the JTE was shown to result in the distorted D_{2d} configuration with the stabilization energy $E_{JT} = 264$ cm^{-1}, which explains the absorption spectrum.[314]

The distortions for several MX_4 clusters with an electronically 3-fold degenerate T ground state are given in Table 15. There are many other examples in the review articles of refs 15 and 16. The D_{2d} distortions ($\phi \approx 85°$) of the NiX_4 cluster in $Ni(NMTP)_4[BF_4]_2$, where NMTP = *N*-methyl-2-thiooxopyrrolidine, allowed the authors[315] to estimate the vibronic coupling constants $F_E = 3250$ cm^{-1} Å^{-1}, $G_E \approx 0$, $E_{JT} = 1595$ cm^{-1}. In the analogous cluster with Zn (instead of Ni), which has a nondegenerate ground state, there are practically no distortions except those that can be attributed to crystal packing.

An interesting example of a polyatomic T_d structure with a JTE in the excited state $^1T_2$ is presented by $Sn_6(\mu_5\text{-}O)_4(\mu_3\text{-}OH)_4$.[316] By means of ab initio calculations with geometry optimization, it was shown that the system in the $^1T_2$ state undergoes a JT distortion from T_d to C_{2v} (as predicted by the theory) which is 23.7 kcal/mol lower in energy. This explains the observed spectral properties, which were earlier interpreted as being due to the formation of Sn−Sn bonds (the authors[316] show that no such bonding takes place).

D. The Benzene and Cyclopentane Families and Some Larger Systems

1. The Benzene Family Molecular and Radical Cation and Anion Systems

The JT study of benzene-like systems and their derivatives has a long history (see refs 317−349 and references therein). In the earlier works (partly reviewed in refs 3 and 321), the JT parameters of the ground ^2E state of *sym*-$C_6F_3H_3^+$, *sym*-$C_6F_3D_3^+$, and *sym*-$C_6Cl_3H_3^+$ were estimated from emission spectra.[317−325] In these papers the multimode nature of the JTE is ignored.

For a similar system *sym*-triazine cation $H_3C_3N_3^+$, the authors[326] calculated the vibronic energy spectrum in the ground E state linearly and quadratically coupled to a single-active ring-distortion e mode v_6. The calculated energy levels and transition intensities were compared with those observed in the two-photon absorption spectrum of the $3s^1E'$ Rydberg state, and a good agreement between them was obtained for the JT parameters $k = 2.14$ and $g = 0.046$. This gives $D = E_{JT}/\hbar\omega_E = 2.29$ and $\delta' = \delta/\hbar\omega_E = 0.21$, and with $\omega_E = 661$ cm^{-1}, $E_{JT} = 1514$ cm^{-1} and $\delta = 139$ cm^{-1}, which means hindered pseudo-rotation in the ground vibronic state.[326]

The pseudo-rotation with a frequency of $\omega_\phi = 150$ cm^{-1} in the excited E state of cyclohexane was revealed[328] based on the analysis of the ultraviolet spectrum of the two-photon transition from the lowest excited $^1A_{1g}$ state to the $3s^1E_g$ Rydberg state. The E−e problem in this system is a multimode one;[329] the major contribution to the linear JT distortion comes from five E-type modes with a total of $E_{JT} = 2550$ cm^{-1}. The barrier of pseudo-rotations is approximately $\delta \approx 140$ cm^{-1}.

The JTE in the benzene cation $C_6H_6^+$ was subject to multiple investigations.[310,319,334,347] Using high-resolution threshold photoionization spectra of benzene in combination with the theoretical predictions for the JT E⊗e problem (section II.B.1), the structure of the ground E state of this system was shown[338] to follow the APES of the Mexican hat (Figure 3) along the E-type C−C−C in-plane bending vibration ($\omega_6 = 536$ cm^{-1}) with $\rho_0 = 0.12$ Å and $E_{JT} = 208$ cm^{-1}. At the minimum, the C−C−C angle is 118.1°. The vibronic constants, according to eq 20, are $k = 0.88$ and $g = 0.02$, which give an estimate of the barrier between the minima $\delta = 8.32$ cm^{-1}. This δ value was confirmed recently[339] in ab initio calculations (BLYP with a 6-311G* basis set) and ZEKE (zero-electron kinetic energy) PE spectra. Compared with the zero-

Table 16. Vibronic Coupling Parameters for the JTE in the Ground $\tilde{X}^2E_{1g}$ State (via the $\nu_6(e_{2g})$ Mode) and PJT Mixing between the Excited $\tilde{B}^2E_{2g}$ and $\tilde{C}^2A_{2u}$ States via the $\nu_{16}(e_{2u})$ and $\nu_{17}(e_{2u})$ Modes in $C_6H_6^+$ and $C_6D_6^+$ (from[341])

system	vibrational mode	ω_E, cm^{-1}	$D_{JT} = E_{JT}/\hbar\omega_E$	$g = \delta/2E_{JT}$	$D_{PJT} = E_{PJT}/\hbar\omega_E$
$C_6H_6^+$	$\nu_6(e_{2g})$	540	0.377	0.020	
	$\nu_{16}(e_{2u})$	333			0.44
	$\nu_{17}(e_{2u})$	673			0.17
$C_6D_6^+$	$\nu_6(e_{2g})$	506	0.345	0.024	
	$\nu_{16}(e_{2u})$	259			0.75
	$\nu_{17}(e_{2u})$	642			0.18

Table 17. Vibronic Coupling Constants for the JTE in the Excited $\tilde{D}^2E_{1u}$ State and PJT Mixing between this State and the $\tilde{E}^2B_{2u}$ State in $C_6H_6^+$ (in eV)[340]

b_{2g} mode	ω	JT linear coupling	PJT coupling
ν_{15}	0.4048	0.0971	0.0664
ν_{16}	0.2055	0.1032	0.1701
ν_{17}	0.1497	0.0579	0.1288
ν_{18}	0.0757	0.1755	0.0417

Table 18. JT Parameters for the Ground State $\tilde{X}^2E_{1g}$ of $C_6F_6^+$ (after ref 321)

	ν_{15}	ν_{16}	ν_{17}	ν_{18}
E_{JT} (cm^{-1})	370	61	289	101
k	0.68	0.32	1.17	0.87
g	~0	~0	0.006	~0
ω_E (cm^{-1})	1609	1220	247	116
δ (cm^{-1})	~0	~0	3.5	~0

point energy, this small barrier means almost free rotations.

The PJTE plays an essential role in the structure and spectra of all benzenoid cations. The excited state $\tilde{B}^2E_{2g}$ of $C_6H_6^+$ is close to the $\tilde{C}^2A_{2u}$ electronic state with a 0.31 eV energy separation.[347] The calulations[337,346] show that there is a rather strong PJT coupling and an interstate conical intersection between these two electronic states via two e_{2u} vibrational modes υ_{16} and υ_{17}. Together with the JTE on the $\tilde{B}^2E_{2g}$ state, which involves the e_{2g} modes υ_6 and υ_8, this explains the origin of the photoelectron band profile of the two overlapping states and the diffuse appearance of the $\tilde{C}$ state in the band. The same PJT coupling in $C_6H_6^+$ and $C_6D_6^+$ between the two states, $\tilde{B}$ and $\tilde{C}$, was employed[341] to interpret the vibrationally resolved photoinduced Rydberg ionization spectra of the dipole-forbidden $\tilde{C}^2E_{2g} \leftarrow \tilde{X}^2E_{2g}$ transition. For the calculations, the authors[341] employed a two-mode PJT model.[350,351] The JT coupling parameters used to fit the calculated spectral lines to the observed ones are given in Table 16.

For higher excited states $\tilde{D}^2E_{1u}$ and $\tilde{E}^2B_{2u}$ of $C_6H_6^+$, multiple surface intersections and strong PJT coupling between them was revealed.[340] Using Green's function calculations (with correlation effects included), the coupling constants for the JTE in the E_{1u} state and the PJT mixing of the E_{1u} and B_{2u} states were estimated (Table 17). Note that both the JTE and the PJTE are triggered by the same four e_{2g} modes, υ_{15}, υ_{16}, υ_{17}, and υ_{18}.

The calculated envelope of the corresponding transitions explains the origin of the observed diffuse photoelectron band. The authors[340] also performed wave packet dynamical simulations and showed that the $\tilde{E} \rightarrow \tilde{D}$ internal conversion process is very fast, several fs. This result is important to the explanation of the mechanism of fragmentation dynamics of $C_6H_6^+$ in the electronically excited state as a stepwise $\tilde{E} \rightarrow \tilde{D} \rightarrow \tilde{C} \rightarrow \tilde{B} \rightarrow \tilde{X}$ internal conversion (nonradiative) process. The $\tilde{C}^2A_{2u} \rightarrow \tilde{B}^2E_{2g} \rightarrow \tilde{X}^2E_{2g}$ fast nonradiative decay (~250fs) was studied earlier[334] based on the investigation of the conical intersections, JTE and PJTE, and wave packet dynamical calculations of this process.

In $C_6F_6^+$, as in $C_6H_6^+$, all four e_{2g} modes υ_{15}, υ_{16}, υ_{17}, and υ_{18} are active in the JTE[321,349] in the ground state $\tilde{X}^2E_{1g}$. Table 18 lists the contribution of each of these modes to the JT distortions. The total JT stabilization energy equals 831 cm^{-1}. The quadratic coupling is shown to be negligible, except for υ_{17} where it is small, $g = 0.006$.

A series of works are devoted to the JTE and PJTE in substituted benzene radical anions (see refs 352−360 and references therein). Using ab initio ROHF approximation with a 6-31G* basis set plus MP2 level correlation calculations at the extrema points of the APES, the authors[356] obtained a detailed structure of this surface produced by the JTE and PJTE in $C_6F_6^-$. In the planar configuration D_{6h}, the ground state is $^2A_{1g}$ with low-lying excited states $^2E_{2u}$ at 15.3 kcal/mol and $^2E_{1u}$ at 24.2 kcal/mol. The small separation of these states allows for their vibronic mixing under the appropriate nuclear displacements. The JTE on the $^2E_{2u}$ term produces e_{2g} distortions within the planar configuration with three D_{2h} minima and three saddle points corresponding to electronic states $^2B_{1u}$ and ^2A_u, respectively. The PJT $^2A_{1g}$−$^2E_{2u}$ mixing under the out-of-plane e_{2u} distortions further reduces the symmetry at each minimum, forming two mirror-symmetry C_{2v} structures, while at the saddle points two D_2 structures are formed. As a result, the system has six minima and six saddle points illustrated in Figure 40. The JT stabilization energy at the minima is estimated as 16.9 kcal/mol. In comparison with neutral C_6F_6, it is seen that the electron affinity of this system is due to combined JT and PJT effects.

2. Cyclopentadienyl Radical and Cyclopentane: Puckering

The JTE in cyclopentadienyl (Cp) radical C_5H_5 and its ionic, deuterated, and substituted states were considered in a series of papers beginning with A. D. Liehr[361] (see refs 360−368 and references therein). In more recent calculations,[362,363] the ground E term of planar C_5H_5 in D_{5h} symmetry is shown to have a distorted C_{2v} configuration at the minima due to the JTE. In a relatively simple ab initio UHF/STO-3G approximation,[362] the JT stabilization energy $E_{JT} =$ 14.5 kcal/mol with a barrier between the minima δ = 3.5 kcal/mol and contraction of the most distorted C−C bond ΔR_{CC} = 70 mÅ. In a more elaborate

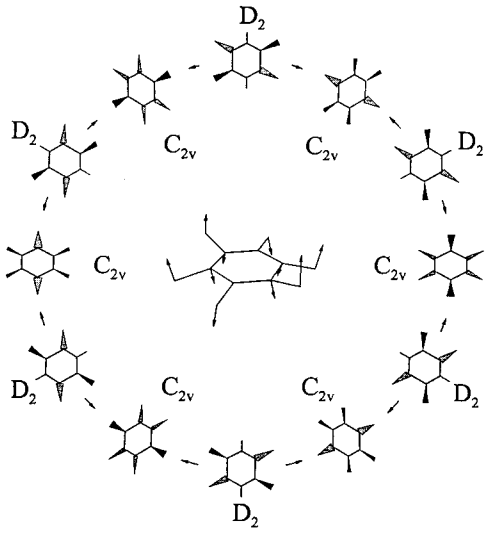

Figure 40. Combined JT plus PJT pseudo-rotation in $C_6F_6^-$. $C_{2v(z)}$ and D_2 structures correspond to the APES minima and saddle points, respectively. Equivalent structures are congruent upon the S_6 symmetry operation. The pseudo-rotation coordinate $Q(b_1)$ is shown in the center. (Reprinted with permission from ref 356. Copyright 1999 Elsevier Science Publishers.)

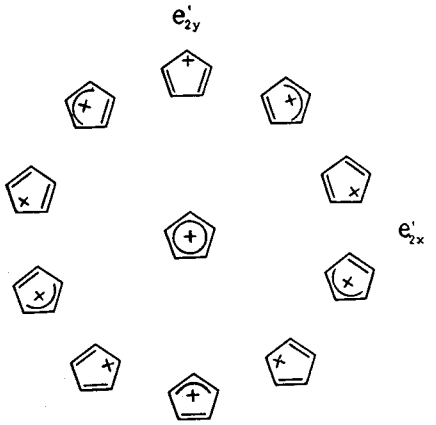

Figure 41. Pseudo-rotation in the lowest singlet state of the cyclopentadienyl cation, distorted in an e_2' mode. (Reprinted with permission from ref 363. Copyright 1979 American Chemical Society.)

calculation that also includes CI in the π space,[363] $E_{JT} = 7.1$ kcal/mol and $\delta \approx 0$ which means free pseudo-rotation of the distortion. In distorted configuration $^2A_2$ and $^2B_1$ states, the interatomic distances (in parentheses for the $^2B_1$ state) are (in Å) $R(C_1-C_2) = 1.407$ (1.457), $R(C_2-C_3) = 1.496$ (1.371), $R(C_3-C_4) = 1.360$ (1.509), with almost unchanged angles of the pentagon. The authors[363] also calculated the APES of the cyclopentadienyl cation $C_5H_5^+$ taking into account the PJT mixing of the ground state $^1A_1'$ with the lowest excited $^1E_2'$ state (at 23 kcal/mol) by e_2' distortions, which produces deeper minima at $E_{JT} = 13.4$ kcal/mol, but without a considerable barrier between the minima (meaning free pseudo-rotation). Note that in both cases, C_5H_5 and $C_5H_5^+$, the distortion coordinate E allows for pseudo-rotation that avoids the high-symmetry D_{5h} configuration. Figure 41 illustrates the pseudo-rotation pattern for $C_5H_5^+$.

The APES of fluorinated Cp cations $C_5H_4F^+$ and $C_5H_4CH_3^+$ in singlet states were studied[364] by MNDO and ab initio MP2/6-31G* methods. The results are related to the pseudo-rotation surface of $C_5H_5^+$.

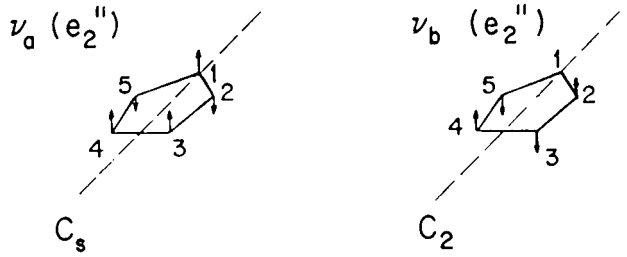

Figure 42. Two components of the e″-type displacements (puckering) in a five-membered ring with D_{5h} symmetry. (Reprinted with permission from ref 369. Copyright 1975 American Chemical Society.)

In the papers[366–368] the rotationally resolved laser-induced fluorescence spectrum of the $\tilde{A}^2A_2'' \leftrightarrow \tilde{X}^2E_1''$ transition in C_5H_5, C_5D_5, C_5H_4D, and C_5HD_4 are analyzed in detail in view of the JTE implications. While the authors found clear evidence of the JT pseudo-rotation in the ground state, the parameter values of the JT distortions that emerge from the spectral data are significantly smaller than in the ab initio calculations, discussed above.

Cyclopentane C_5H_{10}, distinguished from C_5H_5, has no degenerate ground state, but like $C_5H_5^+$ above, it may have PJT distortions due to the vibronic mixing to the excited states. On the other hand, C_5H_{10} is a good example to illustrate the phenomenon of puckering.

In any system with more than three atoms and a reference planar configuration some atoms or atomic groups may undergo out-of-plane displacements resulting in the so-called puckering. Several examples mentioned in the subsections above illustrate such distortions. The out-of-plane bending of the C−O bond in H_2CO[186] considered in section III.A.2 may also be regarded as an element of puckering.

Puckering is shown mostly as an effect of nonplanarity of organic ring structures. In the saturated five-membered ring of cyclopentane C_5H_{10}, the reference planar configuration has D_{5d} symmetry and the puckering distortion has e″ symmetry. Figure 42 shows the two components of the e″ displacements of the atoms in the five-membered ring. The Z-displacements of the individual carbon atoms along the 5-fold axis in this symmetrized "concerted" e″ displacement is given by the following equation[369]

$$Z_i = (2/5)^{1/2} q \cos[\phi + (4\pi/5)(i-1)] \quad i = 1, 2,...,5 \tag{54}$$

where q is the amplitude of distortion and ϕ is the phase angle: by changing ϕ from 0 to 2π the structure goes from one component of displacement (at $\phi = 0°$, 36°, 72°,..., 324°) to the other one (at $\phi =$ 18°, 54°,..., 342°). This kind of typical puckering has been revealed first from thermodynamic data[370] and then confirmed by various experimental techniques (see ref 371 and references therein). Calculations of APES[369] confirm that in cyclopentane the planar configuration is unstable: the puckered configuration is lower in energy by ~4.2 kcal/mol (the experimental value is 5.2 kcal/mol) and the motion of the puckering

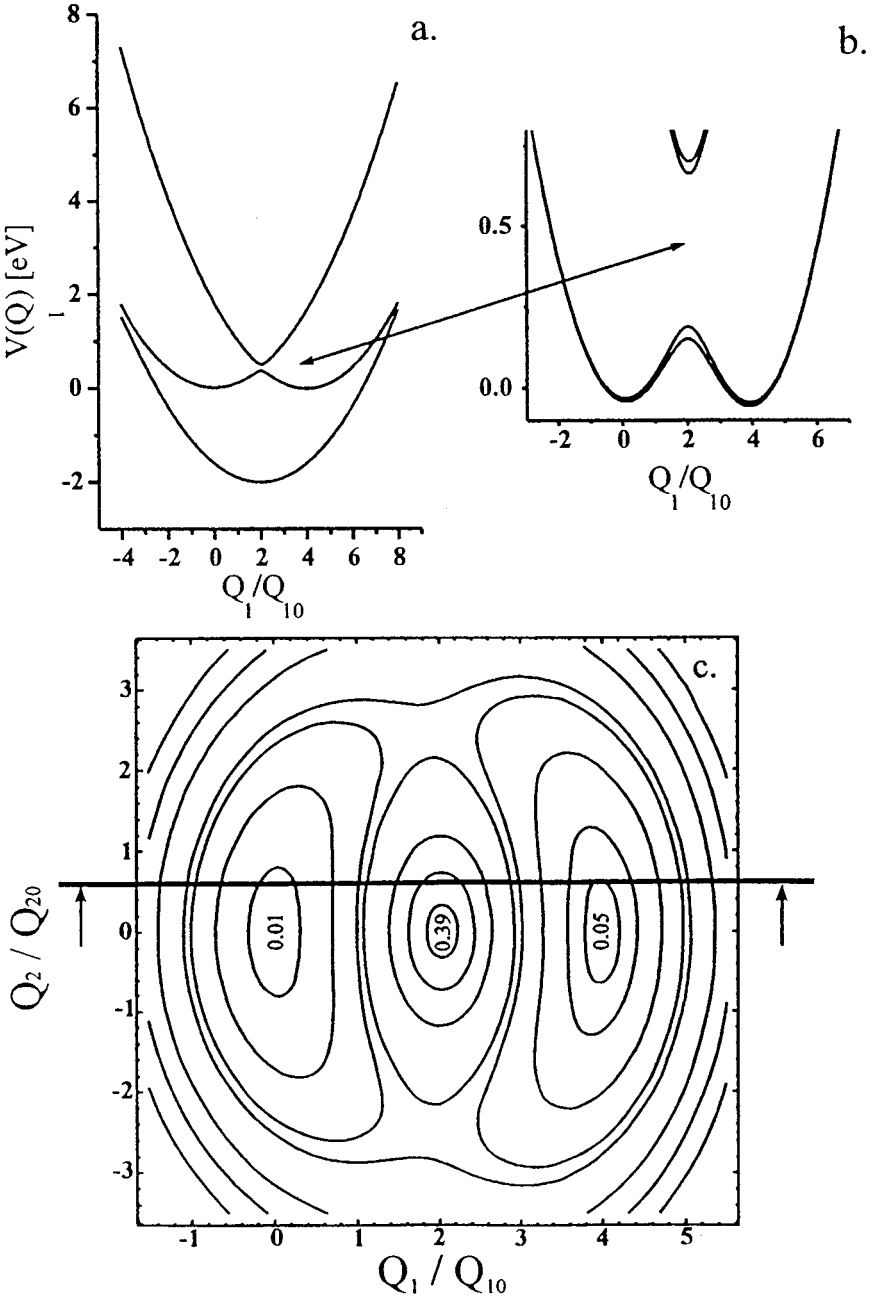

Figure 43. (a) Effective potentials for the totally symmetric C=C stretching coordinate around 1700 cm^{-1} in the three vibronically coupled states of diphenylhexatriene (DPH). In the $2A_g$ state, the pseudo-Jahn−Teller effect leads to a double-well potential (abscissa values of elongation are normalized to the zero-point oscillation for this mode Q_{10}). (b) Enlarged segment of the range of avoided level crossing between the $1B_u$ and $2A_g$ singlet states; potential curves are given for two different vibronic coupling constants. (c) Contour diagram of the effective 2-d vibrational potential for the first excited singlet state of DPH resulting from strong vibronic coupling; the cut at $Q_2 = Q_{20}/2$ represents the lower potential in b. (Reprinted with permission from ref 372. Copyright 1998 Elsevier Science Publishers.)

distortion along the ring is rather a free internal rotation (pseudo-rotation).

The planar configuration of cyclopentane has a closed-shell A_1 electronic ground state and a variety of excited states, among which there are those belonging to the E″ type. Obviously, the vibronic mixing of the ground-state A_1 with the excited E″ under e″ vibrations ($A_1 \times E'' = E''$) softens the former with respect to e″ displacements. If this softening is strong enough (the vibronic coupling is strong and the inequality in eq 31 holds), the ground state becomes unstable with regard to these displacements.

To my knowledge, the PJT origin of this puckering has not been explored so far. The numerical data show as a fact that the system is distorted, giving no information concerning its origin as due to the implication of the E″ excited electronic state that causes the instability of the ground state with respect to e″ displacements. The authors[369] explain the puckering as determined by the balance between the increased strain produced by the decrease in the bond angle (which is smaller in the puckered configuration) and decreased torsion strain (which is the greatest in the planar configuration). The PJT ex-

planation is much more general and straightforward: the puckering distortion, by mixing the A_1 and E″ electronic states, *provides additional covalent bonding* that lowers the energy of the system, quite similar to many other cases considered above. As mentioned in section II.C, in the general formulation employed in this trend, the PJT implication of the excited electronic states is the only possible source of instability of the ground state in the high-symmetry configuration.

3. Larger Systems

Similar to C_5H_5, cycloheptatrienyl C_7H_7 has a E⊗e trough (section II.B.1) with $E_{JT} = 0.859$ kcal/mol.[360] In triphenylene and coronene negative ions, $E_{JT} =$ 0.385 and 0.299 kcal/mol, respectively.[360] Note that these numerical data[360] were obtained by semiempirical calculations and may change significantly when more sophisticated ab initio methods are used.

An interesting case of the PJTE in the excited state of a relatively large molecule diphenylhexatriene (DPH) is described in ref 372. DPH is planar and has C_{2h} symmetry in the ground state A_{1g} with lowest excited states $2A_g$ and $1B_u$ related to the Raman spectra. The observed spectral properties are explained based on significant vibronic mixing of the $2A_g$ and $1B_u$ states by a b_u-type vibrational mode (Q_2) near 40 cm^{-1} also involving the totally symmetric A_g-type vibrational mode (Q_1) at 1700 cm^{-1}. A three-level problem in which the ground-state A_{1g} is coupled to Q_1 only (with a 1.65 eV $Å^{-1}$ amu $^{-1/2}$ coupling constant) while the two excited states are mixed by Q_2 only (with a 0.2 eV $Å^{-1}amu^{-1/2}$ coupling constant) yield the APES illustrated in Figure 43. The results explain the origin of the observed two bands and the broadening in the Raman spectra.

The JTE in much larger systems with trigonal symmetry, triptycene[373] (9,10-dihydro-9, 10 [1′,2″] benzenoanthracene) (I) and 9-fluorotripticene[374] (II) was investigated to explain the origin of the vibronic structure of their resolved $S_1(E) \leftarrow S_o(A_1)$ two-photon ionization spectrum. For I, a single-mode E⊗e problem with $k = 1.65$, $g = 0.426$, and excited-state frequency $\omega_E = 47.83$ cm^{-1} accounts for ∼98% of the observed absorption band intensities in the 0−350 cm^{-1} region. For II, three models were considered: E⊗e, (A + E)⊗e, (A + E)⊗(e + a_2). The E⊗e interpretation yields essentially correct frequencies, while the coupling to the $^1A_1$ state improves the intensities. In the (A + E)⊗e model, $k = 1.145$, $g = 0.152$, and $\omega_E = 61.4$ cm^{-1}. The tunneling splitting A_2−E due to pseudo-rotation and quadratic barriers is 1.5 cm^{-1}.

The ESR spectra of corannulene monoanion $C_{20}H_{10}^-$ were interpreted in terms of pseudo-rotation about the C_{5v} JT crossing.[375] The barrier between the (five) equivalent minima was estimated as $\sim 2.2 \times 10^{-3}$ eV. The JTE in monoanions and trianions of {6}- (I) and {18}hetero(A,B)annulenes (II) was discussed in ref 376. These systems have a 3-fold axis of symmetry and a degenerate E term, thus being subject to the JT E⊗e problem. On the B3LYP/6-31G* level of theory, the authors calculated orbital (section II.D) and integral vibronic coupling constants, which are shown to be most significant for the modes of 1500 cm^{-1} in I and <500 cm^{-1} in II.

Although the main works on the JTE theory in application to the family of fullerenes are cited in section II.B.4, further developments and spectroscopic investigations can be found in recent publications.[377−380]

E. MX_5 an MX_6 Systems

1. Some MX_5 Clusters and Molecules

The general validity of the vibronic approach allows for its applications to any stereochemical problems. References 381 and 382 provide an illustrative example on how this approach can be used to solve the problem of the PJT origin of significant differences in stereochemistry of transition-metal MX_5 compounds that differ by the number of d electrons only.

Consider two crystal structures, $[Co(NH_3)_6]$ $[CuCl_5]$ (I) and $[Co(NH_3)_6]$ $[ZnCl_5]$ (II), which differ by substitution of the Cu atom by Zn, next in the periodic table. The X-ray analysis and other investigations[383−387] show that the pentacoordinated polyhedrons $CuCl_5^{3-}$ (I) and $ZnCl_5^{3-}$ (II) in these crystals have essentially different shapes. Both are unstable in the D_{3h} trigonal-bipyramidal (TBP) configuration. The $CuCl_5^{3-}$ ion is unstable with respect to E′-type distortion describing the conversion toward a square-pyramidal (SP) configuration, TBP → SP (Figure 44a), it has three equivalent (almost) SP configurations, and performs fast conversions between them (molecular pseudo-rotations). The $ZnCl_5^{3-}$ ion is also not TBP, but it forms a distorted tetrahedron plus one chlorine ion on (almost) the trigonal axis, and there are no pseudo-rotations. This configuration can be regarded as being produced by the A_2'' distortion of the TBP configuration, as shown in Figure 44b.

Since the crystal environment for the two clusters is the same, the differences in their geometries are deemed to be due to the inside structure of the clusters themselves. The two different directions of distortions are evidently due to the difference in the electronic configuration of the central atom, d^9 (I) versus d^{10} (II), and the question is whether this effect can be described by the vibronic coupling, i.e., by evaluating the ground and excited electronic states of the reference TBP configuration, estimating the values of the constants K_0, $F^{(oi)}$, and Δ in eq 31, and the contribution of vibronic coupling to the instability of the ground state in different directions (eq 34).

The calculations[381] were carried out by the semiempirical MO LCAO iterative extended Huckel method with the excited states taken in the "frozen orbital" approximation. By estimating the occupied and unoccupied one-electron MO, the excited states of E′ and A_2'' symmetry (for which the vibronic constants $f^{(A'E'')}$ and $f^{(A'A'')}$ are nonzero) were constructed, and the values K_0, Δ, and F^2/Δ were evaluated for each excited state of appropriate symmetry. Some results are given in Tables 19 and 20.

Among the excited states of E′ type, there are three states in I and two states in II whose vibronic admixture to the ground state gives the major negative contribution to the force constant. The first arises from the excitation of one electron from the fully occupied MO $|1e'\rangle = 0.41(2|3s_3\rangle - |3s_4\rangle - |3s_5\rangle)$

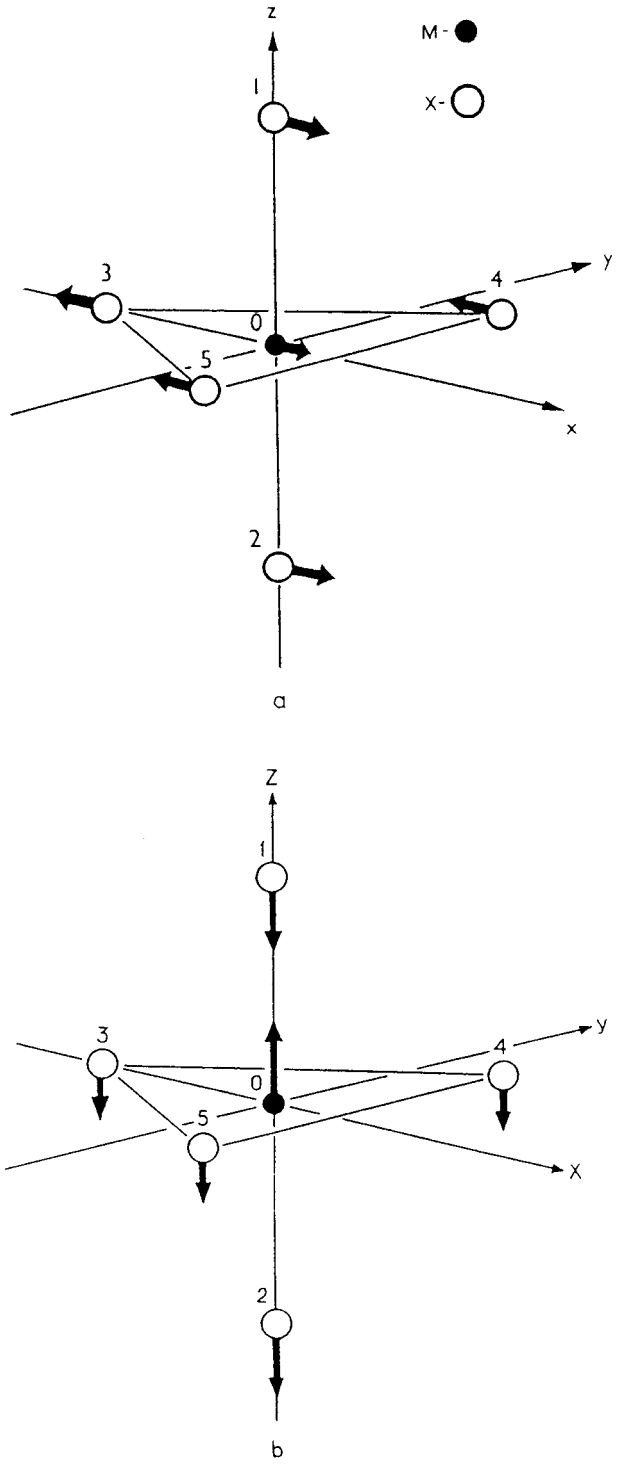

Figure 44. Symmetrized distortions in MX_5 systems with D_{3h} symmetry: (a) E′-type displacements realizing TBP → SP conversion; (b) A'_2-type displacements realizing the transformation MX_5 (TBP) → MX_4 (tetr.) + X. (Reprinted with permission from ref 25. Copyright 1996 John Wiley & Sons, Inc.)

(formed from the 3s AO of the equatorial atoms) to the $5a_1'$ MO. This latter is occupied by one electron in I and two electrons in II, and therefore, in the Zn complex there is no contribution of this $1e' \rightarrow 5a_1'$ excited state.

Although the energy gap to this E′ term in I is large, the PJTE on the E′ displacements is rather strong because of the relatively large vibronic constant $F^{(A'E'')}$ of the mixing of the A_1' and E′ states under consideration, which, in turn, is due to the strong changes in the above MO by the distortion of the TBP configuration. Indeed, in the TBP configuration the overlap of the $5a_1'$ and 1e′ orbitals is zero by symmetry restrictions, and hence, these orbitals do not contribute to the metal−ligand bonding. The E′ nuclear displacements lower the D_{3h} symmetry of the system to C_{2v}. As a result, the e′ MO splits into a_1 and b_2 while the $5a_1'$ one transforms to a_1. Now the overlap of a_1 (e′) and a_1 ($5a_1$) is nonzero, resulting in additional bonding of the AO $3d_{z^2}$ of the copper atom with the AO's 3s of the three equatorial ligands. This effect is not possible in II.

The second active excited E′ term is formed by the promotion of one electron from the same occupied MO 1e′ to the virtual MO $6a_1'$ that has the predominant contribution of the AO 4s of the metal. Despite large energy gaps $E(6a_1') - E(1e')$ equal to 25.0 eV in I and 21.6 eV in II, the vibronic constants are also quite significant and the corresponding negative contribution to the curvature (although somewhat smaller than for $1e' \rightarrow 5a_1'$) is of the same order of magnitude as from the first excited E′. This result is also due to the essential changes in the chemical bonding produced by the 1e′ and $6a_1$ mixing by distortion. Similar to the previous case, the overlap of 1e′ with $6a_1'$ in the TBP configuration is zero by symmetry; the E′ distortion makes it nonzero, resulting in an additional chemical bonding between the metal AO 4s and the appropriate combination of AO's 3s of the equatorial ligands as stipulated by the general theory (section II.C).

Similar analysis explains the PJT contribution of other excited states.[381]

To conclude whether the negative vibronic contribution K_v results in instability, the nonvibronic contribution K_0 must be calculated. The semiempirical method used in refs 381 and 382 does not allow one to do that: for calculation of K_0, the values of the wave function at the nuclei $\psi(0)$ are required. Nevertheless, the computational data allowed the authors to estimate the relative instabilities induced by the vibronic coupling in different symmetrized directions of the same system, for which the K_0 value in its part depending on $\psi(0)$ can be assumed to be the same. One can compare the vibronic instabilities of the same system, I or II, with respect to the two possible distortions, E′ and A_2''. The contribution of the closed-shell core electrons (and all the ns electrons) that make the $\psi(0)$ quantity nonzero are assumed to be the same for both distortions, whereas the contributions of the d hole to these two displacements are different. Fortunately the d state contributions K_o^d to K_o can be easily calculated.[381] The hole in the d^{10} configuration is d_{z^2}, and K_o^d is negative for E′ distortions and positive for A_2'' (the opposite signs are due to the field gradient created by the d_{z^2} hole, which is positive in the *z* direction and negative in the *xy* plane).

The data in Tables 19 and 20 show explicitly that the $CuCl_5^{3-}$ complex is more unstable with respect to the E′ distortion that transforms the TBP configuration into SP (or near SP) (Figure 44a), whereas

Table 19. Excited States of E′ and A_2'' Symmetry Produced by One-Electron Excitations $j \rightarrow k$, Energy Gaps $\Delta = E(k) - E(j)$, Orbital Vibronic Constants $F^{(oi)}$, and Vibronic Contributions $K_v^{(i)}$ and $K_0^{(d)}$ to the Relative Value of the Force Constant K_{Rel} for the E′ and A_2'' Displacements in $CuCl_5^{3-}$ (TBP configuration)[381]

	$j \rightarrow k$	Δ eV	$F^{(oi)}$ 10^{-4} dyn	$K_v^{(i)}$ mdyn/Å	$K_v - \Sigma_i K_v^{(i)}$ mdyn/Å	$K_0^{(d)}$ mdyn/Å	$K_{rel} = K_0^{(d)} + K_v$ mdyn/Å
E′	$1e' \rightarrow 5a_1'$	11.225.0	9.03	−0.91			
	$1e' \rightarrow 6a_1'$	23.9	12.24	−0.75			
	$1a_{1'} \rightarrow 6e''$	2.8	10.44	−0.57			
	$5e' \rightarrow 5a_1'$	12.1	0.58	−0.015			
	$5a_1' \rightarrow 6e'$		1.87	−0.036			
					−2.28	−0.35	−2.63
$A_{2''}$	$1a_2'' \rightarrow 6a_1'$	24.4	11.68	−0.70			
	$3a_2'' \rightarrow 6a_1'$	14.4	6.87	−0.41			
	$1a_1' \rightarrow 4a_2''$	26.5	7.97	−0.30			
	$1a_2'' \rightarrow 5a_1'$	10.6	8.63	−0.88			
	$3a_2'' \rightarrow 5a_1'$	0.8	1.72	−0.46			
					−2.75	0.55	−2.20

Table 20. Excited States of E′ and A_2'' Symmetry Produced by One-Electron Excitations $j \rightarrow k$, Energy Gaps $\Delta = E(k) - E(j)$, Orbital Vibronic Constants $F^{(oi)}$, and Vibronic Contributions $K_v^{(i)}$ to the Relative Value of the Force Constant K_{Rel} for the E′ and A_2'' Displacements in $ZnCl_5^{3-}$ (TBP configuration)[381]

	$j \rightarrow k$	Δ eV	$F^{(oi)}$ 10−4 dyn	$K_v^{(i)}$ mdyn/Å	$K_v^{(i)} = \Sigma_i K_v^{(i)}$ mdyn/Å
E′	$1e' \rightarrow 6a_1'$	21.6	11.61	−0.78	
	$1a_1' \rightarrow 6e'$	24.4	10.07	−0.52	
					−1.30
A_2''	$1a_2'' \rightarrow 6a_1'$	20.7	10.84	−0.71	
	$3a_2'' \rightarrow 6a_1'$	11.3	6.16	−0.42	
	$1a_1' \rightarrow 4a_2''$	26.9	8.92	−0.37	
					−1.51

in $ZnCl_5^{3-}$ the instability is stronger with respect to the A_2'' distortion that describes the transformation of the TBP configuration toward a distorted tetrahedron plus one ligand on the trigonal axis at a larger distance (Figure 44b), in full qualitative agreement with the experimental data, mentioned above.

These examples show how the electronic structure of the ground and excited states control the nuclear configuration making it, under certain conditions, unstable with respect to nuclear displacements of specific symmetry.

As mentioned above, the instability of the TBP configuration of the $CuCl_5^{3-}$ cluster with respect to E′ distortions results in three equivalent almost square-planar configurations with a relatively small energy barrier between them resulting in internal pseudo-rotations. Seemingly similar pseudo-rotations take place in many other molecular systems, and PF_5 is one of the well-known examples. Experimental data and calculations (see refs 388 and 389 and references therein) show that this system has equivalent TBP configurations with a barrier of about 0.17 eV between them at the C_{4v} symmetry and performs the so-called Berry pseudo-rotations. The latter is thus significantly different from the pseudo-rotations in the JT $CuCl_5^{3-}$ system (see ref 25 for more details). The PF_5 system can be regarded as an unstable C_{4v} configuration due to the PJTE. To my knowledge the exploration of such a possibility was not reported as yet.

2. Octahedral Systems

The number of studied JT octahedral systems is innumerable. The majority of them come from *transition-metal coordination compounds mostly in the crystalline state*. As mentioned in section I, the latter is *not reviewed in this article*. Many examples can be found in some earlier reviews on the JTE[1−33] including the bibliographic review.[11]

For examples of more recent work, ab initio SCF and correlated pair functional (CPF) calculations[390] of the APES of the octahedral systems of $Cu(H_2O)_6^{2+}$, $Cr(H_2O)_6^{2+}$, and $Mn(H_2O)_6^{3+}$ in their ground E state (JT E⊗e problem) show that they are tetragonally distorted at the minima with the ratio of, respectively, axial to equatorial $(Cu-O_{ax})/(Cu-O_{eq})$ distances (in Å) of 2.25/2.05, 2.36/2.15, and 2.15/1.99, JT stabilization energy E_{JT} (cm^{-1}) = 930, 749, and 1170, and energy barrier between the minima δ(cm^{-1}) = 136, 256, and 193. These energy values are much lower than those experimentally observed.

For $M(H_2O)_6^{3+}$ with M = Zn, Cd, and Hg, where the ground state is nondegenerate, a PJT coupling to the excited state was revealed using Hartree−Fock and effective core potential calculations.[391] The results show a rather flat potential in these systems that explains the softness of, e.g., the Hg−O bonds and a large spread in their mean values (see also the plasticity effect[25,29]). The JTE in hydrated transition-metal ions definitely influences the water-exchange reactions.[392] The change of the PJTE in the CrF_6^{3-} ion in $(NH_4)_3[CrF_6]$ under pressure that changes the energy gap Δ between the PJT mixing states was demonstrated in ref 393. The role of the PJTE in understanding enzymatic catalysis is discussed in ref 394.

For some gas-phase octahedral systems the discussion of the JT origin of their properties is continuing. A sound example is XeF_6 and isoelectronic systems. There is a rather long history of electronic structure investigation of these systems (see refs 395−402 and references therein). In principle, the PJT mixing of the ground nondegenerate A_{1g} state (formed by the two ns electrons that occupy the antibonding MO)

with the low-lying excited T_{1u} states (formed by the $A_{1g} \rightarrow t_{1u}$ excitation to the t_{1u} MO that originates from the np states) may lead to the trigonal (T_{1u} type) distortion of the octahedron, provided the inequality in eq 31 holds.[25,102] This PJT distortion may be complicated by the proper JTE on the degenerate T_{1u} state.

Dependent on relations between the coupling parameters,[25,102] the resulting distortion of the octahedral configuration are (a) combined PJT dipolar T_{1u} with JT either tetragonal E_g or trigonal T_{2g} distortions; this is the so-called stereochemically active lone pair effect; (b) pure JT either tetragonal or trigonal distortions (when the JTE on the excited T_{1u} term dominates over the PJTE); (c) no distortions (regular octahedra) when neither the PJTE nor the excited state JTE are sufficiently strong (inert lone pairs).

Ab initio and other calculations[395−402] and experimental data (see in ref 401) confirm this qualitative prediction: XeF_6, SeF_6^{2-}, and IF_6^- are trigonally distorted, ClF_6^-, BrF_6^-, and $BiCl_6^{3-}$ seem to be regular octahedra (in the condensed phase), while $SeCl_6^{2-}$, $SeBr_6^{2-}$, $TeCl_6^{2-}$, and TeI_6^{2-} may be either distorted or regular octahedra dependent on the counterions (the environment may stabilize the pseudo-rotations). PJT polar distortions in theTiO_6^{8-} clusters in $BaTiO_3$ explain the origin of ferroelectricity in this and similarly in other crystals (see the review article in ref 33).

The mixed distortions, mentioned above, are most important in explaining the origin of complicated (helicoidal) crystal structures and chirality.[403,404] In particular, in the InCl crystal ($InCl_6^{5-}$ clusters), both types of combined dipolar distortions, dipolar T_{1u} plus trigonal T_{2g} and dipolar T_{1u} plus tetragonal E_g, are observed in two phases of the crystal, yellow and red, respectively.[403,404]

Recent more elaborate calculations of the electronic structure of some of the above systems[401] shows that correlation and relativistic effects diminish the PJT distortions stabilizing nondistorted octahedral configurations (for this reason RuF_6, AtF_6^-, and PoF_6^{2-} emerge as regular octahedra). This result seems to be quite reasonable: higher symmetry favors a more correlated electron distribution (and this will be reflected directly in the vibronic coupling constants of the PJTE), while the relativistic contraction of the ns electrons increases the $A_{1g}-T_{1u}$ energy gap Δ; both of these factors decrease the PJTE contribution to the softening of the system with respect to distortions (eq 31) as well as the possible contribution of the JTE in the excited T_{1u} state.[102,25] The authors[401] claim that "none of the available simple models... is able to predict or rationalize all these structures". This statement is at least ungrounded: the PJTE contains the necessary tool that qualitatively explains all these structural observations. The authors[401] just did not try this possibility for which the estimation of the excited states and vibronic coupling constants would be required.

The JTE in Cu(II) in macrobiocyclic cage complexes studied by EPR methods is reported in refs 405 and 406. A similar study of Ag(II) in a variety of six-coordinated systems is described in ref 407. The JTE in Ni_6 clusters is discussed in ref 408.

Here we mention several topics which, although related directly to the JTE in crystal structures (not discussed in this review article, see section I.B), seem to be of interest in use for molecular systems. The Lanczos method[409] and the related recursion method,[410,411] widely employed in numerical calculations, were applied to a series of JT problems in localized centers in crystals.[49,412−415] Elongated versus compressed octahedra of Cu(II) in crystalline environment are discussed in ref 416. Vibronic coupling constants were calculated for octahedral MF_6 systems, $M = Mn^{2+}$, Cr^{3+}, mostly in a crystalline environment[417,418] and for tetrahedral FeO_4^{2-} and CrO_4^{4-} in oxides.[419] The relation between JTE and Kondo effect is considered in ref 420. Multiwell potentials of complexes with icosahedral symmetry are discussed in ref 421.

The method of pulsed neutron diffraction measurements was applied to a series of transition-metal ceramics of primary interest to high-temperature superconductivity in order to reveal the local distortions around Cu and Mn centers.[422−424] It is shown that the JT distortions are locally present even when the crystallographic structure suggests otherwise; the local distortions are observed even in the metallic phase. These results, in addition to their general importance, also demonstrate how the JT distortions can be observed in conditions when many other methods fail because of the JT dynamics and crystalline environment (somewhat similar to the EXAFS methods[425]). A view on the JT vibronic coupling effects in high-temperature superconductivity theory is given in ref 426. PJT origin of local instabilities and formation of stripes is considered in ref 427.

F. Other Related Problems

There are many other fields of chemistry where the ideas of the JT, PJT, and RT effects are employed, and we just mention here some of them as a link accompanied by references where the reader may find detailed accounts. We remind the reader that, as indicated in section I.B, a great deal of very important fields of JT vibronic coupling effects (mostly in local and cooperative phenomena in crystalline states) are excluded from this review. More global relations to other problems,[35−43] mainly in physics, are mentioned in section I.A.

1. Electron Delocalization in Exchange-Coupled Mixed-Valence Compounds

This is an important problem with applications as molecular magnets, redox catalysts, models of metalloenzymes, local interactions in semiconductors and superconducting ceramics, molecular electron devices, etc., in which the intercenter localization−delocalization alternative plays one of the main roles. By localizing an excess electron on one of the centers of such polycenter compounds, we change its electronic state and vibronic coupling to the nuclear displacements of the near-neighbor environment. Together with the structure of the bridge between the centers, this vibronic coupling determines the rate

of electron delocalization and all the related optical, magnetic, and redox properties. Obviously, the JT and PJT coupling (especially the latter) may be most important in these effects,[17] and the great variety of work devoted to this problem (see in refs 11, 17, 25, 116, and 428−443) confirms this statement.

2. Degenerate Vibronic Coupling Effects in Scattering Processes

Although qualitatively the possible implications of degenerate states in scattering processes due to the JT coupling were understood long ago, the relevant calculations began just recently. It came out that the vibronic coupling implications are most essential. For references, see refs 444−447 and references therein.

3. Others

For the generation of chirality via JTE using polarized light, see ref 448. Cooperative PJTE effects in chirality formation are discussed in refs 449 and 450. The PJT interaction between two chain structures resulting in Payerls-type charge-density waves is considered in ref 451.

IV. Conclusions

A brief outline and some generalizations of the latest achievements in the theory and applications of the JTE, PJTE, and RTE (jointly JT vibronic effects) to molecular systems is given in this review. This paper does not consider a variety of important JTE in application to localized and cooperative solid-state problems such as crystal lattice defects and impurities, ferroelectricity, superconductivity, and colossal magnetoresistance.

The most general conclusion from this review is that the *JT vibronic effects are not just specific effects restricted to a narrow group of systems* with a degenerate electronic state as it is usually presented in the literature. In fact, the *JT vibronic coupling theory is an approach to the investigation of any polyatomic system* without a priori exceptions.

From the point of view of modern theoretical and computational chemistry, the JT vibronic theory is an important extension which allows one to *rationalize the data* (obtained by numerical computation) based on physically sound models. For the large variety of molecular systems reviewed in this paper, the physical meaning of the results of numerical calculations cannot be elucidated without involving the JT theory.

The novel aspects of JT vibronic theory include several achievements of the last 1−2 decades.

An important extension of the theory was reached when it was shown that the strong PJT coupling to the excited states is not only *sufficient* for the instability of the ground state, but it is also the *necessary condition* of such instability, thereby making all unstable high-symmetry systems subjects to the PJTE.

Essential results were achieved in elucidation of the role of conical intersections and the Berry phase implications in the theory of JT vibronic coupling. In particular, the *paradigm* that the ground vibronic state should have the same degeneracy and symmetry as the initial electronic state was reversed by the results of direct numerical solutions of the vibronic coupling equations and explanation of the results based on the analysis of the conical intersections and tunneling splitting. Further developments in the theory of JT distortions, tunneling splitting, and vibronic reduction factors were reported.

Increasing applications of the JT theory to icosahedral systems was inspired by the discovery of fullerenes.

Many stimulating results and developments of the JT vibronic theory were possible due to further achievements of the experimental methods involved in its investigation, especially to new techniques in spectroscopy, such as optical−optical double resonance with high-resolution resonant two-photon ionization in jet-cooled supersonic beam expansion. Sound examples are given in the papers devoted to small molecules in the gas phase, e.g., Na_3. Further developments are expected in the interpretation of JT-induced reactivity and chemical activation.

Finally, the JT-type instability may serve as a basis for a wider understanding of the origin of symmetry breaking in condensed matter in a time and temperature scale. Speculatively, the present state of matter can be regarded as resulting from a sequence of symmetry breaking triggered by JT- and/or PJT-type instability.

V. Acknowledgments

This publication is based in part upon work supported by Texas Advanced Research Program under Grant No. 003658-345. I am grateful to all the persons who sent me reprints and preprints of their publications on my request.

VI. Abbreviations

APES	adiabatic potential energy surface
BLYP	Becke−Lee−Yang−Parr (DFT functional)
CASSCF	complete active space SCF
CI	configuration interaction
CPF	correlated pair functional
DFT	density functional theory
GVB	generalized valence bond
HF	Hartree−Fock
HOMO	highest occupied MO
JT	Jahn−Teller
JTE	Jahn−Teller effect
LSD	local spin density
LUMO	lowest unoccupied MO
MO	molecular orbital
MP	Möller−Plesset (perturbation theory)
MRCI	multireference CI
MRSDCI	MRCI with single and double excitations
PE	photoelectron spectrum
PJTE	pseudo-JTE
QCISD	quadratic CI with single and double excitations
ROHF	restricted open-shell HF
RTE	Renner−Teller effect
SB	symmetry breaking
SCF	self-consistent field
UQCISD	unrestricted QCISD
ZEKE	zero-electron kinetic energy

VII. References

(1) Bersuker, I. B.; Polinger, V. Z. *Vibronic Interactions in Molecules and Crystals*; Springer: New York, 1989.
(2) Englman, R. *The Jahn−Teller Effect in Molecules and Crystals*; Wiley: London, 1972.
(3) Bersuker, I. B. *The Jahn−Teller Effect and Vibronic Interactions in Modern Chemsitry*; Plenum: New York, 1984.
(4) Fischer, G. *Vibronic Coupling: The Interaction Between the Electronic and Nuclear Motions*; Academic Press: London, 1984.
(5) Kaplan, M. D.; Vekhter, B. G. *Cooperative Phenomena in Jahn−Teller Crystals*; Plenum Press: New York, 1995.
(6) Köppel, M.; Domcke, W.; Cederbaum, L. S. *Adv. Chem. Phys.* **1984**, *57*, 59.
(7) *Dynamical Jahn−Teller Effect in Localized Systems*; Perlin, Yu. E., Wagner, M., Eds.; Elsevier: Amsterdam, 1984.
(8) Ham, F. S. In *Electron Paramagnetic Resonance*; Geschwind, S., Ed.; Plenum: New York, 1972; p. 1−484.
(9) Ballhausen, C. J. In *Vibronic Processes in Inorganic Chemistry*; Flint, C. D., Ed.; Kluwer: Dordrecht, 1989; p 53
(10) Bersuker, I. B.; Vekhter, A. G.; Ogurtsov, I. Ya. *Uspekhi Fiz. Nauk (Sov. Phys.-Uspekhi)*, **1975**, *116*, 605.
(11) *The Jahn−Teller Effect. A Bibliographic Review*; Bersuker, I. B., Ed.; IFI/Plenum: New York, 1984; pp 1−590.
(12) *Vibronic Processes in Inorganic Chemistry*; Flint, C. D., Ed.; Kluwer: Dordrecht, 1989.
(13) Sturge, M. D. *The Jahn−Teller Effect in Solids*, In *Solid State Physics*; Seitz, F., Turnbull, D., Ehrenreich, H., Eds.; Academic Press: New York, 1967; Vol. 20.
(14) Ceulemans, A.; Vanquickenbourne, L. G. *Struct. Bonding* **1989**, *71*, 125.
(15) Reinen, D.; Friebel, C. *Struct. Bonding (Berlin)* **1979**, *37*, 1.
(16) Reinen, D.; Atanasov, M. *Magn. Reson. Rev.* **1991**, *15*, 167.
(17) Bersuker, I. B.; Borshch, S. A. In *Advances in Chemical Physics*; Prigogine, I., Rice, S. A., Eds.; Wiley: New York, 1992; Vol. 81, pp 703−782.
(18) Burdett, J. K. *Molecular Shapes. Theoretical Models of Inorganic Stereochemistry*; Wiley: New York, 1980
(19) Bersuker, I. B. *Coord. Chem. Rev.* **1975**, *14*, 357
(20) Whetten, R. L.; Ezra, G. S.; Grant, E. R. *Annu. Rev. Phys. Chem.* **1985**, *36*, 277.
(21) Bersuker, I. B.; Stavrov, S. S. *Coord. Chem. Rev.* **1988**, *8*, 1.
(22) Levin, A. A. In *Soviet Science Reviews B, Chemistry Reviews*; Vol'pin, M. E., Ed.; Harwood: 1987; Vol. 9, p 279; *New J. Chem.* **1993**, *17*, 31.
(23) Bersuker, I. B.; Ogurtsov, I. Ya. *Adv. Quantum Chem.* **1986**, *18*, 1.
(24) Sugano, S.; Tanabe, Y.; Kamimura, H. *Multiplets of Transition Metal Ions in Crystals*; Academic Press: New York, 1970.
(25) Bersuker, I. B. *Electronic Structure and Properties of Transition Metal Compounds. Introduction to the Theory*; Wiley: New York, 1996.
(26) Ceulemans, A. *Top. Curr. Chem.* **1994**, *171*, 27.
(27) Chancey, C. C.; O'Brien, M. C. M. *The Jahn−Teller Effect in C60 and other Icosahedral Complexes*; Princeton University Press: Princeton, NJ, 1997.
(28) Bersuker, I. B. *J. Coord. Chem.* **1995**, *34*, 289.
(29) Gažo, J.; Bersuker, I. B.; Garaj, J.; Kabesova, M.; Kohout, J. Langfelderova, M.; Melnik, M.; Serator, M.; Valach, F. *Coord. Chem. Rev.* **1976**, *19*, 253.
(30) *Electron−Phonon Dynamics and Jahn−Teller Effects*; Bevilacqua, G., Martinelli, L., Terzi, N., Eds.; World Scientific: Singapore, 1999.
(31) Watkins, G. D. In *Deep Centers in Semiconductors*; Pantelides, S. T., Ed.; Gordon and Breach: New York, 1986; p 147.
(32) Barckholtz, T. A.; Miller, T. A. *Int. Rev. Phys. Chem.* **1998**, *17*, 435.
(33) Bersuker, I. B. *Ferroelectrics* **1995**, *164*, 75.
(34) Schastnev, P. V.; Schegoleva, L. N. *Molecular Distortions in Ionic and Excited States*; CRC Press: New York, 1995.
(35) Eberhart, M. E.; Johnson, K. H.; Adler, D.; O'Handley, R. C. *Non-Cryst. Solids* **1986**, *83*, 12.
(36) Bersuker, I. B. *Ferroelectrics* **1989**, *95*, 51.
(37) Bersuker, I. B. *Teor. Eksp. Khim.* **1991**, *27*, 261.
(38) Englman, R.; Yahalom, A. In *NATO Advance Research Workshop*; Kaplan, M. D., Zimmerman, G., Eds.; Kluwer: Dordreht, 2001, to be published.
(39) Weinberg, S. *Quantum theory of Fields*; University Press: Cambridge, 1995, Ch. 11.
(40) Slonczewski, J. S. *Phys. Rev.* **1963**, *131*, 1596.
(41) Abulaffio, C.; Irvine, J. *Phys. Lett.* **1972**, *B38*, 492.
(42) Judd, B. R. *Can. J. Phys.* **1974**, *52*, 999.
(43) Lee, B. S. *J. Phys. A*, **1976**, *9*, 573. Allen, L.; Eberly, J. H. *Optical Resonance and Two-Level Atoms*; Wiley: New York, 1975.
(44) Jahn, H. A., Teller, E. *Proc. R. Soc.* **1937**, *161*, 220.
(45) O'Brien, M. C. M. *J. Phys. A.* **1989**, *22*, 1779.
(46) Ham, F. S. *J. Phys.: Condens. Matter* **1990**, *2*, 1163.
(47) Sobolewski, A. L.; Domcke, W. *Chem. Phys.* **2000**, *259*, 181. Ferretti, A.; Lami, A.; Villani, G. *Chem. Phys.* **2000**, *259*, 201. Mahapatra, S.; Köppel, H.; Cederbaum, L. S.; Stampful, P.; Wenzel, W. *Chem. Phys.* **2000**, *259*, 211. Ben-Nun, M.; Martinez, T. J. *Chem. Phys.* **2000**, *259*, 237. Bornemann, C.; Klessinger, M. *Chem. Phys.* **2000**, *259*, 263. Fui, W.; Haas, Y.; Zilberg, S. *Chem. Phys.* **2000**, *259*, 273. Trushin, S. A.; Fui, W.; Schmid, W. E. *Chem. Phys.* **2000**, *259*, 313. Baer, M. *Chem. Phys.* **2000**, *259*, 123. Sadygov, R. G.; Yarkony, D. R. J. *Chem. Phys.* **1999**, *110*, 3639.
(48) Boudon, V.; Michelot, F.; Moret-Bailly, J. *J. Mol. Spectrosc.* **1994**, *166*, 449. Boudon, V.; Rotger, M.; Avignant, D. *J. Mol. Spectrosc.* **1996**, *175*, 327.
(49) Bevilacqua, G.; Martinelli, L.; Parravicini, G. P. *J. Phys: Condens. Matter* **1998**, *10*, 10347.
(50) Bersuker, I. B. *Opt. Spectrosc.* **1961**, *11*, 319; *Zh. Eksp. Teor. Fiz.* **1962**, *43*, 1315 (*Engl. transl.*: *Sov. Phys.−JETP* **1963**, *16*, 933).
(51) Badran, R. I.; Bates, C. A. *J. Phys.: Condens. Matter* **1991**, *3*, 6329.
(52) Koizumi, H.; Bersuker, I. B. *Phys. Rev. Lett.* **1999**, *83*, 3009.
(53) Zwanziger, W.; Grant, E. R. *J. Chem. Phys.* **1987**, *87*, 1954
(54) Davidson, E. R. *J. Am. Chem. Soc.* **1977**, *99*, 397.
(55) Davidson, E. R.; Borden, W. T. *J. Am. Chem. Soc.* **1983**, *87*, 4783.
(56) (a) Krempl, S.; Winterstetter, M.; Domcke, W. J. *Chem. Phys.* **1995**, *102*, 6499. (b) Ceulemans, A.; Chibotaru, L. F. *Theor. Chim. Acta* **1996**, *94*, 205.
(57) Bacci, M. *Phys. Rev. B.* **1978**, *17*, 4495
(58) Bersuker, I. B.; Polinger, V. Z. *Phys. Lett.* **1973**, *44A*, 495; *Zh. Eksp. Teor. Fiz* (*Sov. Phys.-JETP*) **1974**, *66*, 2078.
(59) Bacci, M.; Mihokova, E. Polak, K. *Phys. Rev. B.* **1997-I**, *55*, 14257. Bacci, M.; Porcinai, S. In ref 30, p 3.
(60) Ceulemans, A.; Qui, Q. C. *Phys. Rev. B.* **2000-II**, *61*, 10628.
(61) Dunn, J. L.; Bates, C. A.; Kirk, P. J. *J. Phys.: Condens. Matter* **1990**, *2*, 10379
(62) Polinger, V. Z.; Bates, C. A.; Dunn, J. L. *J. Phys.: Condens. Matter* **1998**, *10*, 1293.
(63) Simpson, J. A. L.; Bates, C. A.; Dunn, J. L. *J. Phys.: Condens. Matter* **1991**, *3*, 6845.
(64) Liu, Y. M.; Bates, C. A.; Dunn, J. L.; Polinger, V. A. *J. Phys.: Condens. Matter* **1996**, *8*, L523.
(65) Polinger, V. Z.; Kirk, P. J.; Dunn, J. L.; Bates, C. A. *J. Phys.: Condens. Matter* **1993**, *5*, 2213.
(66) Polinger, V. Z.; Bates, C. A.; Dunn, J. L. *Zs. Phys. Chem.* **1997**, *200*, 255.
(67) Polinger, V. Z.; Bates, C. A.; Dunn, J. L. *J. Phys.: Condens. Matter* **1991**, *3*, 513.
(68) Bates, C. A.; Dunn, J. L.; Hallam, L. D.; Kirk, P J. Polinger, V. Z. *J. Phys.: Condens. Matter* **1991**, *3*, 3441. Bates, C. A.; Dunn, J. L.; Polinger, V. Z.; Hallam, L. D.; Kirk, P. J.; Jamila, S. *Mater. Sci. Forum* **1992**, *83−87*, 487.
(69) Koizumi, H.; Bersuker, I. B.; Boggs, J.; Polinger, V. Z. *J. Chem. Phys.* **2000**, *112*, 8470.
(70) Khlopin, V. P.; Polinger, V. Z.; Bersuker, I. B. *Teor. Chim. Acta.* **1978**, *48*, 87.
(71) Pooler, D. R. *J. Phys. C: Solid Phys.* **1980**, *13*, 1029.
(72) Ceulemans, A.; Fowler, P. W. *Phys. Rev. A.* **1989**, *39*, 481.
(73) Ceulemans, A.; Fowler, P. W. *J. Chem. Phys.* **1990**, *93*, 1221.
(74) Cullerne, J. P.; O'Brien, M. C. M. *J. Phys.: Condens. Matter* **1994**, *6*, 9017.
(75) Ceulemans, A.; Fowler, P. W. *J. Chem. Soc., Faraday Trans.* **1992**, *88*, 2797.
(76) Cullerne, J. P.; Angelova, M. N.; O'Brien, M. C. M. *J. Phys.: Condens. Matter* **1995**, *7*, 3247.
(77) Dunn, J. L.; Bates, A. C. *Phys. Rev. B.* **1995**, *52*, 5996.
(78) Ceulemans, A.; Chibotaru, L. F. *Phys. Rev. B.* **1996-I**, *53*, 2460.
(79) Chibotaru, L. F.; Ceulemans, A. *Phys. Rev. B.* **1996**, *53*, 15522.
(80) Moate, M. C. P.; O'Brien, M. C. M.; Dunn, J. L.; Bates, C. A.; Liu, Y. M.; Polinger, V. Z. *Phys., Rev. Lett.* **1996**, *77*, 4362.
(81) Ceulemans, A.; Chihotaru, L. F. Cimpoesu, F. *Phys. Rev. Lett.* **1997**, *78*, 3725.
(82) Auerbach, A.; Manini, N.; Tosatti, E. *Phys. Rev. B.* **1999**, *49*, 12998.
(83) Chibotaru, L. F.; Ceulemans, A.; Cojocaru, S. P. *Phys. Rev B.* **1999-II**, *59*, R12728.
(84) Sobolewski, A. L. *Chem. Phys. Lett.* **1997**, *267*, 452.
(85) Judd. B. R. *Adv. Chem. Phys.* **1984**, *57*, 247.
(86) Wang, C.-L. In ref 30, p 280.
(87) Negri, F.; Orlandi, G. In ref 30, p 264
(88) Borshch, S. A. Prassides, K. *J. Phys. Chem.* **1996**, *100*, 9348.
(89) Dunn, J. L.; Eccles, M. R.; Moate, C. P.; Liu, Y. M.; Bates, A. C. In ref 30, p 241. Moate, C. P.; Liu, Y. M.; Dunn. J. L.; Bates, A. C. In ref 30, p 258. Qiu, Q. C.; Dunn, J. L.; Bates, A. C. Liu, Y. M. In ref 30, p 273.
(90) Chibotaru, L. F.; Ceulemans, A. In ref 30, p 233.
(91) Röthlisberger, U.; Andreoni, W.; Giannozzi, P. *J. Chem Phys.* **1992**, *96*, 1248.
(92) Pickett, W. E. In *Solid State Physics*; Ehrenreich, H., Spaepen, F., Eds.; Academinc Press: San Diego, 1994; Vol. 48, p 225.

(93) Lanoo, M.; Baraft, G. A.; Schliiter, M.; Tomanek, D. *Phys. Rev. B*. **1991**, *44*, 12106.
(94) Coulon, de V.; Martins, J. L.; Reuse, F. *Phys. Rev. B*. **1992**, *45*, 13671.
(95) Gu, B.; Li, Z.; Zhu, J. *J. Phys.: Condens. Matter* **1993**, *5*, 5255.
(96) Liu, Y. M.; Dunn, J. L.; Bates, C. A.; Polinger, V. A. *J. Phys.: Condens. Matter* **1997**, *9*, 7119. Oliete, P. B.; Bates, C. A.; Dunn, J. L.; Stedman, G. E. *Phys. Rev. B*. **1999-II**, *60*, 2319. Qiu, Q. C.; Dunn, J. L.; Bates, C. A.; Abou-Ghantous, M.; Polinger, V. Z. *Phys. Rev. B*. submitted for publication.
(97) Breda, N.; Broglia, R. A.; Colo, G.; Roman, H. E.; Alasia, F.; Onida, G.; Ponomarelli, V.; Vigezzi, E. *Chem. Phys. Lett*. **1998**, *286*, 350. Colo, G.; Breda, N.; Broglia, R. A.; Provasi, D.; Roman, H. E.; Onida, G.; Vigezzi, E. In ref 30, p 241. Wiseman, R. D. In ref 30, p 47.
(98) Bersuker, I. B.; Gorinchoi, N. N.; Polinger, V. Z. *Teor. Chim. Acta* **1984**, *66*, 161.
(99) Bersuker, I. B.; Polinger, V. Z.; Gorinchoi, N. N. *J. Struct. Chem. (THEOCHEM)* **1992**, *5*, 369. Bersuker, I. B. *New J. Chem*. **1993**, *17*, 3.
(100) Bader, R. F. W. *Mol. Phys*. **1960**, *3*, 137. Bader, R. F. W. *Can. J. Chem*. **1962**, *40*, 1164. Bader, R. F. W.; Bandrauk, A. D. *J. Chem. Phys*. ***1968***, *49*, 1666.
(101) Bersuker, G. I.; Polinger, V. Z. *Chem. Phys.*, **1984**, *86*, 57.
(102) Maaskant, W. J. A.; Bersuker, I. B. *J. Phys.: Condens. Matter* **1991**, *3*, 337.
(103) Bersuker, I. B. *Nouv. J. Chim*. **1980**, *4*, 139. Bersuker, I. B. *Teor. Eksp. Khim*. **1980**, *16*, 291. Bersuker, I. B. *Pure Appl. Chem*. **1988**, *60*, 1167. Bersuker, I. B. *Fiz. Tverdogo Tela* **1988**, *30*, 1738.
(104) Chibotary. L. F.; Chimpoesu, F. *Int. J. Quantum Chem*. **1997**, *65*, 37.
(105) Renner, R. *Z. Phys*. **1934**, *92*, 172.
(106) Gerzberg, G.; Teller, E. *Z. Phys. Chem*. **1933**, *B21*, 410.
(107) Pople, J. A.; Longuet-Higgins, H. C. *Mol. Phys*. **1958**, *1*, 372.
(108) Dixon, R. N. *Mol. Phys*. **1965**, *9*, 357.
(109) Petelin, A. N.; Kiselev. A. A. *Int. J. Quantum Chem*. **1972**, *6*, 701.
(110) Jungen, Ch.; Merer, A. J. In *Molecular Spectroscopy: Modern Research*; Rao, K. N., Ed.; Acadmic Press: New York, 1976; Vol. 2, p 127.
(111) Köppel, H.; Domcke, W.; Cederbaum, L. S. *J. Chem. Phys*. **1984**, *74*, 2945.
(112) Brown, J. M.; Jorgensen, F. *Adv. Chem. Phys*. **1983**, *52*, 117.
(113) Peric, M.; Engles, E. Peyerimhoff, S. D. In *Quantum Mechanical Electronic Structure Calculations with Chemical Accuracy*; Langhoff, S. R., Ed.; Kluwer: Dordrecht, 1995; p 261.
(114) Bersuker, I. B. *Kinet. Katal*. **1977**, *18*, 1268. Bersuker, I. B. *Chem. Phys*. **1978**, *31*, 85. Bersuker, I. B. *Teor. i Exp. Khim*. **1978**, *14*, 3. Bersuker, I. B. In *(IUPAC) Coordination Chemistry–20*; Banerjea, D., Ed.; Pergamon Press: Oxford and New York, 1980; p 201.
(115) Stavrov, S. S.; Decusar, I. P.; Bersuker, I. B. *New J. Chem*. **1993**, *17*, 71.
(116) Piepho, S. B. *J. Am. Chem. Soc*. **1988**, *110*, 6319, In *Mixed-Valence Systems: Applications in Chemistry, Physics and Biology*; Prassides, K., Ed.; Kluwer: Dordrecht, 1991; p 329.
(117) Letelier, J. R. *Int.. J. Mod. Phys. C* **1999**, *10*, 1117. Letelier, J. R.; Toro-Labbe, A.; Chiu, Y.-N. *J. Chin. Chem. Soc*. **1999**, *46*, 333.
(118) Lu, T.-X. *Chem. Phys. Lett*. **1992**, *194*, 67. Faulhaber, J. C. R.; Ko, D. Y. K.; Briddon, P. R. *Phys Rev*. B. **1993**−**1**, *48*, 661.
(119) Berry, M. V. *Proc. R. Soc*. **1984**, *A392*, 45.
(120) Longuet-Higgins, H. C.; Opik U.; Pryce, M. H. L.; Sack, R. A. *Proc. R. Soc. London, Ser. A* **1958**, *244*, 1.
(121) Born, N.; Huang, K. *Dynamical Theory of Crystal Latices*; Oxford University Press: London, 1954; App. VIII.
(122) Herzberg, G.; Longuet-Higgins, H. C. *Discuss. Faraday Soc*. **1963**, *35*, 77.
(123) Zwanziger, J. W.; Grant, E. R. *J. Chem. Phys*. **1987**, *87*, 2954.
(124) Ham. S. F. *Phys. Rev. Lett*. **1987**, *58*, 725.
(125) Aitchison, I. J. R. *Phys. Script*. **1988**, *T 23*, 12.
(126) *Geometric Phases in Physics*; Shapere, A., Wilczek, F., Eds.; World Scientific: Singapore, 1989.
(127) Zwanziger, J. W.; Koenig, M.; Pines, A. *Annu. Rev. Phys. Chem*. **1990**, *41*, 601.
(128) Apsel, S. E.; Chancey, C. C.; O'Brien, M. C. M. *Phys. Rev. B* **1992 II**, *45*, 525.
(129) Cina, J. A.; Smith, J., Jr.; Romero-Rochin, V. *Adv. Chem Phys*. **1993**, *83*, 1. China, J. A In ref 30, p 117.
(130) Dittrich, W.; Reuter M. *Classical and Quantum Dynamics from Classical Path to Path Intergrals*, 2nd ed.; Springer: New York, 1994.
(131) Sjöqvist, E.; Goschiniski, O. *Chem. Phys*. **1994**, *186*, 17. Sjöqvist, E.; Hedström, M. *Phys. Rev. A* **1997**, *56*, 3417.
(132) Koizumi, H.; Sugano, S. *J. Chem. Phys*. **1995**, *102*, 4472.
(133) Koizumi, H. *Phys. Rev. Lett*. **1996**, *76*, 2370. Koizumi, H. *Phys. Rev*. **1999-I**, *59*, 8428.
(134) Baer, M.; Englman, R. *Chem. Phys. Lett*. **1997**, *265*, 105.
(135) Englman, R.; Yahalom, A.; Baer, M. *J. Chem. Phys*. **1998**, *109*, 6550. Englman, R.; Yahalom, A.; Baer, M. *Phys. Lett*. **1999**, *A251*, 223. Englman, R.; Yahalom, A.; Baer, M. *Eur. Phys. J*. **2000**, *A60*, 1802.
(136) Shon, J.; Köppel, H. *J. Chem. Phys*. **1998**, *108*, 1503.
(137) Yarkony, D. R. *J. Phys. Chem*. **1996**, *100*, 18612. Yarkony, D. R. *J. Chem. Phys*. **1999**, *111*, 4906.
(138) Manini, N.; Rios, P. de Los. In ref 30, p 37.
(139) Wu, X.; Wyatt, R. E.; D'Mello, M. *J. Chem. Phys*. **1994**, *101*, 2953
(140) Bohm, A.; Boya, L. J.; Kendrick, B. *Phys. Rev*. **1991**, *A 43*, 1206.
(141) Mead, C. A. *Rev. Mod. Phys*. **1992**, *64*, 51,
(142) Herzberg, G. *Electronic Spectra and Electronic Structure of Polyatomic Molecules*; Van Nostrand: Toronto, 1966.
(143) Jordan, P. C. H.; Longuet-Higgins, H. C. *Mol. Phys*. **1962**, *5*, 121.
(144) Ramsey, D. A. *Discuss. Faraday Soc*. **1963**, *35*, 90.
(145) Peyerimhoff, S. D.; Buenker, R. J.; Whitten, J. L. *J. Chem. Phys*. **1967**, *46*, 1707.
(146) Herzberg, G.; Johns, J. W. C. *Proc. R. Soc*. **1966**, *A295*, 107.
(147) Reuter, W.; Peyerimhoff, S. D. *Chem. Phys*. **1992**, *160*, 11.
(148) Engels, B.; Perić, M. *J. Chem. Phys*. **1992**, *97*, 7629.
(149) Buenker, R. J.; Perić, M.; Peyerimhoff, S. D.; Marian, R. *Mol. Phys*. **1981**, *43*, 987.
(150) Jungen, C. H.; Hallin, K.-E.; Merer, A. J. *Mol. Phys*. **1980**, *40*, 25.
(151) Perić, M.; Peyerimhoff, S. D.; Buenker R. J. *Can. J. Chem*. **1981**, *59*, 1318.
(152) Perić, M.; Peyerimhoff, S. D.; Buenker, R. J. *Chem. Phys. Lett*. **1984**, *105*, 44.
(153) Perić, M.; Buenker, R. J. Peyerimhoff, S. D. *Astrophys. Lett*. **1984**, *24*, 69.
(154) Reuter, W.; Perić, M.; Peyerimhoff, S. D. *Mol. Phys*. **1991**, *79*, 569.
(155) Nestmann, B.; Perić, M. *Chem. Phys*. **1984**, *89*, 257.
(156) Bruna, P. J. Cited in ref 113.
(157) Perić, M.; Buenker, R. J.; Peyerimhoff. S. D. *Can. J. Chem*. **1979**, *57*, 2491.
(158) Perić, M. *Chem. Phys. Lett*. **1980**, *76*, 573.
(159) Bruna, P. J.; Hirsch, G.; Perić, M.; Peyerimhoff, S. D.; Buenker, R. J. *Mol. Phys*. **1980**, *40*, 521.
(160) Bruna, P. J.; Marian, C. M. *Chem. Phys*. **1979**, *37*, 425.
(161) Perić, M.; Peyerimhoff, S. D.; Buenker, R. J. *Can. J. Chem*. **1983**, *61*, 2500.
(162) Perić, M.; Radić-Perić, J. *Chem. Phys. Lett*. **1979**, *67*, 138.
(163) Perić, M.; Hess, B. A.; Buenker, R. J. *Mol. Phys*. **1986**, *58*, 1001.
(164) Perić, M.; Phanuprakash, K.; Buenker, R. J. *Mol. Phys*. **1988**, *65*, 403.
(165) Perić, M.; Ostojić, B.; Shäter, B.; Engels, B. *Chem. Phys*. **1997**, *225*, 63.
(166) Zhu, Y. F.; Shehadeh, R.; Grant, E. R. *J. Chem. Phys*. **1993**, *99*, 5723.
(167) Köppel, H.; Cederbaum, L. S.; Domcke, W.; Von Niessen. W. *Chem. Phys*. **1979**, *37*, 303.
(168) Tanaka, K.; Davidson, E. R. *J. Chem. Phys*. **1979**, *70*, 2904.
(169) Lorenzen-Schmidt, H.; Peric, M.; Peyerimhoff, S. D. *J. Chem. Phys*. **1993**, *98*, 525.
(170) Perić, M.; Peyerimhoff, S. D. *J. Chem. Phys*. **1993**, *98*, 3587.
(171) Perić, M.; Peyerimhoff, S. D *J. Mol. Struct*. **1993**, *297*, 347.
(172) Gorinchoi, N. N.; Chimpoesu, F.; Bersuker, I. B. *J. Mol. Struct. (THEOCHEM)* **2000**, *530*, 281.
(173) Balasubramanian, K.; Liao, M. Z. *Chem. Phys*. **1988**, *127*, 313.
(174) Bonacić-Koutecky, V.; Cespiva, L.; Fantucci, P.; Pittner, J.; Koutecky, J. *J. Chem. Phys*. **1993**, *98*, 7981; **1994**, *100*, 490.
(175) Patridge, H.; Bauschlicher, C. W., Jr.; Landhoff S. R. *Chem. Phys. Lett*. **1990**, *175*, 531.
(176) Jeschke, H. O.; Garcia, M. E.; Bennemann, K. H. *Phys. Rev*. **1996**, *54*, R4601.
(177) Wolf, S.; Sommerer. G.; Rutz, S.; Schrebier, E.; Leisner, T.; Woste, L.; Berry, R. S. *Phys. Rev. Lett*. **1995**, *74*, 4177.
(178) Boo, D. W.; Ozaki, Y.; Andersen, L. H.; Lineberger, W. C. *J. Phys. Chem*. **1997**, *A101*, 6688.
(179) Passmore, J.; Shuterland G.; White, P. S. *Inorg. Chem*. **1981**, *20*, 2169.
(180) Mahapatra, S.; Cederbaum, L. S.; Köppel, H. *J. Chem Phys*. **1999**, *111*, 10452.
(181) Bawagan, A. D. O.; Chanty, T. K.; Davidson, E. R.; Tan, K. H. *Chem. Phys. Lett*. **1998**, *287*, 61.
(182) Cederbaum, L. S.; Domcke, W.; Köppel, H. *Chem. Phys*. **1978**, *33*, 319.
(183) Woywod, C.; Domcke, W. *Chem. Phys*. **1992**, *162*, 349.
(184) Thomas, R. K.; Thompson, H. W. *Proc. R. Soc. London*, **1974**, *A339*, 29.
(185) Clouthier, D. J.; Ramsay, D. A. *Annu. Rev. Phys. Chem*. **1983**, *34*, 31.
(186) Ogurtsov, I. Ya.; Munteany, G.; Bersuker I. B.; Bantush, L. *J. Mol. Struct (THEOCHEM)* **2001**, in press.
(187) Porter, R. N.; Stevens, R. M.; Karplus, M. *J. Chem. Phys*. **1968**, *49*, 5163.
(188) King, H. F.; Morokuma, K. *J. Chem. Phys*. **1979**, *71*, 3213.

(189) Raynor, S.; Herschbach, D. R. *J. Phys. Chem.* **1982**, *86*, 3592.
(190) Petsalakis, I. D.; Theodorakopoulos, G.; Wright, J. S. *J. Chem. Phys.* **1988**, *89*, 6850.
(191) Miller, W. H. *Annu. Rev. Phys. Chem.* **1990**, *41*, 245.
(192) Krause, J. L.; Kulander, K. C.; Light, J. C.; Orel, A. E. *J. Chem. Phys.* **1992**, *96*, 4283.
(193) Hagelberg, F. *Int. J. Quantum Chem.* **1999**, *75*, 367.
(194) Mahapatra, S.; Köppel, H. *Phys. Rev. Lett.* **1998**, *81*, 3116.
(195) Mahapatra, S.; Köppel, H. *J. Chem. Phys.* **1998**, *109*, 1721.
(196) Köppel, H.; Mahapatra, S.; Thiel, A. In *Electron Phonon Dynamics, and Jahn−Teller Effect*; Bevilacqua, G., Martinelli, L., Terzi, N., Eds.; World Scientific: Singapore, 1999; p 327.
(197) Martins, J. L.; Car, R.; Buttet, J. *J. Chem. Phys.* **1983**, *78*, 5646.
(198) Thompson, T. C.; Truhlar, D. G.; Mead, C. A. *J. Chem. Phys.* **1985**, *82*, 2392.
(199) Martin, R. L.; Davidson, E. R. *Mol. Phys.* **1978**, *35*, 1713.
(200) Delacretaz, G.; Grant, E. R.; Whetten, R. L.; Wöste, L.; Zwanziger, J. W. *Phys. Rev. Lett.* **1986**, *56*, 2598.
(201) Cocchini, F.; Upton, T. H.; Andreoni, W. *J. Chem. Phys.* **1988**, *88*, 6068.
(202) Bonacić-Koutecky, V.; Fantucci, P.; Koutecky, J. *Phys. Rev. B.* **1988**, *37*, 4369.
(203) Dugourd, Ph.; Chevaleyre, J.; Antoine, R.; Broyer, M.; Wolf, J. P.; Wöste, L. *Chem. Phys. Lett.* **1994**, *225*, 28.
(204) Ernst, W. E.; Rakowsky, S. *Phys. Rev. Lett.* **1995**, *74*, 58. Ernst, W. E.; Rakowsky, S. *Ber. Bunsen-Ges. Phys. Chem.* **1995**, *99*, 441. Ernst, W. E.; Rakowsky, S. *Can J. Phys.* **1994**, *72*, 135.
(205) Higgins. J.; Ernst, W. E.; Callegari, C.; Reho, J.; Lehmann, K. K.; Scoles, G.; Cutowski, M. *Phys. Rev. Lett.* **1996**, *77*, 4532.
(206) Ohashi, N.; Tsuura, M.; Hougen, J. T.; Ernst, W. E.; Rakowsky, S. J. *Mol. Spectrosc.* **1997**, *184*, 22.
(207) Vituccio, D. T.; Golonzka, O.; Ernst, W. E. *J. Mol. Spectrosc.* **1997**, *184*, 237.
(208) Meiswinkel, R.; Köppel, H. *Chem. Phys.* **1990**, *144*, 117.
(209) Mayer, M.; Cederbaum, L. S.; Köppel, H. *J. Chem. Phys.* **1996**, *104*, 8932.
(210) Chau, F. T.; Karlsson. L. *Phys. Scr.* **1977**, *16*, 248.
(211) Busch, von H.; Keil, M.; Kramer, H.-G.; Demtroder, W. In ref 30, p 311.
(212) Kramer, H.-G.; Keil, M.; Suarez, C. B.; Demtroder, W.; Meyer, W. *Chem. Phys. Lett.* **1999**, *299*, 212. Keil, M.; Kramer, H.-G.; Kudel, A.; Baig, M. A.; Zhu, J.; Demtroder, W.; Meyer, W. *J. Chem. Phys.* **2000**, *113*, 7414.
(213) Dobbyn, A. J.; Hutson, J. M. *J. Phys. Chem.* **1994**, *98*, 11428.
(214) Gerber, W. H. Ph.D. Thesis, University of Bern: 1980.
(215) Bush, von H.; Dev, V.; Eckel, H.-A.; Kasahara, S.; Wang. J.; Demtroder W.; Sebald, P.; Meyer, W. *Phys. Rev. Lett.* **1998**, *81*, 4584.
(216) Carter, S.; Meyer, W. *J. Chem. Phys.* **1990**, *93*, 8902.
(217) Walch, S. P.; Laskowski, B. C. *J. Chem. Phys.* **1986**, *84*, 2734.
(218) Walch, S. P.; Bauschlicher, C. W., Jr.; Langhoff, S. R. *J. Chem. Phys.* **1986**, *85*, 5900.
(219) Miyoshi, E.; Tatewaki, H.; Nakamura, T. *J. Chem. Phys.* **1983**, *78*, 815.
(220) Langhoff, S. R.; Bauschlicher, C. W., Jr.; Walch, S P.; Laskowski, B. C. *J. Chem. Phys.* **1986**, *85*, 7211.
(221) Zwanziger, J. W.; Whetten, R. L.; Grant, E. R. *J. Phys. Chem.* **1986**, *90*, 3298.
(222) Morse, M. D. *Chem. Phys. Lett.* **1987**, *133*, 8.
(223) Howard, J. A.; Preston, K. F.; Sutcliffe, R.; Mile, B. *J. Phys. Chem.* **1983**, *87*, 536.
(224) Morse, M. D.; Hopkins, J. B.; Langridge-Smith, P. R. R.; Smalley, R. E. *J. Chem. Phys.* **1983**, *79*, 5316.
(225) Rohlfing, E. A.; Valentini, J. *J. Chem. Phys. Lett.* **1986**, *126*, 113.
(226) Balasubramanian, K.; Liao, M. Z. *Chem. Phys.* **1988**, *127*, 313.
(227) Balasubramanian, K.; Das, K. K. *Chem. Phys. Lett.* **1991**, *186*, 577.
(228) Wedum, E. E.; Grant, E. R.; Cheng, P. Y.; Wiley: K. F.; Duncan, M. A. *J. Chem. Phys.* **1994**, *100*, 6312.
(229) Bauschlicher, C. W. *Chem. Phys. Lett.* **1989**, *156*, 91.
(230) Bishea, G. A.; Morse, M. D. *J. Chem. Phys.* **1991**, *95*, 8779.
(231) Wesendrup. R.; Hunt, T. Schwerdtfeger, P. *J. Chem. Phys.* **2000**, *112*, 9356
(232) (a) Solomonik, V. G.; Boggs, J. E.; Stanton, J. F. *J. Mol. Struct. (THEOCHEM)* **2000**, *496*, 213. (b) Solomonik, V. G.; Boggs, J. E.; Stanton, J. F. *J. Phys. Chem. A* **1999**, *103*, 838.
(233) Solomonik, V. G.; Sliznev, V. V.; Balalbanov, N. B. *Zs. Phys. Chem.* **1997**, *200*, 77. Solomonik, V. G.; Sliznev, V. V.; Balalbanov, N. B. *Zh. Neorg. Khim (Russ. J. Inorg. chem*), **1998**, *43*, 1172.
(234) Hargittai, M.; Reffy, B.; Kolonits, M.; Marsden, C. J.; Heully, J.-L. *J. Am. Chem. Soc.* **1997**, *119*, 9042.
(235) Reffy, B.; Kolonits, M.; Schulz, A.; Klapötke, T. M. *J. Am. Chem. Soc.* **2000**, *122*, 3127.
(236) (a) Schverdtfeger, P.; Boyd, P. D. V.; Brienne, S.; Burrell, A. K. *Inorg. Chem.* **1992**, *31*, 3411. (b) Schverdtfeger, P.; Boyd, P. D. V.; Fisher, T.; Hunt, P.; Liddell, M. *J. Am. Chem. Soc.* **1994**, *116*, 9620. (c) Schverdtfeger, P.; Laakonen, L. J.; Pyykkö, P. *J. Chem. Phys.* **1992**, *96*, 6807.
(237) Balabanov. N. B.; Boggs, J. E. *J. Phys. Chem. A* **2000**, *104*, 1597. Balabanov. N. B.; Boggs, J. E. *J. Phys. Chem. A* **2000**, *104*, 7370.
(238) Valachovic, L.; Riehn, C.; Mikhaylichenko, K.; Wittig, C. *Chem. Phys. Lett.* **1996**, *258*, 644.
(239) Davidson, E. R.; Borden, W. T. *J. Chem. Phys.* **1977**, *67*, 2191.
(240) Borden, W. T.; Davidson, E. R.; Feller, D. *J. Am. Chem. Soc.* **1980**, *102*, 5302.
(241) Zwanziger, J. W.; Ghelichkhani, A.; Grant, E. R. *J. Chem. Phys.* **1988**, *89*, 4012.
(242) Bally, T.; Haselbach, E. *Helv. Chim. Acta* **1975**, *58*, 311. Bally, T. Haselbach, E. *Helv. Chim. Acta* **1978**, *61*, 754.
(243) Komiya, S.; Abbright, T. A.; Hoffmann, R.; Kochi, J. K. *J. Am. Chem. Soc.* **1976**, *98*, 7255.
(244) Barckholtz, T. A.; Miller, T. A. *J. Phys. Chem.* **1999**, *103*, 2321.
(245) Barckholtz, T. A.; Miller, T. A. In *Computational Molecular Spectroscopy*; Bunker, P., Jensen, P., Eds.; Wiley: New York, 2000; p 539.
(246) Barckholtz, T. A.; Yang, M.-C.; Miller, T. A. *Mol. Phys.* **1999**, *97*, 239.
(247) Barckholtz, T. A.; Powers, P. E.; Miller, T. A.; Bursten, B. E. *J. Am. Chem. Soc.* **1999**, *121*, 2576.
(248) Pushkarsky, M.; Barckholtz, T. A.; Miller, T. A. *J. Chem. Phys.* **1999**, *110*, 2016.
(249) Marr, A. J.; Grieman, F.; Steimle T. C. *J. Chem. Phys.* **1996**, *105*, 3930.
(250) Foster, S. C.; Miller, T. A. *J. Phys. Chem.* **1989**, *93*, 5986.
(251) Yarkony, D. R.; Schaefer, H. F., III; Rothenberg, S. *J. Am. Chem. Soc.* **1974**, *96*, 656.
(252) Carter, J. T.; Cook, D. B. *J. Mol. Struct. (THEOCHEM)* **1991**, *251*, 111.
(253) Rubino, R.; Williamson, J. M.; Miller, T. A. *J. Chem. Phys.* **1995**, *103*, 5964.
(254) Hoper, U.; Botschwina, P.; Köppel, H. *J. Chem. Phys.* **2000**, *112*, 4132.
(255) Gonzalez N.; Simons, J. *J. Chem. Phys.* **1994**, *101*, 10746.
(256) Boldyrev, A. I.; Schleyer, P. v. R. *J. Am. Chem. Soc.* **1991**, *113*, 9045. Boldyrev, A. I.; Shamovsky, I. L.; Schleyer, P. v. R. *J. Am. Chem. Soc.* **1992**, *114*, 6469.
(257) Zakrzewski, V. G.; Niessen, von W.; Boldyrev, A. I.; Schleyer, P. v. R. *Chem. Phys.* **1993**, *174*, 167. Boldyrev, A. I.; Simons, J.; Zakrzewski, V. G.; Niessen, von W. *J. Phys. Chem.* **1994**, *98*, 1427.
(258) Schleyer, P. v. P.; Kapp, J. *Chem. Phys. Lett.* **1996**, *255*, 363.
(259) Ghanty, T. K,; Davidson, E. R. *J. Phys. Chem.* **1999**, *103*, 2867.
(260) Muguet, F. F. *Int. J. Chem.* **1998**, *1*, 25; **1999**, *2*, 25.
(261) Marcus. R. A. *J. Phys. Chem.* **1991**, *95*, 8236.
(262) Roeselova, M.; Bally, T.; Jungwirth, P.; Čarsky, P. *Chem. Phys. Lett.* **1995**, *234*, 395.
(263) Borden, W. T.; Davidson, E. R.; Feller, D. *J. Am. Chem. Soc.* **1981**, *103*, 5725.
(264) Bock, H.; Roth, B.; Maier, G. *Chem. Ber.* **1984**, *117*, 172.
(265) Shiotani, M.; Ohta, K.; Nagata, Y.; Sohma, J. *J. Am. Chem. Soc.* **1985**, *107*, 2562.
(266) Tachikawa, H.; Shiotani, M.; Ohta, K. *J. Phys. Chem.* **1992**, *96*, 164.
(267) Metropoulos, A.; Chiu, Y.-N. *J. Mol. Struct. (THEOCHEM)* **1996**, *365*, 119, **1997**, *417*, 95.
(268) Hrouda, V.; Bally, T.; Čarsky, P.; Jungwirth, P. *J. Phys. Chem.* **1997**, *101*, 3918.
(269) Bally, T.; Bernhard, S.; Matzinger, S.; Roulin, J.-L.; Sastry, G. N.; Truttmann, L.; Zhu, Z.; Marcinek, A.; Adamus, J.; Kaminski, R.; Gebicki, J.; Williams, F.; Chen, G. F.; Fulscher, M. R. *Chem. Eur. J.* **2000**, *6*, 11.
(270) Bally, T.; Truttmann, L.; Dai. S.; Williams, F. *J. Am. Chem. Soc.* **1995**, *117*, 7916.
(271) Jungwirth, P.; Čarsky, P.; Bally, T. *J. Am. Chem. Soc.* **1993**, *115*, 5776.
(272) Lee, T.-S.; Lien, M. H.; Jen, S.-F.; Ou, M.-C.; Wu, H.-F.; Gau Y.-F.; Chang, T.-Y. *J. Mol. Struct. (THEOCHEM)* **1998**, *170*, 121.
(273) Dewar, M..S.; Merz, K. M. *J. Mol Struct. (THEOCHEM)* **1985**, *122*, 59.
(274) Pabon, R. A.; Bauld, N. L., *J. Am. Chem. Soc.* **1984**, *106*, 1145.
(275) Bauld, N. L.; Bellville, D. J.; Pabon, R. A.; Chelsky, R.; Green, G. *J. Am. Chem. Soc.* **1983**, *105*, 2378. Bellville, D. J.; Bauld, N. L. *J. Am. Chem. Soc.* **1982**, *104*, 5700.
(276) Ohta, K.; Nakatsuji, H.; Kubodera, H.; Shida, T. *Chem. Phys.* **1983**, *76*, 271.
(277) Bouma, W. J.; Poppinger, D.; Radom, L. *J. Mol. Struct. (THEOCHEM)* **1983**, *103*, 205. Bouma, W. J.; Poppinger, D.; Radom, L. *Isr. J. Chem.* **1983**, *23*, 21.
(278) Ushida, K.; Shida, T.; Iwasaki, M.; Toriama, K.; Nunome, K. *J. Am. Chem. Soc.* **1983**, *105*, 5496.
(279) Egawa, T.; Fukuyama, T.; Yamamoto, S.; Takabayashi, F.; Kambara, H.; Ueda T.; Kuchitsu, K. *J. Chem. Phys.* **1987**, *86*, 6018.
(280) Bally, T.; Buser, U.; Haselbach, E. *Helv. Chim. Acta* **1978**, *61*, 38.
(281) Frey, R. F.; Davidson, E. R. *J. Chem. Phys.* **1988**, *88*, 1775.
(282) Reeves, M. S.; Davidson, E. R. *J. Chem. Phys.* **1991**, *95*, 6551.

(283) Katriel, J.; Davidson, E. R. *Chem. Phys. Lett.* **1980**, *76*, 259.
(284) Coulson, C. A.; Strauss, H. L. *Proc. R. Soc. London* **1962**, *A 269*, 442.
(285) Arents, J.; Allen, L. C. *J. Chem. Phys.* **1970**, *53*, 73.
(286) Dixon, R. N. *Mol. Phys.* **1971**, *20*, 113.
(287) Meyer, W. *J. Chem. Phys.* **1973**, *58*, 1017.
(288) Garcia De La Vega, J. M.; Rico, J. F.; Paniagua, M.; Fernandez-Alonso, J. I. *J. Mol. Struct.* **1983**, *105*, 31;
(289) Garcia De La Vega, J. H.; Segovia, A.; Rico, J. F.; Fernandez-Alonso, J. I. *J. Mol. Struct. (THEOCHEM)* **1985**, *123*, 203.
(290) Paddon-Row, M N.; Fox, D. J.; Pople, J. A.; Houk, K. N.; Pratt, D. W. *J. Am. Chem. Soc.* **1985**, *107*, 7696.
(291) Takeshita, K. *J. Chem. Phys.* **1987**, *86*, 329.
(292) Marinelli, F.; Roche, M. *Chem. Phys.* **1990**, *146*, 219.
(293) Knight, L. B.; Steadman, J.; Feller, D.; Davidson, E. R. *J. Am. Chem. Soc.* **1984**, *106*, 3700.
(294) Corchado, J. C.; Espinosa-Garcia, J.; Roberto-Neto, O.; Chuang, Y.-Y.; Truhlar, D. G. *J. Phys. Chem.* **1998**, *102*, 4899. Espinosa-Garcia, J.; Garcia-Bernaldez, J. C. *Phys. Chem. Chem. Phys.* **2000**, *2*, 2345.
(295) Chiu, Y.-N. *J. Phys. Chem.* **1988**, *92*, 4352.
(296) Frey, R. F.; Davidson, E. R. *J. Chem. Phys.* **1988**, *89*, 4227.
(297) Gordon, M. S. *Chem. Phys. Lett.* **1978**, *59*, 410.
(298) Power, D.; Brint, P.; Spalding, T. *J. Mol. Struct.* **1984**, *108*, 81.
(299) Caballol, R.; Catala, J. A.; Problet, J. M. *Chem. Phys. Lett.* **1986**, *130*, 278.
(300) Pople, J. A.; Curtiss, L. A. *J. Phys. Chem.* **1987**, *91*, 155.
(301) Curtis, L. A.; Pople, J. A. *Chem. Phys. Lett.* **1988**, *144*, 38.
(302) Kudo, T.; Naguse, S. *Chem. Phys.* **1988**, *122*, 233.
(303) Garcia de la Vega, J. M.; Miguel, B.; Fabian, San E. *Int. J. Quantum Chem.* **1997**, 61, 533.
(304) Wright, L. R.; Borkman, R. F. *J. Chem. Phys.* **1982**, *77*, 1938.
(305) Jungwirth, T.; Čarsky, P.; Bally, T. *Chem. Phys. Lett.* **1992**, *195*, 371.
(306) Jiang, G.; Wang, H. Y.; Zhu, Z. H. *Chem. Phys. Lett.* **1998**, *284*, 267.
(307) Wang, L.-S.; Niu, B.; Lee, Y. T.; Shirley, D. A.; Ghelichkhani, A.; Grant, E. R. *J. Chem. Phys.* **1990**, *93*, 6318.
(308) Wang, L.-S.; Niu, B.; Lee, Y. T.; Shirley, D. A.; Ghelichkhani, A.; Grant, E. R. *J. Chem. Phys.* **1990**, *93*, 6327.
(309) Meiswinkel, R.; Köppel, H. *Chem. Phys. Lett.* **1993**, *201*, 449.
(310) Köppel, H. *Zs. Phys. Chem.* **1997**, *200*, 3.
(311) Ferguson, J. *J. Chem. Phys.* **1964**, *40*, 3406.
(312) Deeth, R. J.; Hitchman, M. A.; Lehmann, G.; Sachs, H. *Inorg. Chem.* **1984**, *23*, 1310.
(313) Bruyndonckx, R.; Daul, C.; Manoharan, P. T. *Inorg. Chem.* **1997**, *36*, 4251.
(314) Stavrev, K. K.; Zerner, M. C. *Chem. Phys. Lett.* **1996**, *263*, 667.
(315) Wilk, A.; Hitchman, A.; Massa, W.; Reinen, D. *Inorg. Chem.* **1993**, *32*. 2483.
(316) Arnold, F. P.; Burdett, J. K.; Sita, L. R. *J. Am. Chem. Soc.* **1998**, *120*, 1637.
(317) Sears, T. J.; Miller, T. A.; Bondybey, V. E. *J. Chem. Phys.* **1980**, *72*, 6070; **1981**, *74*, 3240.
(318) Bondybey, V. E.; Miller, T. A.; English, J. H. *Phys. Rev. Lett.* **1980**, *44*, 1344.
(319) Raghavachari, K.; Haddon, R. C.; Miller, T. A. Bondybey, V. E. *J. Chem. Phys.* **1983**, *79*, 1387.
(320) Miller, T. A.; Bondybey, V. E. *Appl. Spectrosc. Rev.* **1982**, *18*, 105.
(321) Miller, T. A. *Annu. Rev. Phys. Chem.* **1982**, *33*, 257.
(322) Cossart-Magos, C.; Cossart, D.; Leach, S. *J. Chem. Phys.* **1978**, *69*, 4313;
(323) Cossart-Magos, C.; Cossart, D.; Leach, S. *Mol. Phys.* **1979**, *37*, 793.
(324) Cossart-Magos, C.; Cossart, D.; Leach, S. *Chem. Phys.* **1979**, *41*, 345; **1979**, *41*, 363.
(325) Cossart-Magos, C.; Leach, S. *Chem. Phys.* **1980**, *48*, 329. Cossart-Magos, C.; Leach, S. *Chem. Phys.* **1980**, *48*, 349.
(326) Whetten, R. L.; Haber, K. S.; Grant, E. R. *J. Chem. Phys.* **1986**, *84*, 1270.
(327) Cossart-Magos, C.; Cossart, D.; Leach, S. Maier, J. P.; Miser, L. *J. Chem. Phys.* **1983**, *78*, 3673.
(328) Whetten, R. L.; Grant, E. R. *J. Chem. Phys.* **1984**, *80*, 1711.
(329) Whetten, R. L.; Grant, E. R. *J. Chem. Phys.* **1986**, *84*, 654.
(330) Whetten, R. L.; Grant, E. R. *J. Chem. Phys.* **1984**, *80*, 5999.
(331) Whetten, R. L.; Grant, E. R *J. Chem. Phys.* **1984**, *80*, 691.
(332) Whetten, R. L.; Grubb, S. G.; Otis, C. E.; Albrecht, A. C.; Grant E. R. *J. Chem. Phys.* **1985**, *82*, 1115.
(333) Grubb, S. G.; Otis, C. E.; Whetten, R. L.; Grant, E. R.; Albrecht, A. C. *J. Chem. Phys.* **1985**, *82*, 1135.
(334) Köppel, H. *Chem. Phys. Lett.* **1993**, *205*, 361.
(335) Miller, T. A. *Angew. Chem., Int. Ed. Engl.* **1994**, *33*, 962.
(336) Pulay, P.; Fogarasi, G.; Boggs J. E. *J. Chem. Phys.* **1981**, *74*, 3999.
(337) Köppel, H.; Cederbaum, L. S.; Domcke, W. *J. Chem. Phys.* **1988**, *89*, 2023.
(338) Lindner, R.; Muller-Dethlefs, K.; Wedum, C.; Haber, K.; Grant, E. R. *Science* **1996**, *271*, 1698.
(339) Muller-Dethlefs, K.; Peel, J. B. *J. Chem. Phys.* **1999**, *111*, 10550.
(340) Döscher, M.; Köppel, H. *Chem. Phys.* **1997**, *225*, 93.
(341) Goode, J. G.; Hofstein, J. D.; Johnson, P. M. *J. Chem. Phys.* **1997**, *107*, 1703.
(342) Kato, H.; Hirao, K.; Sano, M. *J. Mol. Struct.* **1983**, *104*, 489.
(343) Huang, M.; Lunell, S. *J. Chem. Phys.* **1990**, *92*, 6081.
(344) Takeshita, K. *J. Chem. Phys.* **1994**, *101*, 2192.
(345) Eiding, J.; Schneider, R.; Domcke, W.; Koppel, H.; Niesen, von W. *Chem. Phys. Lett.* **1992**, *177*, 345.
(346) Eiding, J.; Domcke, W. *Chem. Phys.* **1992**, *163*, 133.
(347) Niessen, von W.; Cederbaum, L. S.; Kraemer, W. P. *J. Chem. Phys.* **1976**, *65*, 1378
(348) Whetten, R. L.; Fu, K.-Y.; Grant, E. R. *Chem. Phys.* **1984**, *90*, 155.
(349) Sears, T. J.; Miller, T. A.; Bondybey, V. E. *J. Chem. Phys.* **1981**, *74*, 3240.
(350) van der Waals, J. H.; Berghuis, A. M. D.; Groot, de M. S. *Mol. Phys.* **1967**, *13*, 301. van der Waals, J. H.; Berghuis, A. M. D.; Groot, de M. S. *Mol. Phys.* **1971**, *21*, 497.
(351) van Egmond, J.; van der Waals, J. H. *Mol. Phys.* **1974**, *28*, 457.
(352) Shchegoleva, L. N.; Bilkis, I. I.; Schastnev, P. V. *Chem. Phys.* **1983**, *82*, 343.
(353) Shchegoleva, L. N.; Schastnev, P. V. *Chem. Phys.* **1989**, *130*, 115.
(354) Hiraoka, K.; Mizume, S.; Yamabe, S. *J. Phys. Chem.* **1990**, *94*, 3689.
(355) Nash, J. J.; Squires, R. R. *J. Am. Chem. Soc.* **1996**, *118*, 11872.
(356) Shchegoleva. L. N.; Beregovaya, I. I.; Schastnev, P. V. *Chem. Phys. Lett.* **1999**, *312*, 325.
(357) Konovalov, V. V.; Laev, S. S.; Beregovaya, I. V.; Shchegoleva, L. N.; Shteingarts, V. D.; Tsvetkov, Yu, D.; Bilkis, I. I. *J. Phys. Chem. A* **2000**, *104*, 152.
(358) Beregovaya, I. V.; Shchegoleva, L. N. *Chem. Phys. Lett.* **2000**, submitted.
(359) Starichenko, V. F.; Shundrin, L. A.; Shchegoleva, L. N.; Shteingarts, V. D. *Zh. Struct. Khim.*, **2000**, *41* (5), in press.
(360) Hobey, W. D.; Mclachlan, A. D. *J. Chem. Phys.* **1960**, *33*, 1695.
(361) Liehr, A. D. *Z. Phys. Chem.* **1956**, *9*, 338.
(362) Meyer, R.; Grof. F.; Ha, T.-K.; Gunthard, H. H. *Chem. Phys. Lett.* **1979**, *66*, 65.
(363) Borden, W. T.; Davidson, E. R. *J. Am. Chem. Soc.* **1979**, *101*, 3771.
(364) Shchegoleva, L. N.; Karpov, V. M.; Platonov, V. E. *Zh. Struct. Khim.* **1996**, *37*, 1023.
(365) Schchegoleva, L. N.; Karpov, V. M.; Platonov, V. E. *Zh. Struct. Khim.*, **1999**, *40*, 184.
(366) Yu, L.; Foster, S. C.; Williamson, J. M.; Hearen, M. C.; Miller, T. A. *J. Phys. Chem.* **1988**, *92*, 4263.
(367) Yu. L.; Williamson, J. M.; Miller, T. A. *Chem. Phys. Lett.* **1989**, *162*, 431.
(368) Yu, L.; Cullin, D. W.; Williamson, J. M.; Miller, T. A. *J. Chem. Phys.* **1993**, *98*, 2682.
(369) Cremer, D.; Pople, J. A. *J. Am. Chem. Soc.* **1975**, *97*, 1358.
(370) Kilpatrick, J. E.; Pitzer, K. S.; Pitzer, R. *J. Am. Chem. Soc.* **1947**, *69*, 2483; Pitzer, K. S.; Donath, W. E. *J. Am. Chem. Soc.* **1959**, *81*, 3213.
(371) Carreira, L. A.; Jiang, G. J.; Person, W. B.; Willis, J. N., Jr. *J. Chem. Phys.* **1972**, *56*, 1440.
(372) Pfeiffer, M.; Werncke, W.; Hogin, S.; Kummrow, A.; Lau, A. *Chem. Phys. Lett.* **1998**, *295*, 56.
(373) Furlan, A.; Riley, M. J.; Leutwyler, S. *J. Chem. Phys.* **1992**, *96*, 7306.
(374) Furlan, A.; Leutwyler, S.; Riley, M. J.; Adcock W. *J. Chem. Phys.* **1993**, 99, 4932.
(375) Sato, T.; Yamamoto, A.; Tanaka, H. *Chem. Phys. Lett.* **2000**, *326*, 573.
(376) Tachibana, H.; Yoshizawa, K. *Chem. Phys.* **2000**, *260*, 303.
(377) Long, V. C.; Musfeldt, J. L.; Kamaras, K. *Phys. Rev. B* **1998**, *58*, 14338.
(378) Tosatti, E.; Manini, N.; Gunnarson, O. *Phys. Rev. B* **1996**, *54*, 17184.
(379) Tian, L.; Yi, Y. S.; Wang, C. L. *Int. J. Mod. Phys. B* **1997**, *11*, 1969.
(380) Wang, W. Z.; Wang, C. L.; Bishop, A. R. *Phys. Rev. B* **1995**, *51*, 10209.
(381) Polinger, V. Z.; Gorinchoy, N. N.; Bersuker, I. B. *Chem. Phys.* **1992**, *159*, 75.
(382) Gorinchoy, N. N.; Bersuker, I. B.; Polinger, V. Z. *New J. Chem.* **1993**, *17*, 125.
(383) Meek, D. W.; Ibers, J. A. *Inorg. Chem.* **1970**, *9*, 405.
(384) Reinen, D.; Friebel, C. *Inorg. Chem.* **1984**, *23*, 792.
(385) Reinen, D.; Atanasov. M. *Chem. Phys.* **1989**, *136*, 27.
(386) Reinen, D.; Atanasov. M. *Chem. Phys.* **1991**, *155*, 157.
(387) Atanasov. M.; König, W.; Craubner, H.; Reinen, D. *New J. Chem.* **1993**, *14*, 115.
(388) Wasada, H.; Hirao, K. *J. Am. Chem. Soc.* **1992**, *114*, 16.
(389) Daul, C.; Frioud, M.; Shafer, O.; Selloni, A. *Chem. Phys. Lett.* **1996**, *262*, 74.
(390) Akesson, R.; Petterson, L. G. M.; Sandström, M.; Wahlgren, U. *J. Phys. Chem.* **1992**, *96*, 150.

(391) Strömberg, D.; Sandström, M.; Wahlgren, U. *Chem. Phys. Lett.* **1990**, *172*, 49.
(392) Akesson, R.; Pettersson, M.; Sandström, M.; Siegbahn, E. M.; Wahlgren, U. *J. Phys. Chem.* **1993**, *97*, 3765.
(393) Kenney, J. W., III; Clymire, W.; Agnew, S. F. *J. Am. Chem. Soc.* **1995**, *117*, 1645.
(394) Bacci, M. *New J. Chem.* **1993**, *17*, 67.
(395) Bash, H.; Moskowitz, J. W.; Holister, C.; Hankin, D. *J. Chem. Phys.* **1971**, *55*, 1922.
(396) Rothmann, M. J.; Bartell, L. S.; Ewig, C. S.; Wazer, van J. R. *J. Chem. Phys.* **1988**, *73*, 375.
(397) Klobukowski, M.; Huzinaga, S.; Seijo, L.; Barandiaran Z. *Theor. Chim Acta* **1987**, *71*, 237.
(398) Klobukowski, M. *Can. J. Chem.* **1993**, *71*, 141.
(399) Klobukowski, M. *J. Comput. Chem.* **1993**, *14*, 1234.
(400) Kutzelnigg W.; Schmitz, F. In *Unkoventionelle Wechselwirkungen in der Chemie metallischer Elemente*; Krebs, B., Ed.; Verlag Chemie: Weinheim, 1992; p 17.
(401) Kaupp, M.; Willen, van Ch.; Franke, R.; Schmitz F.; Kutzelnigg, W. *J. Am. Chem. Soc.* **1996**, *118*, 11939.
(402) Wheeler, R. A.; Kumar, P. N. V. P. *J. Am. Chem. Soc.* **1992**, *114*, 4776.
(403) Maaskant, W. J. A. *New J. Chem.* **1993**, *17*, 97.
(404) Maaskant, W. J. A. *J. Alloys Compd.* **1998**, *281*, 211.
(405) Kundu, T. K.; Manoharan, P. T. *Mol. Phys.* **1999**, *97*, 709. Kundu, T. K.; Bruyndonckx, R.; Daul, C.; Manoharan, P. T. *Inorg. Chem.* **2000**, in press.
(406) Kundu, T. K.; Manoharan, P. T. *Chem. Phys. Lett.* **1997**, *264*, 338.
(407) Kundu, T. K.; Manoharan, P. T. *Mol. Phys.* **2000**, in press.
(408) Michelini, M. C.; Diez, R. P.; Jubert, A. H. *J. Mol. Struct. (THEOCHEM)* **1999**, *490*, 181.
(409) Lanczos, C. *J. Res. Natl. Bur. Stand.* **1950**, *45*, 255. Lanczos, C. *J. Res. Natl. Bur. Stand.* **1952**, *49*, 33. *Applied Analysis*; Prentice Hall: Englewood Cliffs, NJ, 1956.
(410) Haydock, R.; Heine, V.; Kelly, M. J. *J. Phys. C.* **1972**, *5*, 2845. Haydock, R.; Heine, V.; Kelly, M. J. *J. Phys. C.* **1975**, *8*, 2591.
(411) Bullet, D. W,; Haydock, R.; Heine, V.; Kelly, M. J. In *Soilid State Physics: Advances in Researsh and Applications*; Erhenreich, H., Seitz, F., Turnbull, D., Eds.; Academic Press: New York, 1980; Vol. 35.
(412) Martinelli, L.; Parravicini, G. P. *Phys. Rev. B.* **1988-II**, *37*, 10612. Martinelli, L.; Parravicini, G. P. *Phys. Rev. B.* **1989-II**, *39*, 13343. Martinelli, L.; Parravicini, G. P. *Phys. Rev. B.* **1992-II**, *46*, 15795.
(413) Martinelli, L.; Passaro, M.; Parravicini, G. P. *Phys. Rev. B.* **1991**, *43*, 8395; **1989-II**, *40*, 1044.
(414) Grosso, G.; Martinelli, L.; Parravicini, G. P. *Phys. Rev. B.* **1995-I**, *51*, 13033.
(415) Bevilacqua, G.; Martinelli, L.; Parravicini, G. P. *Phys. Rev. B.* **1996-I**, *54*, 7626. Bevilacqua, G.; Martinelli, L.; Orue, de M. A.; Rivera-Iratchet, J.; Vogel, E. E. In ref 30, p 178.
(416) Reinen, D.; Hitchman, M. A. *Z. Phys. Chem.* **1997**, *200*, 11.
(417) Barriuso, M. T.; Aramburu, J. A.; Moreno, M. *Phys. Stat. Sol. (b)* **1996**, *196*, 193.
(418) Moreno, M.; Aramburu, J. A.; Barriuso, M. T. *Phys. Rev. B* **1997-II**, *56*, 14423.
(419) Wissing, K.; Barriuso, M. T. Aramburu, J. A.; Moreno, M. J. *Chem. Phys.* **1999**, *111*, 10217.
(420) Gogolin, A. O. *Phys. Rev. B.: Condes. Matter* **1996**, *53*, R5990.
(421) Roitsin, A. B.; Klimov, A. A.; Artamonov, L. V. *Zh. Eksp. Teor. Fiz. (Sov. Phys. JETP)* **1998**, *87*, 123.
(422) Louca, D.; Kwei, G. H.; Mitchell, J. F. *Phys. Rev. Lett.* **1998**, *80*, 3811.
(423) Louca, D.; Egami, T. *Phys. Rev. B* **1999-I**, *59*, 6193.
(424) Louca, D.; Kwei, G. H.; Dabrowski, B.; Bukowski, A. *Phys. Rev. B.* **1999-II**, *60*, 7558. Louca, D.; Sarrao, J. L.; Thompson, J. D.; Röder, H.; Kwei, G. H. *Phys. Rev. B.* **1999-II**, *60*, 10378. Louca, D.; Brosha, E. L.; Egami, T. *Phys. Rev. B.* **2000-II**, *61*, 1351.
(425) EXAFS: Basic Principles and Data Analysis. In *Inorganic Chemistry Concepts*; Teo, B. K., Ed; Springer: Berlin, 1986; Vol. 9.
(426) Chiu, Y.-N. *Phys. Rev. B* **1997**, *55*, 6022.
(427) Bersuker, G. I.; Goodenough, J. B. *Physica C* **1997**, *274*, 267.
(428) Piepho, S. B.; Krausz, E. R.; Shatz, P. N. *J. Am. Chem. Soc.* **1978**, *100*, 2996. Wong, K. Y.; Shatz, P. N. *Prog. Inorg. Chem.* **1981**, *28*, 369.
(429) *Mixed-Valence Systems: Applications in Chemistry, Physics and Biology*, Prassides, K., Ed.; NATO ASI Series C; Kluwer: Dodrecht, 1991; Vol. 343.
(430) Borshch, S. A.; Bominaar, E. L.; Blondin, G.; Girerd, J.-J. *J. Am. Chem. Soc.* **1993**, *115*, 5155. Bominaar, E. L.; Borshch, S. A.; Girerd, J.-J. *J. Am. Chem. Soc.* **1994**, *116*, 5362.
(431) Riley, M. J.; Güdel, H. U.; Norton, A. H. *Chem. Phys.* **1992**, *166*, 19.
(432) Riley, M. J.; Krausz, E. R. In ref 429, p 341.
(433) Root, D. E.; Henson, M. J.; Machonkin, T. *J. Am. Chem. Soc.***1998**, *120*, 4982.
(434) Borshch, S. A.; Girerd, J.-J. *Chem. Phys.* **1994**, *181*, 1.
(435) *Molecular Magnetism: From Molecular Assemblies to the Devices*; Coronado, E., Delhaes, P., Gatteschi, D., Miller, J. S., Eds.; NATO ASI Series E; Kluwer: Dodrecht, 1996; Vol. 321.
(436) Borras-Almenar, J. J.; Coronado, E.; Tsukerblat, B. S.; Georges, R. In ref 435, p 105.
(437) Robert, V.; Borshch, S. A.; Bigot, B. *J. Phys. Chem.* **1996**, *100*, 580.
(438) Borras-Almenar, J. J.; Clemente-Juan, J. M.; Coronado, E., Paii, A. V.; Tsukerblat, B. S. *J. Phys. Chem. A.* **1998**, *102*, 200.
(439) Borras-Almenar, J. J.; Clemente-Juan, J. M.; Coronado, E., Palii, A. V.; Tsukerblat, B. S. *Phys. Lett. A.* **1998**, *238*, 164.
(440) Borshch, S. A. *J. Mol. Struct. (THEOCHEM)* **1995**, *330*, 139.
(441) Borshch, S. A.; Chibotaru, L. F. *Chem. Phys.* **1989**, *135*, 375.
(442) Bominaar, E. L.; Achim, C.; Borshch, S. A. *J. Chem. Phys.* **1999**, *110*, 11411.
(443) Klokishner, S.; Varret, F.; Boukheddaden In ref 30, p 83.
(444) Lepetit, B.; Kupperman, A. *Chem. Phys. Lett.* **1990**, *166*, 581. Wu, Y.-S. M.; Kupperman, A.; Lepetit, B. *Chem. Phys. Lett.* **1991**, *186*, 319. Kupperman, A.; Wu, Y.-S. M. *Chem. Phys. Lett.* **1993**, *205*, 577. Kupperman, A.; Wu, Y.-S. M. *Chem. Phys. Lett.* **1995**, *241*, 229. Wu, Y.-S. M.; Kupperman, A. *Chem. Phys. Lett.* **1995**, *235*, 105.
(445) Marcovic, N.; Billing, G. D. *J. Chem. Phys.* **1994**, *100*, 1089.
(446) Zhu, C.; Nikitin, E. E.; Nakamura, H. *J. Chem. Phys.* **1996**, *104*, 7059.
(447) Charutz, D. M.; Baer, R.; Bayer, M.; *Chem. Phys. Lett.* **1997**, *265*, 629.
(448) Chiu, Y.-N. *J. Phys. Chem.* **1984**, *88*, 5820. Chiu, Y.-N. *Int. J. Quantum Chem.* **1985**, *28*, 843. Chiu, Y.-N. *Phys. Rev. A* **1985**, *32*, 2257.
(449) Bersuker, G. I. *J. Chem. Phys.* **1999**, *110*, 10907.
(450) Bersuker, G. I.; Pekker, M. *J. Chem. Phys.* **1999**, *110*, 10923.
(451) Yoshizawa, K.; Hoffman, R. *J. Chem. Phys.* **1995**, *103*, 2126. Yoshizawa, K. *Nippon Kagaku Kaishi* **2000**, *7*, 443.

CR0004411